

Erythrocyte Carriers: Tool Development for Erythrocyte Mediated Diagnostic and
Drug Delivery

Nathan Paul Oien

A dissertation submitted to the faculty at the University of North Carolina at Chapel
Hill in partial fulfillment of the requirements for the degree of Doctor of Philosophy
in the Eshelman School of Pharmacy in the Division of Chemical Biology and
Medicinal Chemistry

Chapel Hill
2014

Approved By:

David S. Lawrence

Jian Liu

Stephen Frye

James E. Bear

Kenneth A. Jacobson

© 2014
Nathan Paul Oien
ALL RIGHTS RESERVED

ABSTRACT

Nathan Paul Oien: Erythrocyte Carriers: Tool Development for Erythrocyte Mediated Diagnostic and Drug Delivery
(Under the direction of David S. Lawrence)

Carrier erythrocytes have become increasingly popular in literature and in the clinical setting due to their low immunogenic response, ease of use, and well defined structure and physiology. Small molecules, therapeutic proteins, and optical biosensors have each successfully been loaded into erythrocytes, establishing a strong methodological foundation for our work that utilizes erythrocytes as “carriers” of fluorescent biosensors and therapeutic agents.

The initial stage of our research focused primarily on optimization of erythrocyte loading procedures using exogenous fluorophore labeled peptides and proteins (the term ‘loading’ refers to addition of exogenous material to the cytosol of erythrocytes). We visualized loading using widefield and confocal fluorescence microscopy. Upon our establishment of an optimized erythrocyte loading method, we used photo responsive cassettes to investigate whether erythrocytes can be manipulated to contain the cassette, and that upon microscope-mediated photolysis a fluorescence increase (without significant leakage) is observed.

With the successful development of our erythrocyte loading method, we next sought to determine whether such innovative technology could be utilized to monitor endogenous kinase activity. Erythrocytes possess highly complex biochemical

pathways, which include enzymes important in glycolysis and maintenance of extracellular homeostasis. One of the most prominent enzymes in cells, including enucleated erythrocytes, is cAMP dependent protein kinase (PKA). PKA in red blood cells is particularly relevant to the study of Malaria as it is a vital player in the protozoan parasite invasion of erythrocytes.^[1] Thus, we proposed developing a method to monitor endogenous PKA activity in erythrocytes. This ability to monitor the endogenous PKA activity will be beneficial in assessing erythrocyte response during exogenous stimuli, serving as both a biological sensor and as a diagnostic tool to detect malarial invasion. We first aimed to monitor PKA activity through the development of a bi-molecular assay. Our innovative work demonstrates that the interaction between a positively charged peptide that is covalently bound to a far-red fluorophore and a negatively charged quencher that interacts with our labeled-peptide results in quenched fluorescence. More importantly, our work demonstrates that after phosphorylation, the quencher is displaced and a fluorescence increase is observed. Upon verification of optimization and reproducibility, our carefully designed continuous assay was then used to monitor real-time endogenous PKA activity in erythrocyte lysates and within intact erythrocytes, the latter of which is possible through our established erythrocyte loading method.

With the completion of both our erythrocyte loading method and novel real-time detection of endogenous PKA activity, our next objective was to determine whether we could utilize erythrocytes for spatial and temporal- specific delivery of therapeutics using cobalamin-drug conjugates, where cobalamin acts as a light responsive photoprotecting group. In this instance, as opposed to intracellular

loading, we use lipids to anchor the drug conjugates to the exterior surface of the erythrocyte membrane. To test drug release from membranes, we utilized near-infrared (NIR) light to release anti-inflammatory therapeutics from the vitamin B12 derivative, hydroxyl-cobalamin. Cobalamin is an organometallic compound containing a cobalt center surrounded by a corrin ring. The cobalt axial bound ligand is readily cleaved using light. Interestingly, cobalamin also contains a modifiable hydroxyl sugar. We show by lipidating the hydroxyl sugar and attaching therapeutics to the cobalt axial bond, that we could anchor the complex to erythrocyte membranes. Furthermore, we demonstrated photo-release of axially bound therapeutics using 525 nm light. Lastly, we were able to extend the wavelengths of light-mediated delivery into the NIR region by introducing lipidated NIR fluorophores to the erythrocyte membranes. Excitation of the lipidated fluorophore led to photocleavage of the cobalt small molecule bond.

Using erythrocytes as carriers represents a simple and attractive method as a delivery tool. Our work demonstrates the utility of erythrocytes as carriers for delivering diagnostic tools and therapeutics that respond to light resulting in spatial and temporal control of delivery and activation.

To my best friend and wife, Jaime, I could not have done this without you. Thank you for being my balance and my rock. You have always been there when I needed you.

To my Mom, Nancee, my Dad, Tim, and my Sisters, Amanda and Kassie, for pushing me from a young age to pursue my dreams and for keeping me grounded.

To Debbie and Tom, without your support and guidance my life would be less fulfilled.

To Cinnamon, who has always been there to happily greet me when I get home.

ACKNOWLEDGEMENTS

I would like to thank Dr. David S. Lawrence for agreeing to be my advisor and accepting me into his lab. Dr. Lawrence has been a wonderful advisor and has encouraged me to pursue my research interests. I would also like to thank Dr. Lawrence for all of his feedback in reviewing my dissertation. I will always look toward Dr. Lawrence for his advice and guidance.

I would like to acknowledge all the current and former members of the Lawrence lab that have helped me along the way. I would like to thank Melanie Priestman for all of her guidance, both in the technical aspects and scientific aspects. Without her assistance my projects would have been significantly more difficult. I would like to acknowledge Finith E. Jernigan, Hsien-Ming Lee, and Luong T. Nguyen for synthesizing all of the necessary compounds to complete Chapters 2 and 3 of this dissertation. I would like to thank Weston Smith and Zack Rodgers for synthesizing all of the compounds necessary to complete Chapter 4. I would also like to thank Thomas Shell for synthesizing the compounds necessary to demonstrate proof-of-concept for future directions. I would like to thank Marissa Cann and Colin O'Banion for all their experimental support in Chapter 2. I would like to thank Finith E. Jernigan and Luong T. Nguyen for all of their additional support in completing Chapter 3. I would like to thank Robert Hughes, Weston Smith, Zach Rodgers, and Christina Marvin for all of their experimental support and guidance in

completing Chapter 4. The members of the Lawrence lab have been critical to the success of this dissertation and I would not have been able to complete it without their support and guidance.

I would like to thank the UNC Eshelman School of Pharmacy and the Division of Chemical Biology and Medicinal Chemistry for accepting me into the program and their support throughout these years. I would like to thank each of my committee members for all of the support and advice in completing my objectives.

Finally, I would like to acknowledge my reviewers. I would like to especially thank Jaime Brozowski for agreeing to be the first reviewer of my dissertation. I am extremely grateful for your patience and quality suggestions. I would also like to thank and acknowledge Nancee Oien for all of the additional support with Chapter 1 and Chapter 4. The comments and suggestions provided by both Jaime and Nancee have dramatically improved the quality and clarity of this dissertation. I would also like to acknowledge Jennifer Shell, Melanie Priestman, Robert Hughes, and Tim Oien for all of their additional comments and suggestions in reviewing Chapters 2, 3, 4, and 5 respectively.

TABLE OF CONTENTS

LIST OF TABLES.....	xii
LIST OF FIGURES.....	xiii
LIST OF ABBREVIATIONS.....	xvii
CHAPTER 1: Utilizing Erythrocytes as Highly Advanced Carrier Vesicles	
for Diagnostic and Therapeutic Purposes.....	1
Overview.....	1
Erythrocytes as carrier vesicles.....	2
Erythrocyte carriers: membrane bound delivery systems.....	5
Protein-bound targeting via antibodies.....	5
Chemically-induced targeting.....	7
Lipid targeting.....	8
Erythrocyte carrier delivery strategies: Intracellular loading.....	9
Osmosis.....	10
Electroporation.....	13
Endocytosis.....	14
Erythrocyte carriers: diagnostic assays.....	16
Optical window of tissue.....	17
Selection of long wavelength fluorophores.....	20
Fluorescence signal in erythrocyte lysates.....	23

Conclusion: research aims.....	24
Summary.....	25
CHAPTER 2: Method Development and Optimization for Loading	
Fluorescent Molecules into Erythrocytes.....	27
Overview.....	27
Introduction.....	28
Materials and Methods.....	29
Results.....	40
Discussion.....	49
CHAPTER 3: Monitoring Endogenous Erythrocyte PKA53	
Overview.....	53
Introduction.....	54
Materials and Methods.....	57
Results.....	73
Discussion and Future Directions.....	87
CHAPTER 4: Erythrocyte Mediated Delivery of Anti-inflammatory	
Therapeutics.....	91
Overview.....	91
Introduction.....	92
Materials and Methods.....	96
Results.....	119
Discussion and Future Directions.....	134

CHAPTER 5: Final Thoughts and Future Directions.....	139
Overview.....	139
Erythrocytes as carriers.....	139
Anchoring therapeutics to erythrocyte membranes.....	140
Loading therapeutics into erythrocytes.....	143
Other carriers (hybrid erythrocytes nano-vesicles, nanoparticles, liposomes/micelles).....	145
Using cobalamin to control enzymatic activity.....	146
REFERENCES.....	148

LIST OF TABLES

Table 1.1 - Various fluorophores for visualization within the optical window of tissue.....	21
Table 3.1 - Quenchers used in kinase assay screen.....	74
Table 3.2 - Fluorescent increase of peptides associated with quenchers.....	75
Table 3.3 - Effect of salt on the fluorescent response upon phosphorylation.....	75
Table 3.4 - Effect of salt on the fluorescent response upon phosphorylation of peptides with Evans Blue.....	76

LIST OF FIGURES

Figure 1.1 – Loading methods of erythrocytes used as carriers.....	4
Figure 1.2 – Antibody-urokinase conjugates bind to erythrocytes and target urokinase activity to hemorrhage site.....	6
Figure 1.3 – Loading erythrocytes using hypotonic swelling.....	10
Figure 1.4 – Loading erythrocytes using electroporation.....	12
Figure 1.5 – Loading erythrocytes by endocytosis.....	14
Figure 1.6 – Optical window of tissue.....	18
Figure 1.7 – Signal loss of Cy5.5 in various tissue samples.....	19
Figure 1.8 – Erythrocyte lysate absorbance vs fluorophore absorbance.....	24
Figure 1.9 – Signal loss of fluorophores due to various hematocrit of erythrocyte lysates.....	24
Figure 2.1 – HPLC of photolabile cassette.....	34
Figure 2.2 – Synthesis of lipidated protease sensor.....	35
Figure 2.3 – LC/MS analysis of protease sensor.....	38
Figure 2.4 – Loading erythrocytes via hypotonic dialysis.....	42
Figure 2.5 – Loading erythrocytes via hypotonic dilution.....	42
Figure 2.6 – loading erythrocytes via electroporation.....	42
Figure 2.7 – Loading erythrocytes using hypotonic dilution with fluorophore labeled peptides and fluorophore labeled PKA.....	43
Figure 2.8 – Erythrocytes loaded with 10,000 MW OG dextran and TAMRA labeled peptide.....	44
Figure 2.9 – Photolabile cassette.....	46
Figure 2.10 – Widefield microscopy mediated photolysis of the quenched cassette using a microwell plate.....	46

Figure 2.11 – Photolysis of erythrocytes loaded with photolabile cassette.....	47
Figure 2.12 – Erythrocytes loaded with cassette and imaged using confocal microscopy.....	47
Figure 2.13 – Confocal images of erythrocytes loaded with membrane anchored photocleavable protease substrate.....	48
Figure 2.14 – Fluorescence fold change of protease substrate loaded into erythrocytes.....	49
Figure 3.1 – schematic diagram of erythrocyte kinase activity.....	57
Figure 3.2 – Peptide Atto 680-KRRRLASLAA with quencher Acid Blue 80.....	76
Figure 3.3 – Percent erythrocyte lysis from exposure to Evans Blue and Acid Blue 80.....	77
Figure 3.4 – Job plot analysis of Acid Blue 80 and Evans Blue determined at 556 nm.....	78
Figure 3.5 – EQ ₅₀ of Acid Blue 80 and Evans Blue.....	79
Figure 3.6 – EQ ₅₀ of Acid Blue 80 at various salt concentrations.....	80
Figure 3.7 – Quenching of Atto633-Aoc-GRTGRRFSY in erythrocyte lysates.....	80
Figure 3.8 – Fluorescence increase of Atto633-Aoc-GRTGRRFSY And TAMRA-Aoc-GRTGRRFSY in 10% erythrocyte lysates and In 100% erythrocyte lysates.....	81
Figure 3.9 – Inhibition of PKA activity.....	82
Figure 3.10 – Inhibition of erythrocyte PKA activity using non-specific PKA inhibitors.....	83
Figure 3.11 – Immunodepletion of PKA from erythrocyte lysates.....	83
Figure 3.12 – Photoactivation of Atto633-Aoc-GRTGRRFS(DMNB)Y.....	84
Figure 3.13 – Confocal fluorescence images of Atto633-Aoc-GRTGRRFSY loaded erythrocytes.....	85

Figure 3.14 – Flow cytometry analysis of erythrocytes loaded with Atto633-Aoc-GRTGRRFSY peptide, Atto633-Aoc-GRTGRRFSY peptide and Evans Blue, and no loading control.....	85
Figure 3.15 – Confocal images of atto633-Aoc-GRTGRRFSY and Evans Blue loaded erythrocytes.....	86
Figure 3.16 – Erythrocytes stimulated with DMSO, H89, or CPT-cAMP then analyzed by western blot for phosphorylated PKA substrates.....	90
Figure 4.1 – Wavelength-encoded drug release strategy.....	94
Figure 4.2 – Fluorescent fold change in aqueous fraction after photolysis.....	120
Figure 4.3 – Transfer of methotrexate to aqueous layer after photolysis.....	120
Figure 4.4 – Monitoring FAM and TAM release after fluorescence in erythrocyte supernatants.....	121
Figure 4.5 – TAMRA release (fluorescence fold increase) as function of Cy5-C18 and TAM-Cbl-C18.....	124
Figure 4.6 – Concentration of TAMRA released at 660 nm using various concentration of Cy5-C18 and 1 μ M TAM-Cbl-C18.....	124
Figure 4.7 – Ratio of TAMRA released in the absence of fluorophore-C18 after photolyzing at the fluorophore excitation maximum.....	125
Figure 4.8 – Concentration of TAMRA released using various fluorophore-C18 after photolyzing at their corresponding excitation maximum.....	125
Figure 4.9 – Concentration of fluorescein released using various fluorophore-C18 after photolyzing at their corresponding excitation maximum.....	126
Figure 4.10 – Confocal images of erythrocyte loaded with Cy5-C18.....	127
Figure 4.11 – Release of TAMRA from the RBC membrane into The surrounding medium visualized by widefield microscopy.....	127
Figure 4.12 – Correlation between amount of Drug-Cbl-C18 loaded onto erythrocyte and concentration of drug released into the supernatant.....	128

Figure 4.13 – Inhibition of DHFR using methotrexate and photo-MTX.....	128
Figure 4.14 – Photolyzed colchicine added to HeLa Cells.....	129
Figure 4.15 – HeLa Cells exposed to dexamethasone.....	130
Figure 4.16 – HeLa Cells exposed to Col-Cbl-C18 loaded erythrocytes.....	130
Figure 4.17 – Cellular thermal shift assay of HeLa cells treated with MTX-Cbl-C18 loaded erythrocytes.....	131
Figure 4.18 – Widefield images of HeLa cells after dexamethasone release from Dex-Cbl-C18 and Cy5-C18 loaded erythrocytes using 660 nm light.....	132
Figure 4.19 – Widefield images of HeLa cells after colchicine release from Col-Cbl-C18 and FL800-C18 loaded erythrocytes using 780 nm light.....	133
Figure 4.20 – Cellular thermal shift assay of HeLa cells treated with MTX-Cbl-C18 and Cy7-C18 loaded erythrocytes.....	134
Figure 5.1 – Confocal images of erythrocytes loaded with Cy5-C18 and TAMRA-C18.....	142
Figure 5.2 – Overlay of Cy5-C18 and TAMRA-C18 loaded erythrocytes mixed together.....	142
Figure 5.3 – Chemical structures of phosphatidylcholine, phosphatidylethanolamine, and phosphatidyleserine.....	143
Figure 5.4 – Fluorescence increase in supernatant of BODIPY loaded erythrocytes in the presence and absence of light (660 nm).....	144
Figure 5.5 – Erythrocytes loaded with BODIPY-Cbl and imaged by confocal microscopy.....	145
Figure 5.6 – Schematic representation for long wavelength control to measure erythrocyte kinase activity in real time.....	147

LIST OF ABBREVIATIONS

ATP	Adenosine triphosphate
BODIPY	boron-dipyrromethene
C18	Octadecyl
cAMP	Cyclic adenosine monophosphate
CBL	Cobalamin
COL	Colchicine
CPT-cAMP	8-(4-Chlorophenylthio)adenosine-3',5'-cyclic monophosphorothioate
CETSA	Cellular thermal shift assay
DCI	Delayed Cerebral Ischemia
DEX	Dexamethasone
DHFR	Dihydrofolate reductase
DMSO	Dimethyl sulfoxide
DNA	Deoxyribonucleic acid
DTT	Dithiothreitol
EDTA	Ethylenediaminetetraacetic acid
EET	Epoxyeicosatrienoic acid
ELISA	enzyme-linked immunosorbent assay
FAM	Fluorescein
FBS	Fetal Bovine Serum
FRET	Fluorescence resonance energy transfer
GPCR	G protein-coupled receptors
GPI	Glycophosphatidylinositol

HLA	human leukocyte antigen
igG	Immunoglobulin G
IR	Infrared
LC-MS	Liquid chromatography mass spec
LED	Light emitting diode
MRI	Magnetic resonance imaging
MTX	Methotrexate
NEM	N-Ethylmaleimide
NHS	N-Hydroxysuccinimide
NIR	Near infrared
NO	Nitric oxide
OG-Dextran	Oregon green dextran
PBS	Phosphate buffered saline
PC	Phosphatidylcholine
PDT	Photodynamic therapy
PE	Phosphatidylethanolamine
PEG	Polyethylene glycol
<i>Pf</i> PKA	<i>Plasmodium falciparum</i> cAMP-depedent protein kinase
PS	Phosphatidylserine
RA	Rheumatoid arthritis
ROS	Reactive oxygen species
SM	Sphingomyelin
TAM	Tetramethylrhodamine

TAMRA	Tetramethylrhodamine
tPA	Tissue plasminogen activator
UV	Ultraviolet

Chapter 1 Utilizing Erythrocytes as Highly Advanced Carrier Vesicles for Diagnostic and Therapeutic Purposes

Overview

Erythrocyte carriers represent a method to increase therapeutic drug delivery with demonstrated success in the clinic.^[2] The therapeutic index of these drugs can be increased by using light to control delivery in a spatial and temporal manner. Similarly, diagnostic agents can be delivered using erythrocytes and light could be used to initiate the diagnostic at a specific location. However, an important aspect in using erythrocytes as carriers of light-activated diagnostic and therapeutic agents includes developing tools that can respond to light that is within the appropriate wavelength range to allow penetration of tissue. The objective of my dissertation is to show that we have successfully developed substrates which are able to be carried by erythrocytes and which respond to light that operates within the optical window of tissue. These agents demonstrate the potential for *in vivo* delivery and activation in a spatial and temporal manner.

Erythrocytes as carrier vesicles

Erythrocytes were first discovered in the 1600s followed by a more complete characterization in the 1800s,^[3] with further understanding of a seemingly single vital role in the human body as “sacks of hemoglobin” that deliver oxygen while simultaneously removing carbon dioxide. Erythropoiesis, the formation of erythrocytes, is heavily dedicated to the role of concentrating hemoglobin inside the “young erythrocyte” or erythroblast, which involves multiple levels of gene regulation of highly complex mechanisms.^[4]

Erythropoiesis elicits the eventual ejection of the nucleus and other intracellular organelles, such as the mitochondria, to make room for hemoglobin to support oxygen transport.^[5] Hemoglobin, a porphyrin containing oxygen transport protein, constitutes 90% of the dry weight of a mature erythrocyte and has been shown to exceed 90% upon exclusion of membranes and membrane bound proteins.^[6]

Despite the large accumulation of hemoglobin, Zolla *et al.* performed a proteomic study that demonstrated evidence of 1,900 non-redundant proteins, suggesting the “sacks of hemoglobin” and corresponding microenvironment are more complex than originally believed.^[6] Many of the aforementioned non-redundant proteins were found to be localized to the membrane and classified as integral membrane proteins; membrane-associated proteins, GPI-anchored proteins, and extracellular/cytoskeletal/membrane spanning proteins, all of which have widely varied functions including transport, binding, catalytic, signal transduction, glycolysis, structural and antioxidant activity.^[7, 8] Many of these proteins are involved in protein protection such as glutathione peroxidase.^[9] Interestingly, a

definitive property of erythrocytes, is their elasticity and deformability that is critical for the average 5 to 10 μm cell to pass through 3 to 5 μm vessels.^[8, 10] Elasticity and deformability involves many of the previously mentioned protein classifications. In fact, loss of elasticity and deformability in erythrocytes over the 120 day life cycle corresponds with eventual degradation and clearance of the erythrocyte.^[11] As a result it is important to use fresh erythrocytes when studying or using erythrocytes to ensure 'normal' phenotypes are observed.

When comparing erythrocytes to other carriers such as liposomes or nanoparticles that are short lived in the body (days to weeks) and accumulate in the liver,^[12] the long (120 day) life cycle and ability to circulate through blood vessels located throughout the body make erythrocytes an attractive target as carriers of therapeutics and diagnostics. Since the 1950s, large efforts have been put forth to utilize erythrocytes as a vessel to carry and deliver exogenous substrates *in vivo*. In 1979 such methods of loading erythrocytes with exogenous substrates for *in vivo* use were termed 'carrier erythrocytes' and have subsequently been further developed. Examples of erythrocyte mediated delivery of diagnostic tools, small molecule therapeutics, and even proteins are described in the literature.^[13] Two primary carrier mechanisms with exogenous substrates have been utilized thus far (**Figure 1.1**) 1) binding to the extracellular membrane of erythrocytes through antibody recognition of erythrocyte surface proteins, covalent modification of the extracellular membrane, or use of hydrophobic lipids to anchor substrates to the membrane; or 2) loading into erythrocytes by altering isotonicity and inducing formation of small pores in the erythrocyte membrane. In

fact, combined basic and translational research efforts utilizing these two erythrocyte carrier methods have yielded promising therapies that are currently in all three phases of clinical trials for the treatment of cancer and inflammation related diseases.^[13]

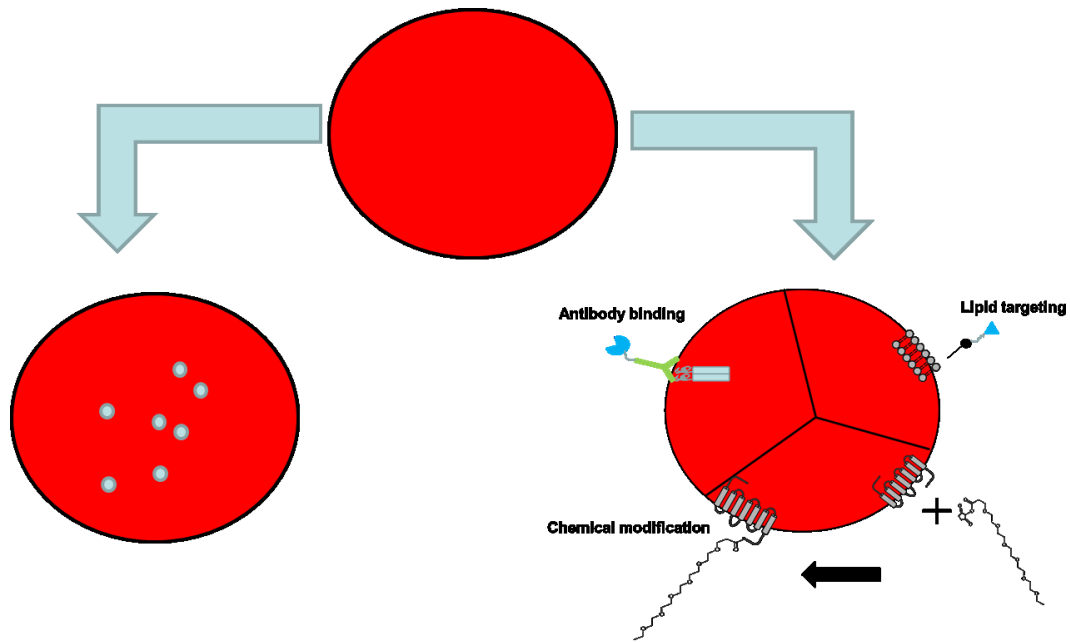


Figure 1.1 Loading methods of erythrocytes used as carriers. Proteins and small molecules can be loaded into erythrocytes (left) or bound to the extracellular surface via membrane protein targeted antibodies (right) or through chemical modification of erythrocyte membranes.^[3]

Erythrocyte carriers: membrane bound delivery systems

The first erythrocyte carrier mechanism involves membrane bound delivery. The erythrocyte membrane is comprised of protein (52%), lipids (40%), and carbohydrates (8%),^[14] the abundant availability of proteins and lipids serve as ideal targets for efficient membrane bound delivery mechanisms of erythrocyte carrier vesicles.

Protein-bound targeting via antibodies: Drug delivery via a membrane bound delivery system may be mediated by an antibody drug conjugate that targets erythrocyte membrane proteins. The erythrocyte membrane proteins are categorized into two subgroups, peripheral membrane proteins and integral membrane proteins. Integral membrane proteins are located at the cytoplasmic side of the erythrocyte membrane and are currently of not much utility for membrane bound delivery systems which use antibodies. Integral membrane proteins are tightly bound to the membrane and span both sides of the erythrocyte membrane exposing protein extracellularly and intracellularly, and thus serve as ideal membrane bound delivery target components. Specifically, band 3 and glycophorins are two major integral membrane proteins of erythrocytes that have been utilized as targets for drug delivery methods via antibody targeting mechanisms.^[15, 16] Using glycophorin as a delivery target has been described to treat delayed cerebral ischemia (DCI) in mice (**Figure 1.2**).^[17] By targeting glycophorin A with an antibody (anti-glycophorin A)-urokinase (a type of tissue-type plasminogen activators) derivative, the detrimental microclot

burden was reduced in mice during subarachnoid hemorrhage. Murciano *et al.* recent findings suggest modifying erythrocytes to carry urokinase (via glycophorin A targeting) specifically localized the thrombolytic agent to dissolve clots that may have the potential to cause cerebral ischemia, thus serving as a therapeutic agent to reduce DCI.^[17]

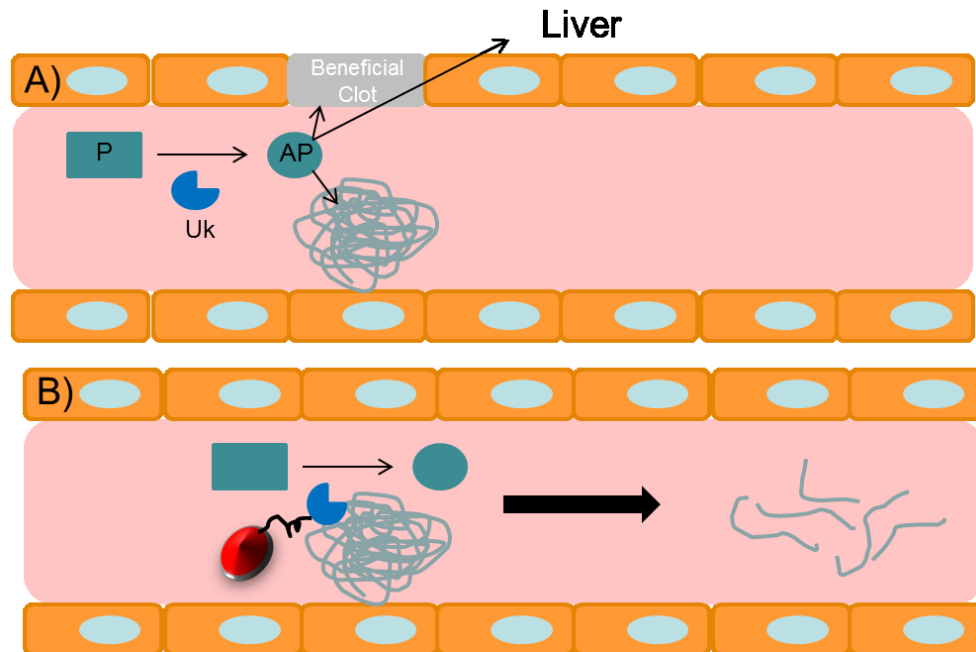


Figure 1.2 Antibody-urokinase conjugates bind to erythrocytes and target urokinase activity to hemorrhage site. A) High doses of Urokinase required for reperfusion and diffusion of urokinase into occlusive pathological clots increases the risk of bleeding. B) Antibody-mediated targeting of urokinase to erythrocytes reduces the clearance rate of urokinase and increases specificity for potentially harmful clots. (Uk urokinase, P plasminogen, AP Plasmin).^[18]

Chemically-induced targeting: Another strategy for membrane based erythrocyte delivery systems is to manipulate the erythrocyte membrane by chemical means, such as through covalent modification. Covalent modifications of membranes is advantageous as a delivery system as it provides permanent modifications to the cell (until cleared), as well as elimination of antibody cross-

reactivity *in vivo* and eliminating the need for erythrocyte membrane protein target identification. However, chemically-induced targeting also has potential pitfalls since covalent modification requires *ex vivo* manipulation of erythrocytes and use of chemical crosslinkers to modify the surface with the potential to damage and reduce integrity of erythrocyte membranes.^[18] Techniques for crosslinking molecules to erythrocytes have been developed since the 1950s, utilizing crosslinking agents, such as cyanuric chloride,^[19] N-hydroxysuccinimide (NHS),^[20] trypsin and phenylhydrazine,^[21] N-ethylmaleimide (NEM),^[22] and glutaraldehyde.^[23] Polyethylene glycol (PEG) modification of erythrocyte membranes using cyanuric chloride has been shown to camouflage erythrocyte antigenic determinants, such that loss of carbohydrate blood-type specific “ABO” groups and HLA typing on the surface of erythrocytes allowed for interspecies transfusion with sufficient erythrocyte lifespan.^[19] The clinical significance of PEGylating erythrocytes for transfusion suggests blood could be used from any donor, and thus eliminating the need for blood-type matched donors. Similar to PEG modification, NHS ester modification of erythrocyte membranes has also demonstrated success.^[20] Covalent crosslinking of biotin via NHS ester modification provides a versatile arm that can be used to attach anything, via a streptavidin handle, from small molecules and peptides to large enzymes.^[24] Under monovalent conditions tissue-type plasminogen activator (tPA) (used to dissolve nascent clots) has been attached to erythrocyte surfaces. tPA attached to the membrane of erythrocytes was demonstrated to have an increased lifespan (versus tPA alone) and function to reduce pulmonary clots in a rat

venous thrombosis model.^[17] Despite a propensity to cause lysis, as demonstrated by the mouse studies performed by Scott *et al.*, covalent modification of erythrocytes remains a strong possibility for clinical use.

Lipid targeting: Exogenous lipids serve as another candidate for an efficient membrane bound delivery mechanism of erythrocyte carrier vesicles. The erythrocyte membrane is comprised largely of lipids, specifically: phosphatidylcholine (PC), sphingomyelin (SM), phosphatidylethanolamine (PE), and phosphatidylserine (PS), as well as smaller fractions of phospholipids phosphatidic acid, phosphatidylinositol 4-phosphate, and phosphatidylinositol 4, 5-diphosphate.^[14] These phospholipids, along with the membrane associated proteins and carbohydrates, form the erythrocyte membrane bilayer is comprised of a hydrophobic interior and a hydrophilic exterior. Specifically, lipids such as PC or PS have been used to anchor small molecules to the erythrocyte membrane with minimal impact on erythrocyte biology. For example, PC has been used to anchor the mitochondrial tracker boron-dipyrromethene (bodipy) and biotin to erythrocyte membranes.^[25, 26] Muzykantov *et al.* compared lipid targeting via PE-biotin bound to the membranes of erythrocytes to chemically-induced targeting via covalently bound NHS-biotin loaded erythrocytes, both methods reported similar amounts of avidin. Importantly, they did not observe erythrocyte lysis when anchoring biotin to erythrocyte membranes using PE.^[25] Muzykantov *et al.* findings represent a potentially simplified option for membrane-bound delivery targeting of erythrocyte carrier methods over covalent modification.

In summary, chemically-induced and exogenous lipid targeting strategies of membrane bound delivery mechanisms show promise for using erythrocytes to deliver therapeutics. The 120 day erythrocyte lifespan, reduced immune response, and the myriad of tools available for membrane anchored delivery contribute to the attractiveness of this technique for therapeutic delivery. Membrane bound delivery systems have the potential to enhance therapeutics by enhancing their circulation lifespan while maintaining therapeutic potency.

Erythrocyte carrier delivery strategies: intracellular loading

A second erythrocyte delivery mechanism involves intracellular loading. Loading requires the removal and isolation of blood from the body. Due to the high hemoglobin content (90%), erythrocytes are easily separated by centrifugation,^[27] allowing for ease of blood cell separation. Over the past 60 years, since the first published erythrocyte loading method, many have been developed to load erythrocytes; methods should be used that minimize alteration to erythrocyte phenotypes if erythrocytes are to be used *in vivo*. A few of the most common erythrocyte loading methods include osmosis-, electroporation-, and endocytosis-based methods.

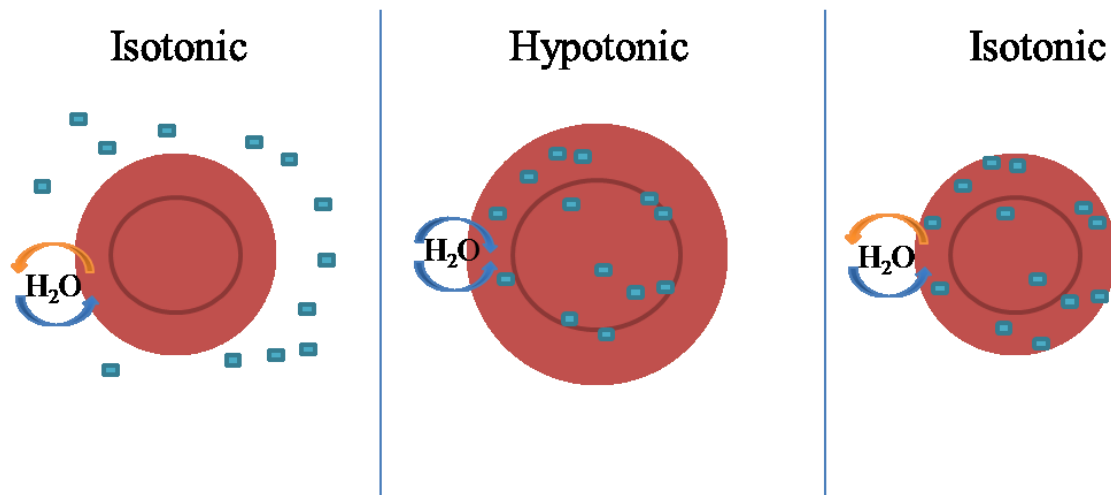


Figure 1.3 Loading erythrocytes using hypotonic swelling. The “cargo” intended to be loaded is mixed with erythrocytes in an isotonic buffer. The mixture is then mixed with a low salt solution to induce swelling and pore formation. Isotonicity is then restored to induce sealing.

Osmosis: The first method for loading erythrocytes uses osmosis, by which manipulations to induce a hypotonic solution causes erythrocyte swelling and formation of pores, allowing for cargo to be loaded. Osmosis based methods for efficient erythrocyte loading of proteins, small molecules, or drugs have been common methods utilized during investigations of drug delivery efficiency, membrane protein analyses, and phenotypic analyses of erythrocyte function.^[3, 13, 18, 28, 29] Although erythrocyte osmosis-based loading methods may be further subcategorized into 5 classifications (hypotonic dilution; hypotonic dialysis; hypotonic pre-swelling; osmotic pulse; and hypotonic hemolysis),^[27] each classification follows a similar process. Erythrocytes are exposed to a hypotonic solution, by which the low salt solution in the buffer induces rapid water influx; this, in combination with the slow salt efflux, causes the erythrocytes to “swell”. As erythrocytes cannot alter the surface area of their membrane, increasing the internal volume induces a single pore to form in each

erythrocyte.^[11] Pore formation allows for the free exchange of cargo between the erythrocyte cytoplasm and the extracellular environment.^[11, 30] When isotonicity is restored the pore begins to reseal. Where typical cells would undergo apoptosis in similar conditions, erythrocytes do not contain the machinery (mitochondria or nucleus) to induce apoptosis and have been shown to be stable for up to 3 months after loading.^[5, 28, 31] Hypotonic dilution and hypotonic dialysis are the two most common forms of erythrocyte loading and will be highlighted here, for information on the other loading methods refer to Magnani *et al.* Although both hypotonic dilution and dialysis methods can be readily established in any laboratory, hypotonic dialysis is the most common method with well-established optimization protocols and documented stable biochemical and physiological cell characteristics.^[32] In brief, loading erythrocytes with hypotonic dialysis requires the use of dialysis kits placed in solutions with specific osmotic pressure to ensure minimal perturbation of erythrocyte physiology. However, this requires a large amount of substrate relative to erythrocyte volume. In contrast, hypotonic dilution mediated erythrocyte loading simply requires dilution of erythrocytes in a hypotonic solution until lysis begins to occur, followed by restoration of isotonicity and incubation, requiring minimal substrate concentrations.^[33] Though hypotonic dilution may not maintain optimal physiological properties of erythrocytes as well as hypotonic dialysis methods do; the simplicity of this method, and minimal substrate utilization, has made this an attractive loading method. Osmosis-based erythrocyte loading has been utilized to load doxorubicin as a method of drug delivery.^[34, 35] Doxorubicin is an extremely cytotoxic small molecule antibiotic that

is used as a chemotherapeutic agent.^[36] To maximize efficacy and reduce cytotoxicity doxorubicin should be delivered in small doses over many increments of time.^[37] De Flora *et al.* showed erythrocytes were able to be loaded with high concentrations of doxorubicin. Furthermore, doxorubicin was protected from semiquinone formation, the semiquinone is thought of as the active form and generates ROS inducing DNA damage. Doxorubicin loaded erythrocytes were efficient in the slow release of unaltered doxorubicin in the vascular system.^[34] Clinical investigations of lymphoma patients treated with doxorubicin-loaded erythrocytes, in comparison to the normal delivery method of free doxorubicin, showed reduced doxorubicin clearance, lack of severe myelosuppression, and no evidence of cardiotoxicity.^[35] Though further studies are warranted to determine the efficacy of this treatment compared to slow intravenous infusion, the preliminary clinical results demonstrate a safer drug delivery method of a typically strong cytotoxic drug over previous free, normal delivery methods.

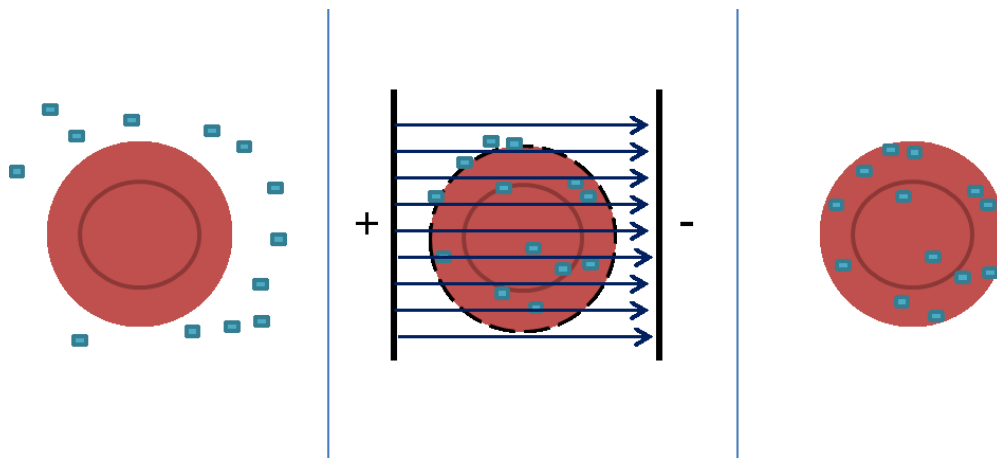


Figure 1.4 Loading erythrocytes using electroporation. Erythrocytes are mixed with isotonic saline containing “cargo” to be loaded and electroporated for a brief time followed by recovery.

Electroporation: A second method for loading erythrocytes involves electroporation. Through electroporation electric field pulses are applied to erythrocyte suspensions altering membrane integrity and increasing permeability, allowing for a potential loading method.^[38] During electroporation, erythrocytes are suspended to 10-20% hematocrit in an isotonic saline solution buffer containing iso-osmotic concentrations of sucrose and the desired cargo to be loaded into the erythrocyte. When the electric field is applied, this induces breakdown of the erythrocyte membrane and allows the cargo to become encapsulated. After the sub-millisecond electric pulse the erythrocytes are incubated at 37 °C to stabilize or “reseal” the membrane.^[39] Previous work established that electroporation-based erythrocyte loading via electric pulses should not exceed 2.5 kV/cm in order to minimize lysis, and erythrocytes incubated at 4 °C for 1 h allowed loading, and approximately 10 min at 37 °C allowed membrane resealing.^[40] Interestingly, Flynn *et al.* demonstrated erythrocytes could be loaded with methotrexate using electroporation and subsequent photosensitization with light exposure resulted in release of methotrexate from erythrocytes,^[41] suggesting erythrocytes loaded with anticancer drugs and photosensitized may be a potential strategy to treat cancer via photodynamic therapy (PDT).^[42] Loading cytotoxic agents into erythrocytes and using light to induce spatially and temporally selective release of the drug near the tumor microenvironment could provide an alternative method to deliver anticancer agents at a high concentration to improve therapeutic efficacy while reducing host cytotoxicity.

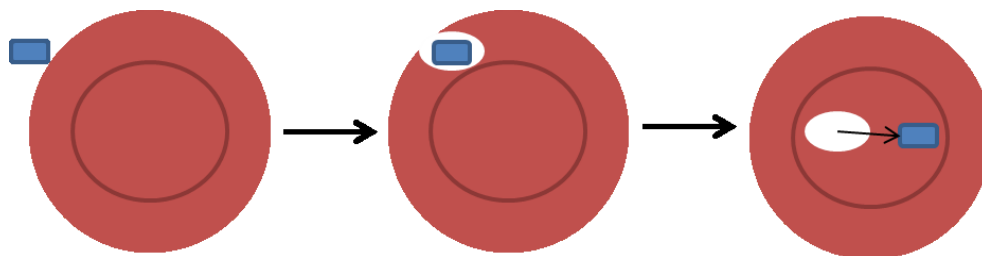


Figure 1.5 Loading erythrocytes by endocytosis. Erythrocytes are mixed with “cargo” to be loaded and agents that induce endocytosis. After membrane invagination and sealing the “cargo” escapes the endosome and become cytosolic.

87

Endocytosis: A third type of erythrocyte loading involves endocytosis.

Endocytosis is the natural cellular process of invagination of the plasma membrane to uptake extracellular fluid and components in the cell. Once the external surfaces of the cell wall closes, an intracellular bi-layered vesicle is formed, housing the extracellular fluid and components, including proteins, small molecules, and/or drugs.^[39] Interestingly, the ability of the erythrocyte to endocytose is inversely correlated with erythrocyte age.^[43] Amphipathic cations (vitamin A, chlorpromazine, primaquine) and small hydrophobic molecules (steroids) can induce endocytosis in cells.^[44, 45] Molecules that are not naturally endocytosed by erythrocytes can be mixed with amphipathic cations, providing a potentially universal mechanism for loading. Endocytosis-mediated loading of erythrocytes has been successfully applied by using hydrocortisone, vinblastine, and chlorpromazine.^[46] Endocytosis-mediated loading of erythrocytes is a particularly attractive strategy since it offers the least perturbation to erythrocytes, absence of lysis or loss of cytoplasmic content, and an increased overall lifespan (maximizing the 120 day lifespan of erythrocytes). Specifically, pravastatin was

demonstrated to be intracellularly carried by erythrocytes via endocytosis-mediated loading, which may serve as a slow release formulation for the potential treatment of many diseases including stroke and Alzheimer's disease. Typically patients receiving pravastatin experience side effects, such as diarrhea, constipation, nausea and indigestion. Due to the low oral bioavailability and subsequent requirement for increasing the dosage side effects on the liver, kidney, and muscular tissue may be exacerbated.^[47, 48] Endocytosis-mediated loading of erythrocytes with subsequent drug release may provide an alternative delivery method to oral delivery. Harisa *et al.* determined that pravastatin, as an amphipathic cation, was able to be loaded via endocytosis into erythrocytes with minimal perturbation. Furthermore, they were able to monitor the slow release of Pravastatin with 70% release over 24 h.^[48] This prolonged ability to circulate *in vivo*, provides an efficient slow release of loaded agents, allowing highly cytotoxic compounds, such as anticancer agents to be delivered while minimizing host cytotoxicity typically observed via oral route delivery. A major pitfall to endocytosis based loading methods is that not all therapeutics can be loaded in this manner. However, it has been demonstrated that even large substrates, such as DNA, can be entrapped in erythrocytes via endocytosis and used to deliver to other cells using fusagens such as PEG.^[49]

The general practice of loading therapeutic agents into the intracellular environment of erythrocytes represents an attractive method for drug delivery. The loading process is simple, fast, and provides consistent results. The cargo loaded into erythrocytes experiences increased circulation lifetime as a result of

being protected from the extracellular environment. Furthermore, the slow release of cytotoxic agents can reduce experienced side effects and provide better treatment options.

Erythrocyte carriers: diagnostic assays

Current diagnostic-based assays include removing erythrocytes from the patient and testing properties, such as: sedimentation rates for inflammation and infection,^[50] loading erythrocytes with contrast agents to assist in MRI,^[51, 52] and using antibodies to monitor erythrocyte changes by enzyme-linked immunosorbent assay (ELISA) or flow cytometry.^[53] None of the current tests utilize erythrocyte based enzymatic activity as reporters for disease. Developing an assay to monitor endogenous erythrocyte enzyme activity could allow for rapid detection of disease *in vivo*. As previously described, erythrocytes contain many biochemical pathways that are all dependent on response to external stimuli. Erythrocytes have been defined as oxygen sensors, which are capable of responding to various oxygen concentrations and altering blood flow to match metabolic needs.^[54] Erythrocytes entering a region with high oxygen demand release ATP and subsequently induce localized vasodilation.^[55] Similarly, nitric oxide (NO) may impact the activity of a G-protein coupled receptor (GPCR) G_i , a transmembrane receptor within the erythrocyte membrane, through stimulation of endogenous mono-ADP-ribosyltransferase to inhibit ATP release and subsequent calcium uptake and release of epoxyeicosatrienoic acids (EETs) for

vasodilation.^[56, 57] On the infectious disease side, malaria has been shown to invade erythrocytes and destroy endogenous proteins and utilize its own proteins to replicate, thereby perturbing the response of erythrocyte proteins to extracellular stimuli.^[58, 59] Therefore, developing an assay to monitor erythrocyte enzymatic responses to external stimuli could provide diagnostics for cardiovascular disease and erythrocyte parasitic infection.

Optical window of tissue

Hemoglobin, melanin, and water are the primary components in biological tissue substrates that impact the therapeutic and diagnostic capabilities of light. Penetration of tissues by short wavelength light is hindered by hemoglobin and melanin, thus blocking either the fluorophore dependent response (as needed by a diagnostic) or providing enough energy to activate a light responsive therapeutic.^[60] Longer wavelength light (>950 nm) is unable to penetrate tissue due primarily to water absorbance. However, between the hemoglobin/melanin absorbance and water absorbance there is an absorbance minimum known as the optical window of tissue, which resides between 600 and 950 nm (**Figure 1.6**).^[61] Therefore, light used to probe tissue should be longer than 600 nm. As proof-of-concept when a green light (~550 nm) or red light (~700 nm) from a laser pointer is held to human tissue (the finger), the red light within the optical window is able to be visualized through a finger while this is not the case for green light. The small optical window is one of the primary constraints preventing

the application of many currently developed enzymatic assays as useful diagnostics or drug delivery tools; therefore, our work aims to elucidate potential manipulation of tools for use within the optical window to be used in the development of diagnostic assays and drug delivery systems.

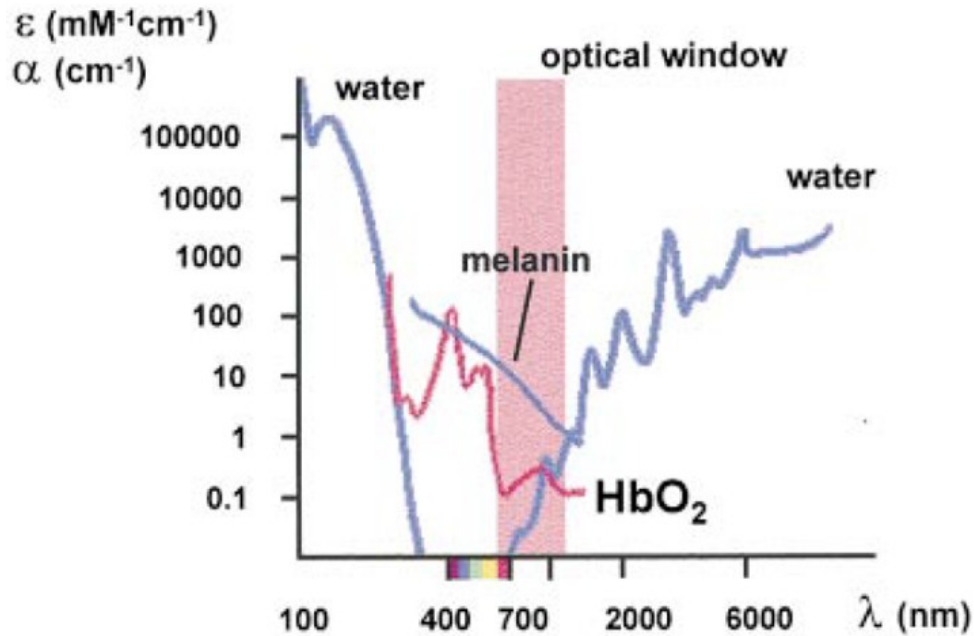


Figure 1.6 Optical window of tissue. The optical window of tissue, shown in pink, occurs at the combined minimum of water, hemoglobin, and melanin. reprinted with permission from the publisher.^[61]

The optical window of tissue is separated into three subgroups: red, far-red, and NIR light. While there is not a specific recognized spectral cutoff for each of these sections, for the purposes of this dissertation; red light is defined as 600 - 710 nm, far-red light as 710 - 850nm, and NIR light as 850 - 1100 nm. *In silico* data demonstrate fluorescent probes for diagnostic purposes require the use of far-red fluorophores to penetrate a majority of tissue types. For example, **Figure 1.7** shows the results of a simulation of tissue penetration of Cy5.5, a red

fluorophore, through various human tissue samples,^[62] such as the lung.

However, light that excites red fluorophores weakly penetrates other tissues, such as the dense tissues of breast and muscle.

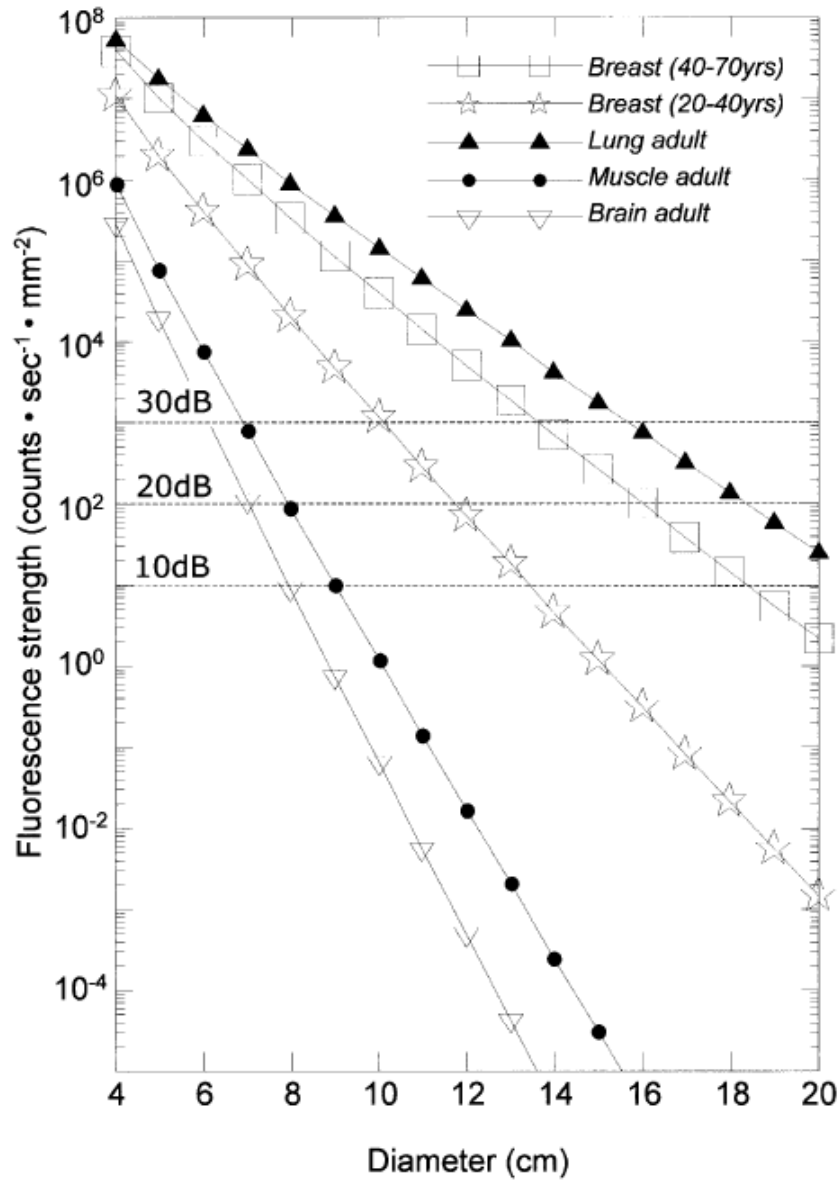


Figure 1.7 Signal loss of Cy5.5 in various tissue samples. Expected signal loss of fluorophore Cy5.5 (Ex: 673 nm Em: 704 nm) in various tissue samples reprinted with permission from the publisher.^[62]

Selection of long wavelength fluorophores

The optical window for penetration of tissue coincides directly with the absorbance minimum of hemoglobin (**Figure 1.6**). As previously described, erythrocytes are the primary carriers of hemoglobin in tissue.^[6] Therefore, we propose erythrocytes and their respective lysates as model systems for the development of diagnostic and therapeutic technologies through proof-of-concept demonstrations. We selected the fluorophores listed in **Table 1.1** for use in an enzymatic assay to monitor intracellular kinase activity (Chapter 3) and for use in the light mediated delivery of anti-inflammatory agents (Chapter 4). Table 1.1 fluorophores were selected since they are within excitation wavelengths of the red and far-red regions, commercially available, and possess large extinction coefficients. Fluorescein, Cy3, and tetramethylrhodamine (TAMRA) are the only exceptions to the above statement, TAMRA and Fluorescein were used as a control to demonstrate the necessity for longer wavelength fluorophores.

Table 1.1 Various fluorophores for visualization within the optical window of tissue.

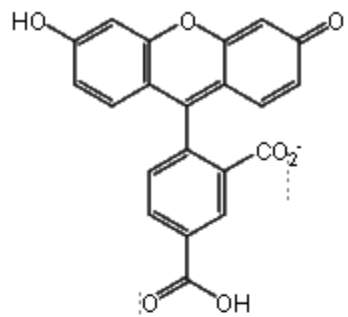
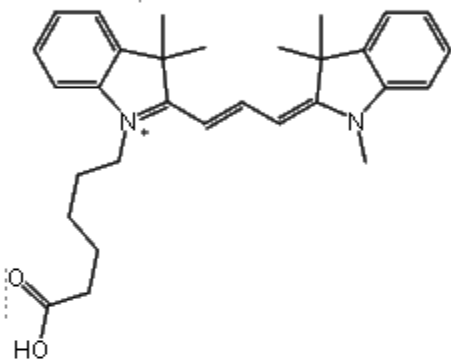
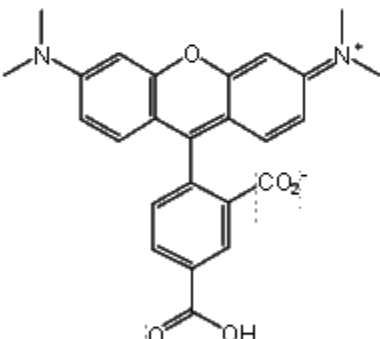
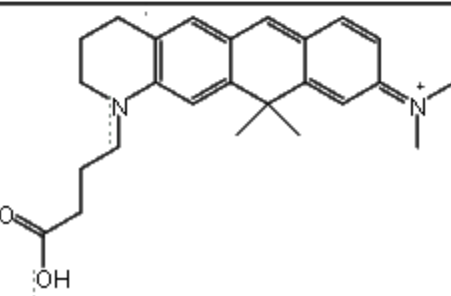
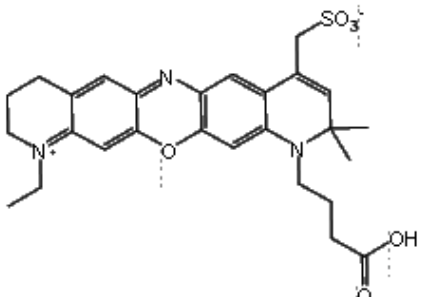
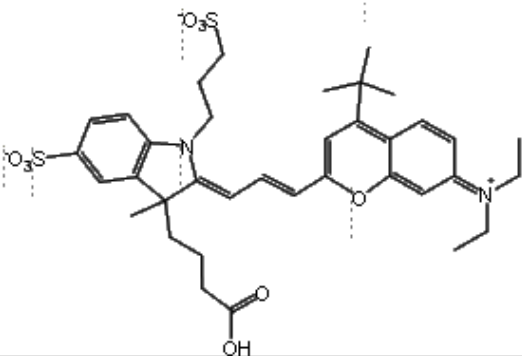
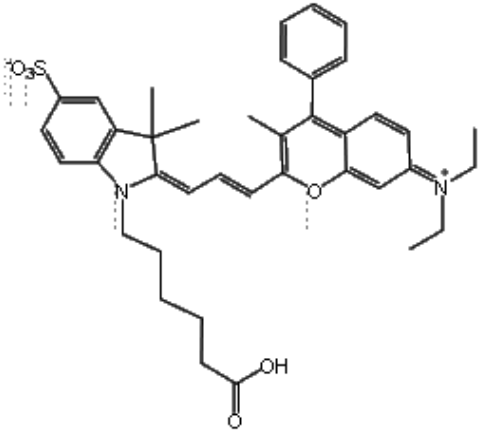
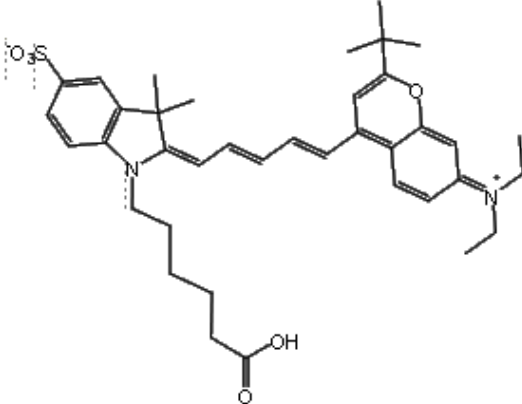
Name	Structure	Excitation wavelength (nm)	Emission wavelength (nm)
5-Fam		494	530
Cy3		544	564
5-Tamra		550	587
Atto610		620	640
Atto620	unknown	620	645

Table 1.1 continued.

Name	Structure	Excitation wavelength (nm)	Emission wavelength (nm)
Atto680		685	705
Red681		685	715
NIR700		691	737
NIR730		727	752

Fluorescence signal in erythrocyte lysates

The concentration of erythrocytes in the blood stream is referred to as the hematocrit. Hematocrit concentrations/levels are determined by centrifuging a sample of blood and calculating the ratio of the red zone (erythrocytes) to all other zones. The average human hematocrit is between 30 - 70%. The higher the hematocrit the more the hemoglobin absorbance will interfere with fluorescent assays. The impact on the fluorescent response is proportional to how much the fluorophore excitation peak overlaps with the hemoglobin excitation peak. We hypothesize that overlaying the absorbance spectrum of erythrocyte lysates between 450 nm and 700 nm (the tailing peak of hemoglobin absorbance) with the absorbance spectrum of five fluorophores (FAM, TAM, Atto620, Atto633, and Atto680) may identify that fluorescein and tetramethylrhodamine should experience more interference due to hemoglobin (**Figure 1.8**); in contrast to Atto633 or Atto680, which we predict will have minimal overlap with the absorbance of hemoglobin and may provide much better signal response in solutions containing erythrocytes. The reduced signal loss experienced by red and far-red fluorophores is supported by the results provided within **Figure 1.9**. Fluorescein and tetramethylrhodamine TAMRA signals are nearly abolished when measuring fluorescence through 10% hematocrit lysates and completely undetectable at 100% hematocrit lysates. However, Atto633 provides significant fluorescence signal even in 100% hematocrit lysates.

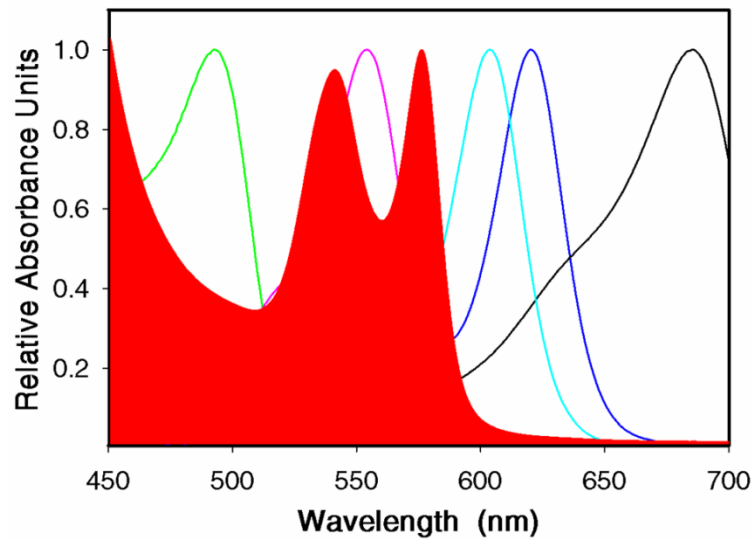


Figure 1.8 Erythrocyte lysate absorbance vs fluorophore absorbance Erythrocyte lysate absorbance (red) compared to FAM, TAMRA, Atto 620, Atto633, and Atto 680 labeled peptide. Reprinted with permission from the publisher.^[63]

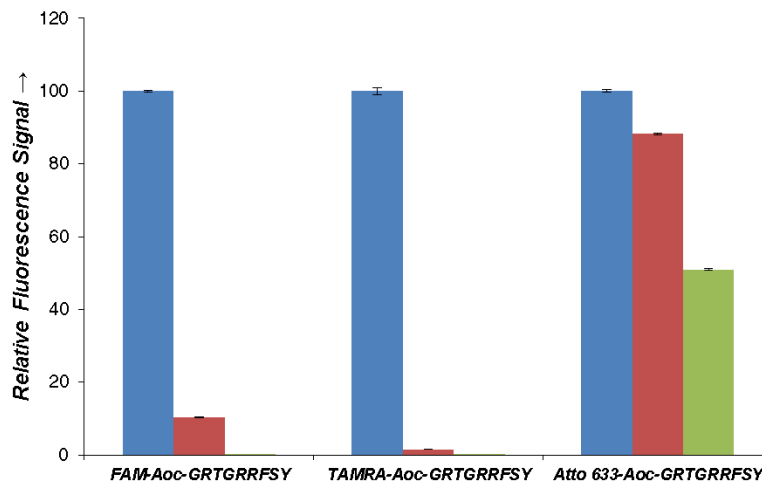


Figure 1.9 Signal loss of fluorophores due to various hematocrits of erythrocyte lysates. Signal loss of FAM, TAM, and Atto633 labeled peptide in 0, 10%, and 100% hematocrit lysed erythrocytes. Reprinted with permission from the publisher.^[63]

Conclusion: research aims

In vivo clinical use of erythrocyte carriers for diagnostic assays or light-dependent delivery of therapeutics requires the development and optimization of model systems that may utilize light capable of penetrating human tissues while also eliciting a spatially and temporally effective release-controlled response to such light, which is currently lacking.^[64] Therefore, our research aims to fill this gap by developing a versatile diagnostic assay to monitor specific protein kinase A (PKA) enzymatic activity in erythrocytes since PKA is vital to the erythrocytes' role in vasodilation and aberrant activity in disease, including sickle cell and malaria. In addition, we hypothesize that using erythrocytes as carriers of anti-inflammatory therapeutics via membrane-bound loading methods may serve as a responsive therapeutic method for enhancement of drug delivery mechanisms.

We aim to describe our work, which tests the following objectives; 1. Develop a method to load exogenous material into erythrocytes and use fluorescence microscopy to visualize loading and enzymatic activity and explore erythrocyte loading of small molecule therapeutics. 2. Develop an assay to monitor endogenous erythrocyte PKA activity. 3. Utilize erythrocytes as carriers of membrane-bound anchored therapeutics.

Summary:

The next three chapters are dedicated toward the accomplishment of each objective. Specifically, Chapter 2 highlights my efforts in the development of an optimized erythrocyte loading method to load exogenous substrates and protect a protease substrate through membrane sequestration. In addition, within the subsequent chapters, I will highlight the main purpose of this dissertation which is to determine 1) whether PKA activity can be monitored in erythrocytes using red shifted fluorophores (Chapter 3); and 2) whether erythrocytes can be manipulated to serve as carriers of therapeutic agents (Chapter 4). Lastly, in the final chapter I end with a discussion of future directions and provide final remarks regarding my work.

Chapter 2 Method Development and Optimization for Loading Fluorescent Molecules into Erythrocytes

Overview

As previously described within Chapter 1, exposing erythrocytes to either electric field pulses or a hypotonic solution induces swelling and cellular membrane pore formation to aid effective exogenous substrate loading and thus form a “carrier erythrocyte”. We investigated electroporation, hypotonic dilution and dialysis loading methods and found that hypotonic dilution offered fast, efficient, and consistent loading. Previous work utilizing the hypotonic dilution loading strategy has established successful loading of erythrocytes to carry a vast array of exogenous materials, such as proteins, small molecules, and therapeutic drugs;^[3] therefore, our work focused on the development and optimization of the hypotonic dilution delivery strategy to load exogenous material that can be visualized *in vitro* by fluorescent microscopy. In addition, we aimed to establish a technique to monitor and visualize enzymatic activity as a means to develop a potential diagnostic assay. Specifically, we demonstrated erythrocytes can be loaded with a photolabile fluorescently quenched small molecule that becomes fluorescent upon stimulation with UV light, showing increases in fluorescence that can be detected and monitored over time using fluorescent

microscopy. We also demonstrated that the biological activity of loaded erythrocytes remains intact via enzymatic activity monitoring through a UV light-activatable fluorescent protease reporter model system.

In summary, our work is significant since we developed a novel, versatile system for efficient erythrocyte loading of exogenous material for *in vitro* monitoring of enzymatic activity, which may serve as a foundation for a potential method for erythrocyte loading of small molecule therapeutic and diagnostic agents.

Introduction

Erythrocytes have a unique metabolism different from all other cells due to their enucleated structure, thus allowing production of ATP exclusively through glycolysis with no mitochondria or gene expression involvement.^[65] As such, erythrocytes are unable to undergo traditional apoptosis; instead erythrocytes rely on a series of pre-defined mechanisms utilizing macrophages for biological clearance in a process known as *eryptosis*. When erythrocytes are exposed to oxidative stress and/or injury, a cascade of signaling events elicits exposure of membrane phosphatidylserine on the extracellular surface subsequently signaling for the recruitment of macrophages for the engulfment of damaged/aged erythrocytes.^[66] Alternatively, erythrocytes may be cleared via IgG binding to band 3 leading to phagocytosis by macrophages within the liver.^[67] In response to extracellular conditions that would normally induce lysis (osmotic shock,

exposure to high concentrations of DMSO, or high voltages) erythrocytes do not lyse. Instead, erythrocytes undergo physiological changes such as swelling and pore formation, which may be utilized to efficiently load exogenous material. Therefore, we utilized these methods for the development and optimization of a versatile method that can be utilized to reliably load exogenous material into erythrocytes. We compared the loading methods using various sized fluorescent molecules and evaluated the loaded erythrocytes using fluorescence microscopy.

Next, we sought to determine whether stimulating the light-sensitive dimethoxynitrobenzyl group with UV light may be accomplished within erythrocytes. We sought to address the question using a UV light responsive small molecule pro-fluorescent cassette.^[68] Using this cassette we compared photolysis in the presence and absence of hemoglobin and determined photolysis conditions necessary for cleaving the nitrobenzyl group. We later used the established photolysis conditions to demonstrate that the nitrobenzyl groups can be used to prevent enzymes from modifying our substrate until light stimulation.

Materials and Methods

Materials: All amino acids, NovaSyn TGR resin, 5-chloro-1-[bis(dimethylamino)methylene]-1H-benzotriazolium 3-oxide hexafluorophosphate (HCTU), 6-chloro-1-hydroxybenzotriazolen (6-Cl-HOBt) were obtained from NovaBiochem or Peptide International. 4 (1-(9

Fluorenylmethyloxycarbonylamino)ethyl]-2-methoxy-5-nitrophenoxy}butanoic acid (Fmoc-photolabile linker) and 3-N α -Fmoc-Amino-3-(2-nitrophenyl) propionic acid (Fmoc-photolabile linker) were from Advanced ChemTech. N,N-dimethylformamide (DMF), methylene chloride (CH₂Cl₂), magnesium chloride, 10 X PBS buffer (137 mM NaCl, 2.7 mM KCl, 10 mM sodium phosphate dibasic, 2 mM potassium phosphate monobasic and a pH of 7.4), and other general solvents were obtained from Fisher Scientific. N,N-diisopropylethylamine (DIEPA), 4-dimethylaminophenylazophenyl-4'-maleimide (Dabcyl maleimide) , and dithiothreitol (DTT) were purchased from Sigma. Fluorescein-5-isothiocynate (5-FITC), were purchased from Invitrogen. 5-Carboxytetramethylrhodamine (5-TAMRA, 4) was purchased from ChemPep. Peripheral erythrocytes were purchased from AllCells. Dialysis cassettes were purchased from VWR.

Erythrocyte loading (hypotonic dilution): Fresh peripheral erythrocytes were washed 3x in 1x PBS containing 1 mM MgCl₂ (centrifuging at 1,000 g for 3 mins). After the final wash erythrocytes were re-suspended in 1x PBS containing 1 mM MgCl₂ to 10% hematocrit. 50 μ L of washed erythrocytes was added to 450 μ L water containing substrates to be added. Erythrocytes were allowed to incubate on ice for 5 minutes and subsequently resealed by adding 50 μ L 10x PBS containing 10 mM MgCl₂ and incubation at RT for 30 minutes.

Erythrocyte loading (hypotonic dialysis): Fresh peripheral erythrocytes were washed 3x in 1x PBS containing 1 mM MgCl₂. After the final wash

erythrocytes were re-suspended in 1x PBS containing 1 mM MgCl_2 to 10% hematocrit. Re-suspended erythrocytes were mixed with 1x PBS containing material to be loaded and added to a prepared dialysis unit (0.5 to 100 kD cutoff filter). The dialysis unit was then added to water and allowed dialyze for 4 hours at 4 °C. The dialysis unit was then added to 1x PBS containing 1 mM MgCl_2 and allowed to reseal at RT for at least 1 hour.

Erythrocyte loading (electroporation): Fresh peripheral erythrocytes were washed 3x in 1x PBS containing 1 mM MgCl_2 . After the final wash erythrocytes were Re-suspended in 1x PBS containing 1 mM MgCl_2 to 10% hematocrit. Re-suspended erythrocytes were mixed with 1x PBS containing material to be loaded and added to the electrode unit. Erythrocytes were then exposed to a brief 2.0 kV/cm² pulse. The erythrocytes were then allowed to incubate (recover) at RT for 2 hours.

Preparation of hemoglobin free ghosts (hypotonic dilution): Fresh peripheral erythrocytes were washed 3x in 1x PBS containing 1 mM MgCl_2 . After the final wash erythrocytes were re-suspended in 1x PBS containing 1 mM MgCl_2 to 10% hematocrit. Erythrocytes were then exposed to 10x volumes of deionized water and spun down at 16,000 g for 10 minutes. The supernatant was removed and the pellet was re-suspended in deionized water. The process was repeated until the pellet was white (generally 4 to 5 times). After the pellet turns white, the

supernatant was removed and the erythrocytes were re-suspended to 10% cell suspension in 1x PBS containing 1 mM MgCl₂.

Synthesis of fluorophore labeled PKA E. Coli containing PKA expression vector (described by Herberg *et al.*) was suspended in LB Broth and grown to OD of 0.6.^[69] IPTG was used to induce expression. After expression and pelleting the cells were re-suspended in lysis buffer (30 mM MES, 1 mM EDTA, 50 mM NaCl pH 6.5) followed by incubation at 40 °C for 1 hour and subsequent lysis by sonication. The lysed cells were then centrifuged at 15,000 RPM for 45 minutes at 4 °C. Purification was using a PII cellulose resin. Lysates were incubated in prepared PII cellulose resin overnight at 4 °C. The solution was then filtered. Then PKA was eluted off using running buffer (30 mM MES, 1 mM EDTA, 5 mM DTT) and increasing concentration of KH₂PO₄ (from 100 mM to 500 mM). The fractions were collected and analyzed by SDS-page for protein content at the expected molecular weight. Fractions containing expected band were pooled together. Atto-633 maleimide was used to label PKA. 5 mgs of Purified PKA was diluted in PBS buffer containing 1.3 equivalents of Atto-633 maleimide was added to the solution and incubated overnight at 4 °C. Purification was performed by dialyzing (using a 10 Kd cutoff filter) against PBS overnight at 4 °C.

Synthesis of photolabile cassette (synthesis completed by and reprinted from Hsien-Ming *et al.*^[68]). Fmoc-photolabile linker was used to make

the peptide backbone configurations on the TGR resin (0.2 mmol/g, 500 mg resin, 0.1 mmol scale). A standard peptide coupling protocol was used for the amino acid couplings including the Fmoc-photolabile linkers (Fmoc-DMNB). Amino acid (3 equiv/equiv resin), HCTU/6-Cl-HOBt (3 equiv/equiv resin) and DIEPA (8 equiv/equiv resin) were mixed with resin in DMF and reacted for 2 h at RT. Fmoc deprotection was achieved using 20% piperidine in DMF for 20 min at RT. The N-terminus was capped using acetic anhydride with 20% DIEPA for 20 min. Following N-terminus acetylation, the Lys side-chain (ivDde) protecting group was deprotected using 2% hydrazine monohydrate in DMF (25 mL/g resin of hydrazine solution, 3 X 3 min). The backbone peptidyl resins was split in half (50 μ mol scale) for the fluorophore labeling reactions. For the 5-TAMRA labeling, 5-TAMRA (3 equiv, 150 μ mol) was preactivated using HCTU (3 equiv, 150 μ mol) with DIEPA (8 equiv) in DMF for 1 min and reacted with the Lys deprotected peptidyl resins for 2 h. After the fluorophore labeling, the eight peptidyl resins were dried and subsequently cleaved in a solution of 95% TFA, 2.5% H₂O and 2.5% triisopropylsilane. The fluorophore-labeled peptides were HPLC (semipreparative C-18 column) purified using a linear gradient binary solvent system (solvent A: 0.1% TFA/H₂O; solvent B: 0.1% TFA/CH₃CN) with a ratio of A:B that varied from 80:20 (0 min) to 30:70 (30 min). The major fraction for each peptide was collected and freeze-dried. The eight individual peptides were dissolved in DMF (10 mM stock solution) and further aliquoted into 4 vials (400 μ L, 4 μ mol each vial, total 32 vials) for the quencher labeling reaction. The thiol-reactive quencher (QSY-35 maleimide), (2 equiv, 8 μ mol) was added to the vials

and the peptide/quencher mixtures further diluted to 1 mL with 50% DMF/ 50% PBS at pH 7.5, and reacted for 2 h to generate the final product. The final product was purified by HPLC (semipreparative C-18 column) using a linear gradient binary solvent system (solvent A: 0.1% TFA/H₂O; solvent B: 0.1% TFA/CH₃CN) with a ratio of A:B that varied from 80:20 (0 min) to 30:70 (30 min). The major fraction from each reaction was collected and characterized by ESIMS. The subsequently prepared DMF stock solutions employed the HPLC purified peptide. Peptide concentration was obtained by using (1) the extinction coefficient of the λ_{max} of quencher or (2) the extinction coefficient summation of quenchers + fluorophores at the λ_{max} of quenchers if there is an overlap between the fluorophore and quencher absorbance spectra: For TAMRA cassette, the concentration QSY 35 containing cassette was determined using only λ_{max} QSY35 (24000 cm⁻¹M⁻¹ @ 476 nm).

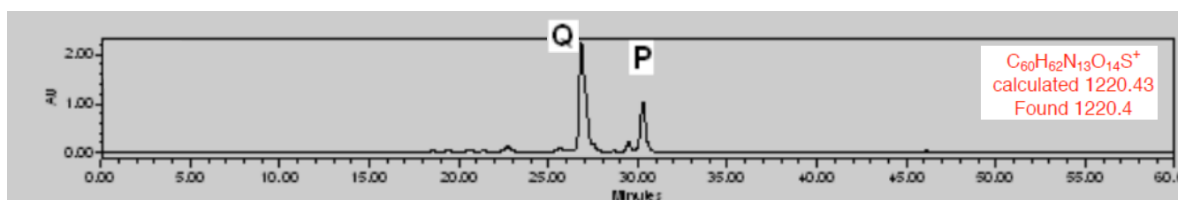


Figure 2.1 HPLC of the photolabile cassette. Photolabile cassette was purified using the following gradient: 80% solvent A/20% solvent B (0 min) to 30% solvent A/70% solvent B (30 min) to 10% solvent A/90% solvent B (40 min). The peptide cassette (P) and excess quencher (Q) are labeled in the chromatograms (characterized and confirmed by mass spectrometry). Reprinted with permission from the publisher^[68]. Copyright 2010 American Chemical Society.

Synthesis of C18-protease substrate (synthesis of protease substrate was obtained from and described by Nguyen *et al.*^[70])

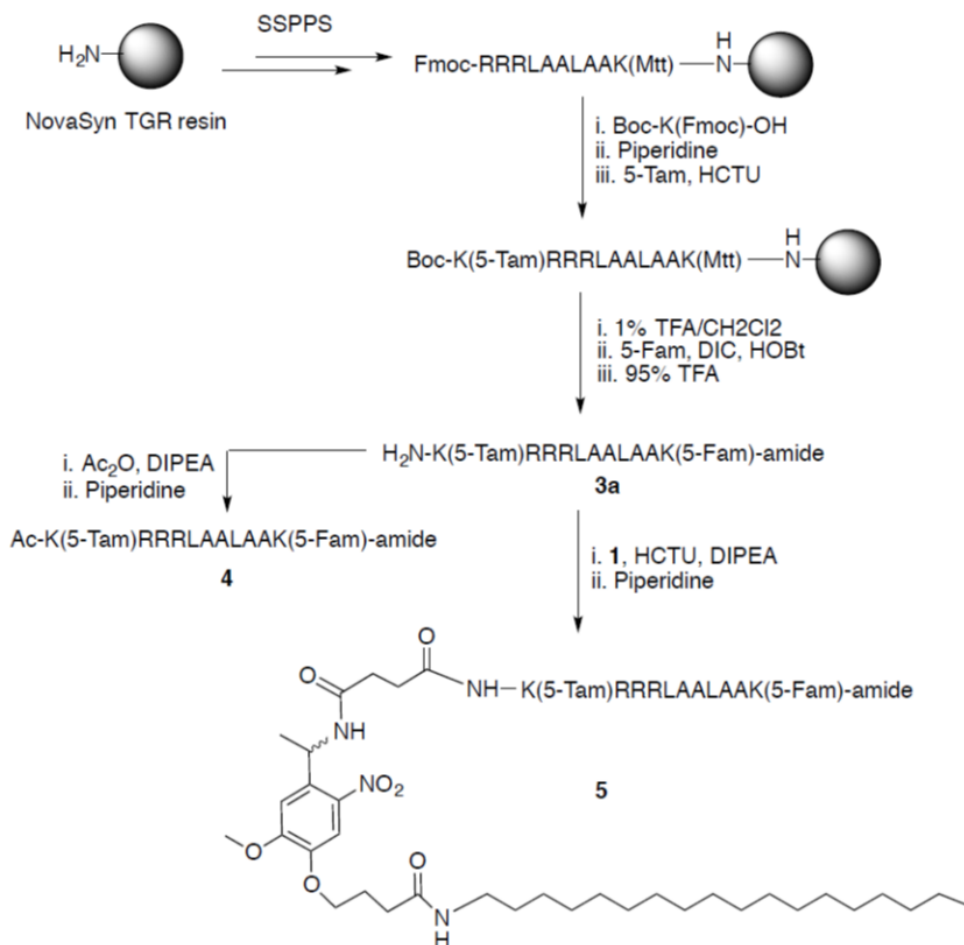


Figure 2.2 Synthesis of lipidated protease sensor. Reprinted with permission from publisher^[70]

Standard solid phase peptide synthesis (SSPPS) was performed on a Prelude peptide synthesizer from Protein Technology using Fmoc-protected amino acids (amino acids 3 eq., HCTU 2.95 eq., DIPEA 10 eq. in DMF, double coupling in 20 and 40 min). Fmoc deprotection was performed using piperidine (25%) in DMF (3 times, 10 min each). The peptide containing a Lys side chain

protected with the acid sensitive 4 methyltrityl group (Mtt), Boc-K(Fmoc)RRRLAALAAK(Mtt), was synthesized on a NovaSyn TGR resin using SSPPS. The Fmoc protecting group on the lysine residue was deprotected by piperidine (25%) in DMF followed by coupling of 5-Tam fluorophore using 5-Tam (1.5 eq.), HCTU (1.5 eq.), and DIPEA (10 eq.) in DMF for 4 h. The Mtt was removed with 1% trifluoroacetic acid (TFA) in CH₂Cl₂ followed by coupling 5-Fam using 5-Fam (1.5 eq.), N,N'-diisopropylcarbodiimide (DIC, 1.7 eq.), and 1-hydroxybenzotriazole (HOBt, 10 eq.) in DMF for 2 h. The peptide was then cleaved from the resin with TFA:H₂O:Triisopropylsilane in a ratio of 95:2.5:2.5, and purified by HPLC using H₂O:CH₃CN with 0.1% TFA to afford 3a. Solution of pure 3a was acidified with HCl and dried. C₁₀₀H₁₃₅N₂₄O₂₂⁺. Exact mass calculated 2024.02, found (ESI+) 675.3 (M + 2 H)³⁺, 506.6 (M + 3 H)⁴⁺, 405.6 (M + 4 H)⁵⁺.

Synthesis of 4. Dried 3a (0.55 μmol) was redissolved in DMF (500 μL). DIPEA (5.5 μmol) and Ac₂O (5.5 μmol) were added to the DMF solution containing 3a. The reaction mixture was shaken at room temperature for 1 h. H₂O (500 μL) was then added and the mixture shaken for 30 min. Piperidine (27.5 μmol) was then added and the mixture shaken for 30 min. Solvent and excess reagents were removed under vacuum and the crude product purified by HPLC using the C18 column to afford pure 4 (**Figure 2.2**). C₁₀₂H₁₃₇N₂₄O₂₃⁺. Exact mass calculated 2066.03, found (ESI+) 1033.6 (M + H)²⁺, 689.2 (M + 2 H)³⁺, 517.2 (M + 3 H)⁴⁺, 414.0 (M + 4 H)⁵⁺.

Synthesis of 5. 1 (21.5 mg, 33 μmol), HCTU (12.4 mg, 30 μmol), and DIPEA (10.9 μL, 66 μmol) were dissolved in minimum amount of DMF (with a small amount of CH₂Cl₂ to help dissolve the compound) and the solution

was stirred for 2 min. The HCTU activated peptide was then added to DMF (20 mL) containing 3a (22 μ mol) and DIPEA (220 μ mol). The reaction mixture was shaken at room temperature for 20 min. H₂O (0.5 mL) was then added to the reaction mixture, which was then shaken for 30 min followed by addition of piperidine (110 μ L, 1.1 mmol) and 30 min stirring. Solvent and excess reagents were then removed under high vacuum and crude product purified by HPLC on the C4 column to afford pure 5 (**Figure 2.2**). C₁₃₅H₁₉₂N₂₇O₂₉⁺. Exact mass calculated 2655.44, found (ESI+) 1328.3 (M + H)²⁺, 885.9 (M + 2 H)³⁺, 664.6 (M + 3 H)⁴⁺, 531.9 (M + 4 H)⁵⁺.

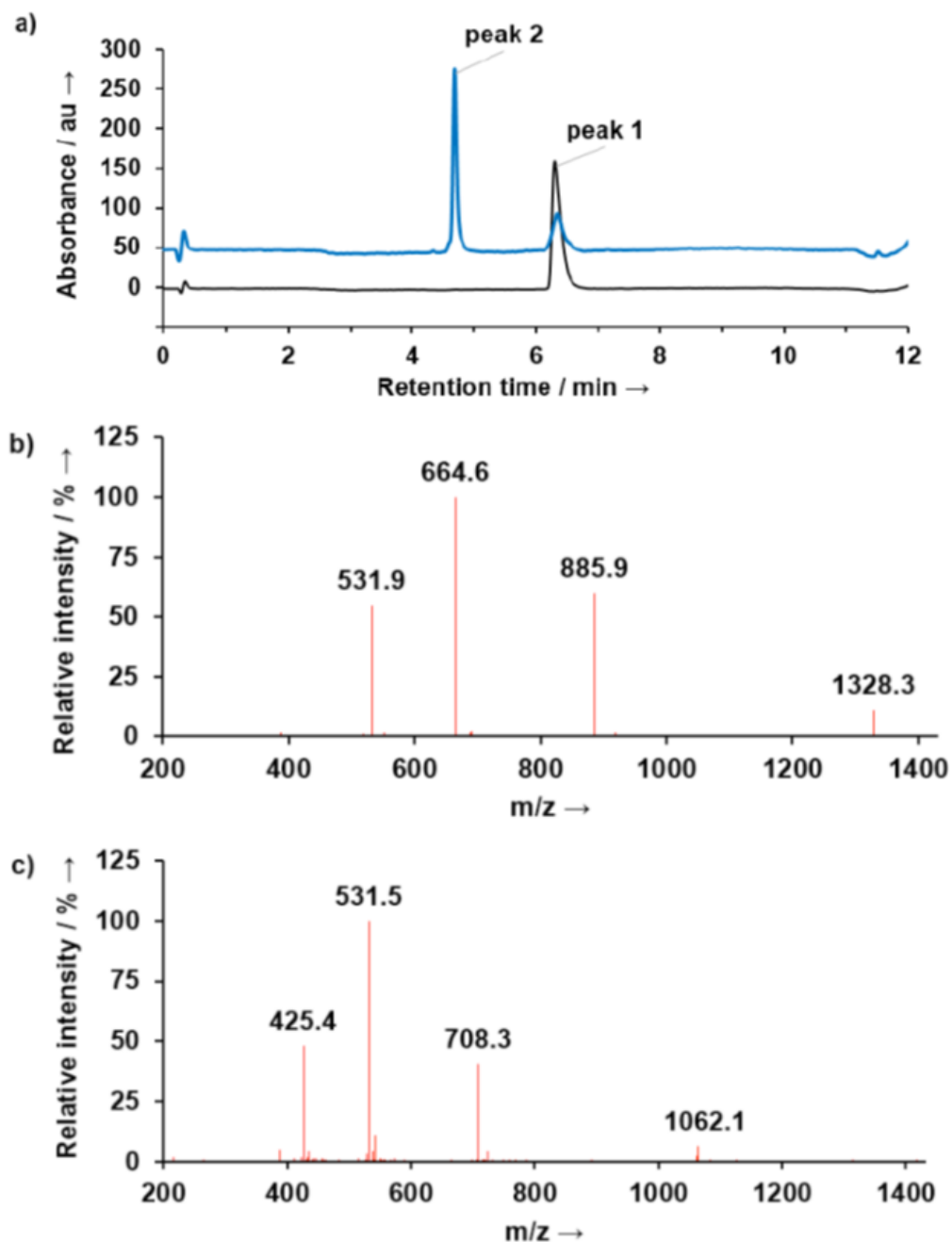


Figure 2.3 LC/MS analysis of proteasome substrate from figure 2.2. (a) LC-MS of the protease substrate before (black) and after photolysis (blue). ESI+ MS of the primary peaks in **a)** PBS 1X (100 μ L) containing 5 (4 μ M), DTT (5 mM) was photolyzed at 360 nm for 2 min. Sample was run on the C4 column. Absorbance was monitored at 550 nm. Photolyzed product of 5 (compound 6, peak 2): $C_{104}H_{140}N_{25}O_{24}^+$, calculated $M+ 2123.0$, found ESI+ 1062.1 ($M + H$) $^{2+}$, 708.3 ($M + 2 H$) $^{3+}$, 531.5 ($M + 3 H$) $^{4+}$, 425.4 ($M + 4 H$) $^{5+}$. Reprinted with permission from publisher.^[70]

Fluorescence assays. Fluorescence assays were monitored using a PTI Technologies QuantMaster-40 equipped with cooled PMT housing. The data was collected using FelixGX Software.

Bench photolysis. Photolysis experiments on the caged cassette or the protease substrate were performed using in PBS [sodium phosphate (8.06 mM), potassium phosphate (1.94 mM), KCl (2.7 mM) and NaCl (137 mM); pH 7.4] or in PBS containing 10% erythrocyte lysate, DTT (20 mM), and Halt protease and phosphatase inhibitors (1x). Photolysis was performed using a Zeiss Colibri 1 LED light source (365 nm light at 100% power) for 5 min or using an Oriel Hg arc lamp (426 mW/cm²) for 2 min. PBS containing 1 mM MgCl₂. Following photolysis, activity was monitored using fluorescence.

Confocal microscopy. All confocal microscopy experiments were performed at room temperature on an Olympus FV1000 scanning confocal with an IX81 microscope base. Laser and region of photolysis were controlled via Fluoview software. Photolysis was performed using the stimulation mode with images collected before and after stimulation. A photolytic dwell time of 20 μs/pixel in tornado mode was employed for the defined region of interest using 25 frames at 405 nm and 2% power level. All imaging was performed with a 100X at 1.9X digital zoom objective using 635 nm at 2% laser power and a dwell time of 12 μs/pixel. The Atto-633 peptide, in the absence of dye quencher, was used to generate a photobleaching curve. ImageJ software was employed for

image analyses. Final fluorescence intensity changes of Atto-633 were corrected for photobleaching effect by equation 2.

$$F_t (\text{corrected}) = F_t \times f_0/f_t \quad (\text{Eq. 2.1})$$

Where F_t are fluorescence values measured at time t , f_0 and f_t are fluorescence values of bleaching curve at $t = 0$ and at t .

Widefield microscopy. All widefield fluorescent microscopy imaging experiments were performed using an inverted Olympus IX81 microscope equipped with a Hamamatsu C8484 camera, a 60X oil immersion Plan S-Apo objective with 1.6x zoom, and a Texas Red filter cube (Semrock). Imaging was collected using Metamorph and processing was performed using Image J software.

Results

Development of an efficient erythrocyte loading procedure. In order to exploit the ability of erythrocytes to form pores and load exogenous material, we compared the loading of three commonly used mechanisms. We evaluated the loading methods based on uniformity and % loading. Erythrocytes were loaded using hypotonic dialysis, hypotonic dilution, or electroporation with 5 μM TAMRA (λ_{ex} : 550 nm λ_{em} : 580 nm). Our experiments determined (depicted in **Figure 2.4**,

Figure 2.5, and **Figure 2.6**) that TAMRA was loaded into nearly all of the cells with high efficiency. However, hypotonic dilution provided the best uniformity (fluorescence appears even in all cells) of loading.

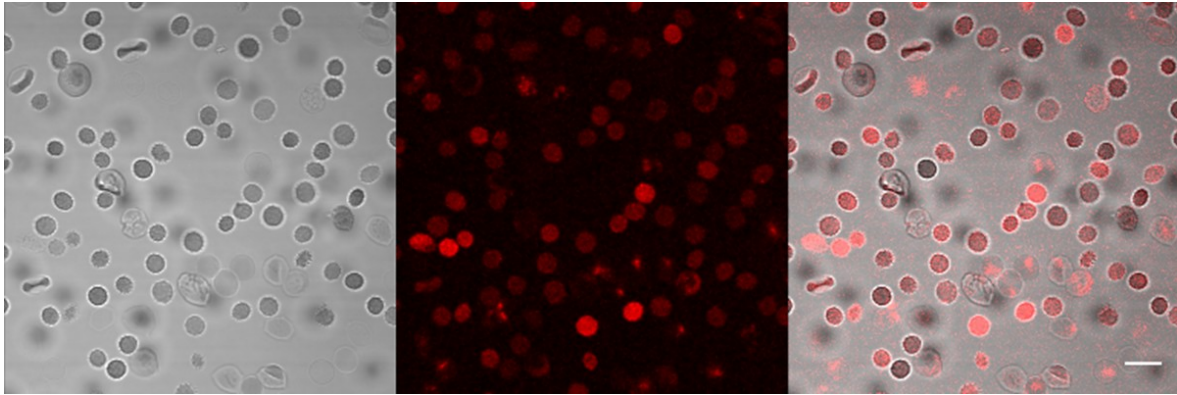


Figure 2.4 Loading erythrocytes via hypotonic dialysis. Nearly all erythrocytes were loaded with TAMRA, however the loading appears highly uneven. White bar represents 10 μ M. Phase contrast (left) Fluorescence (middle) overlay (right)

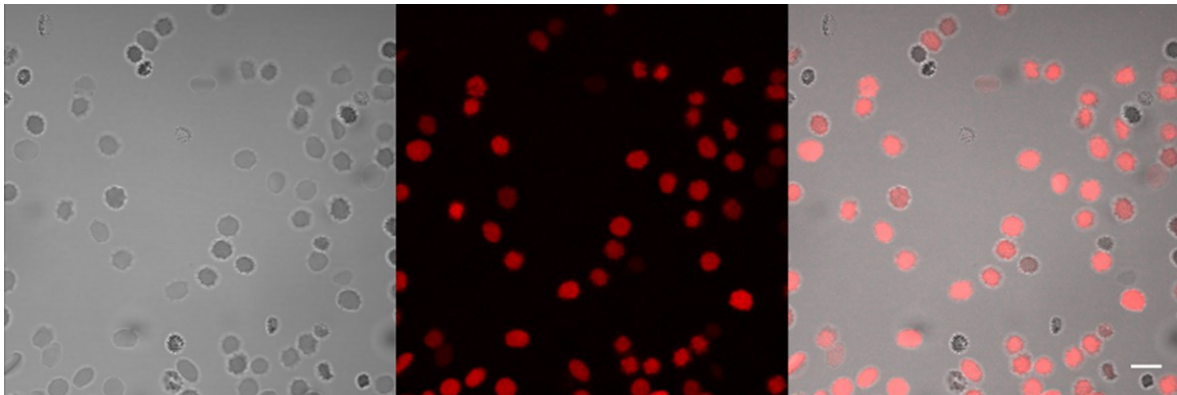


Figure 2.5 Loading erythrocytes via hypotonic dilution. The loading appears highly uniform. White bar represents 10 μ M Phase contrast (left) Fluorescence (middle) overlay (right)

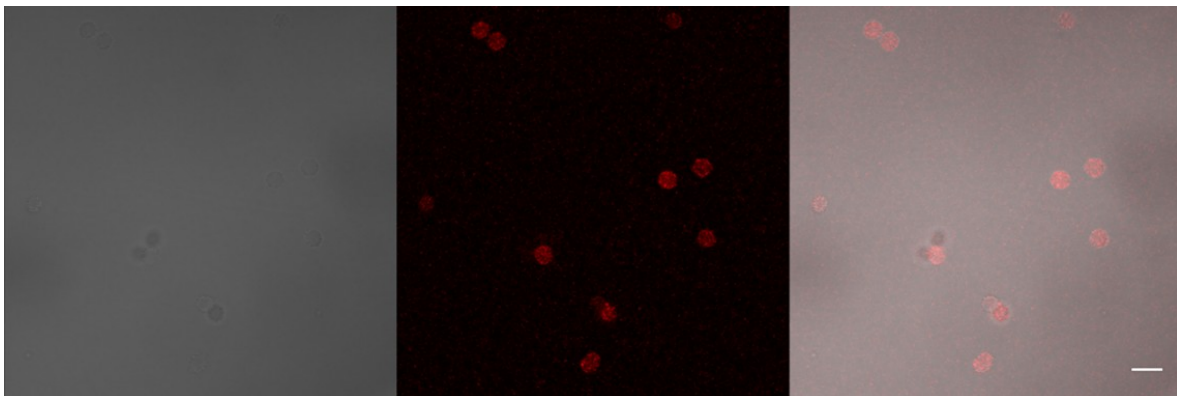


Figure 2.6 Loading erythrocytes via electroporation. While the cells were all loaded, the fluorescence appears punctate. White bar represents 10 μ M Phase contrast (left) Fluorescence (middle) overlay (right)

Loading of erythrocytes with peptides and proteins. We next sought to determine if erythrocytes can be loaded using hypotonic dilution with a fluorescently labeled peptide and a fluorescently labeled protein. **Figure 2.7a** shows a widefield image of an erythrocyte loaded with 1 μM TAMRA labeled PKA substrate. **Figure 2.7b** demonstrates erythrocytes can be loaded using hypotonic dilution with fluorescently labeled PKA. Furthermore, erythrocytes can be co-loaded with TAMRA labeled PKA and a 10,000 MW OG dextran (**Figure 2.8**). The overlay of the red and green channel, shown in **Figure 2.8c**, shows a large number of cells are loaded with both the TAMRA labeled peptide and OG-Dextran (yellow).

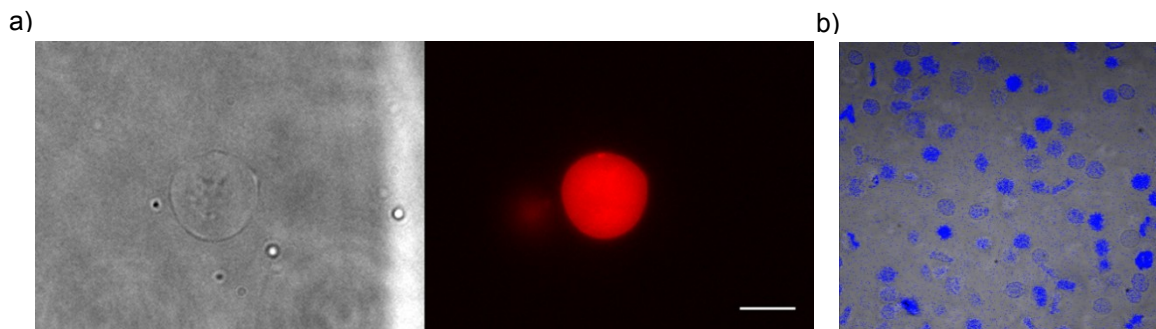


Figure 2.7 Loading erythrocytes using hypotonic dilution with fluorophore labeled peptides and fluorophore labeled PKA. a) Erythrocytes were loaded with TAMRA-GRTGRRFSY and imaged by widefield microscopy left; transmitted image right; fluorescence image b) Overlay of erythrocytes loaded with Atto-633 labeled PKA and imaged by confocal microscopy. White bar represents 5 μM . Image a) reprinted with permission from the publisher^[63].

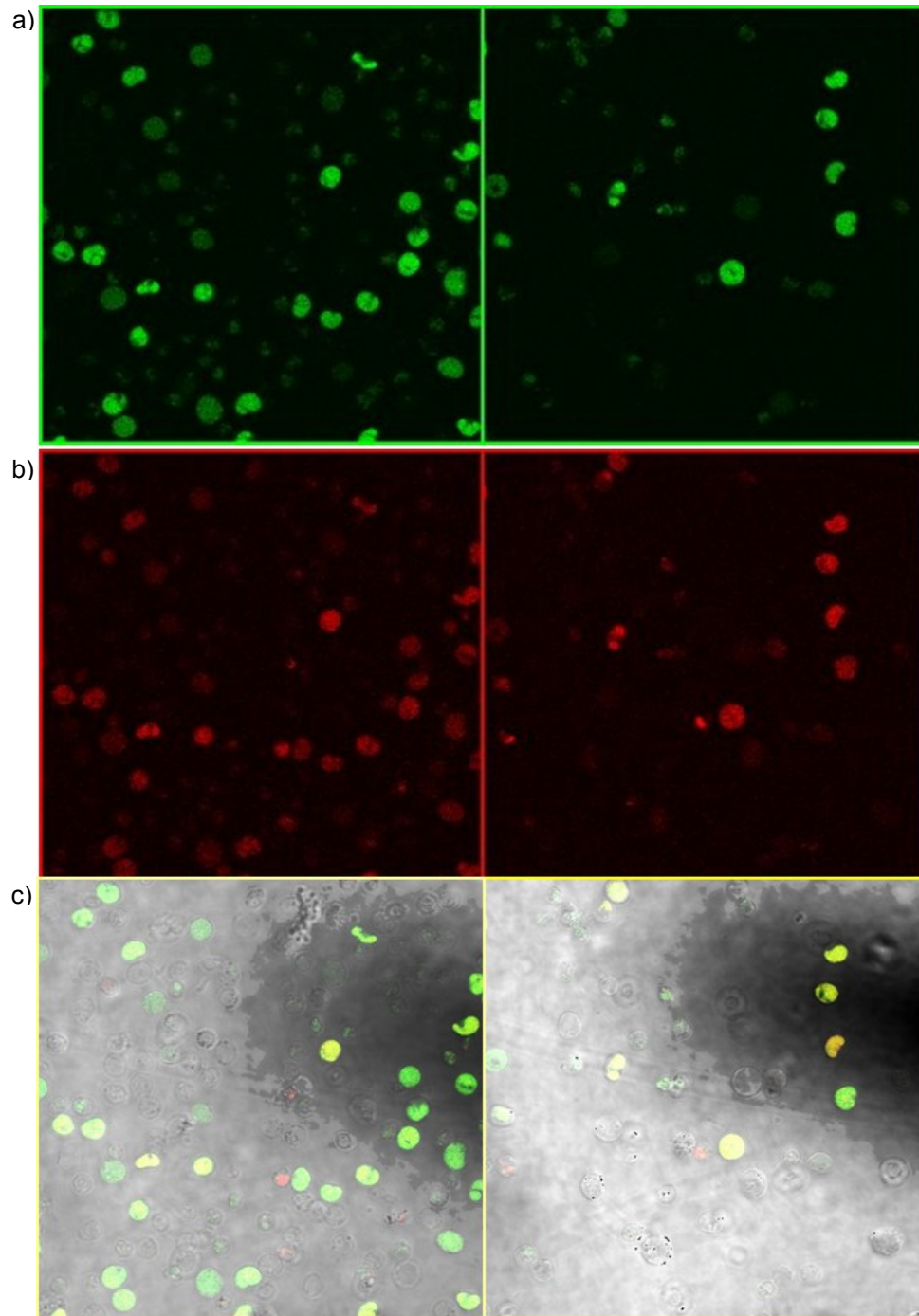


Figure 2.8 Erythrocytes loaded with 10,000 MW OG dextran and TAMRA labeled peptide. a) false color fluorescent confocal image of OG dextran loading into erythrocytes b) false color fluorescent confocal image of TAMRA labeled peptide c) overlay of both channel with transmitted image. Yellow represent erythrocytes that contain both the peptide and dextran.

Photolabile cassette in Fig. 2.9a. Having successfully loaded erythrocytes with exogenous material we sought to determine if UV light could induce photolysis of a nitrobenzyl moiety within intact erythrocytes (both in ghosts which are hemoglobin free and resealed erythrocytes that contain hemoglobin). In order to demonstrate this we utilized a quenched photolabile cassette in Fig. 2.9a that upon photolysis with UV-light furnishes a 45-fold fluorescent enhancement (**Figure 2.9**). Prior to loading the small molecule cassette in Fig. 2.9a into erythrocytes we wanted to demonstrate that photolysis could be carried out under microscopy conditions. To demonstrate photolysis under microscopy conditions we utilized a microwell plate and a 4x objective. Each well was loaded with 5 μ M cassette and photolyzed for 20 s using UV pulses (100 μ W/pulse). We demonstrated (shown in **Figure 2.10**) a 14-fold fluorescence increase in the microwells in the presence of 10 mM DTT (no fluorescence change observed in the absence of DTT). We next loaded erythrocytes with 5 μ M cassette using hypotonic dilution and demonstrated that either a UV or a 405 laser can photolyze the cassette inside erythrocytes (as revealed by a fluorescence increase). Furthermore, as the inner filter effect associated with hemoglobin strongly interferes with nitrobenzyl absorbance, we sought to compare photolysis of the cassette loaded into erythrocytes in the presence (intact) and absence (ghosts) of hemoglobin. Although the cassette photolyzed more rapidly in the absence of hemoglobin, the final fluorescence changes were similar (**Figure 2.11**). Finally, after 20 frames of photolysis (less than 1 s) a 5-fold fluorescence enhancement was observed (**Figure 2.12**).

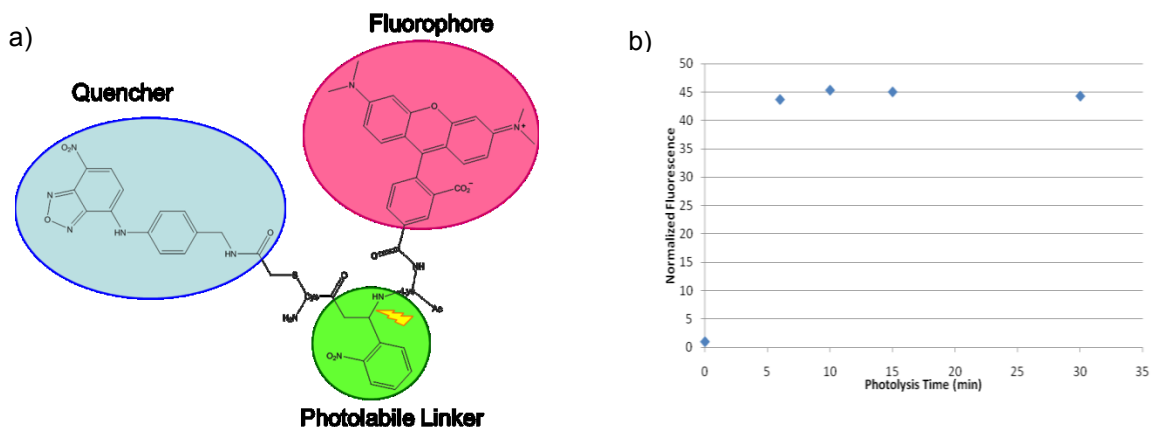


Figure 2.9 Photolabile cassette. a) Molecular structure of photolabile cassette and b) fluorescence increase of photolabile cassette after photolysis using a mercury arc lamp with a 365 band pass filter.

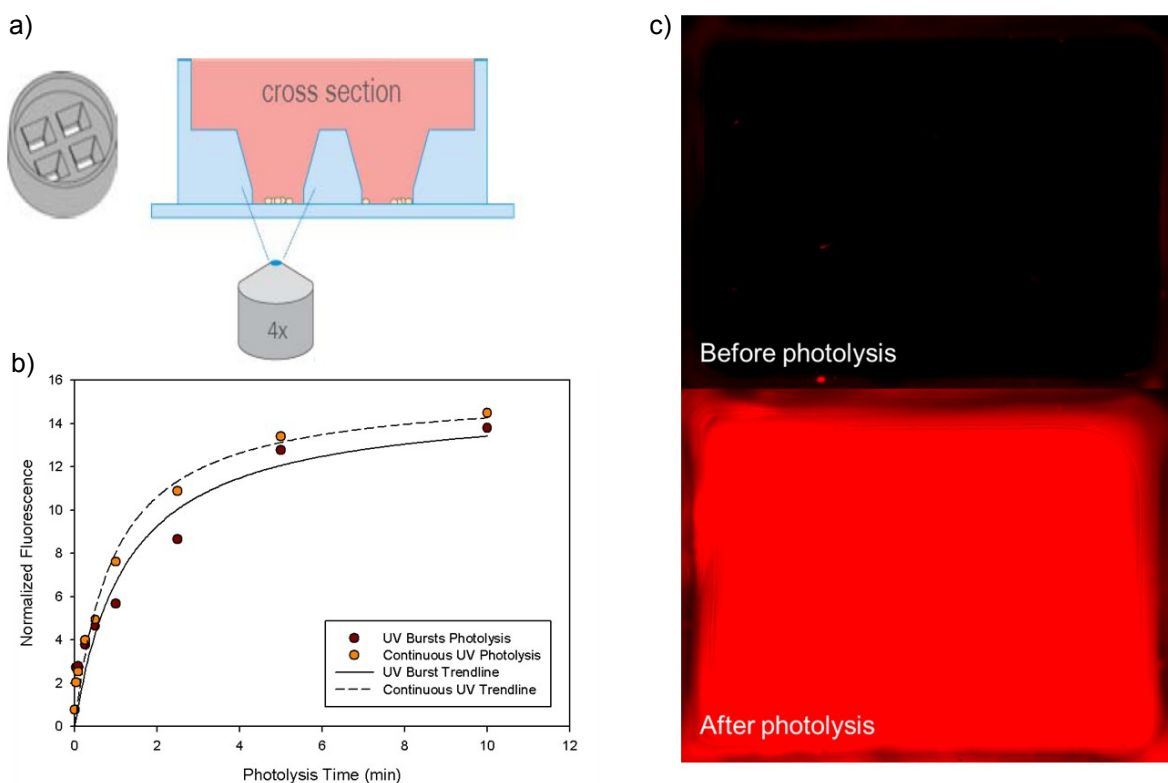


Figure 2.10 Widefield microscopy mediated photolysis of the quenched cassette using a microwell plate. a) Example of a microwell plate, b) fluorescence increase as a function of photolysis time using a UV laser equipped widefield microscope, and c) widefield images of a microwell before and after photolysis.

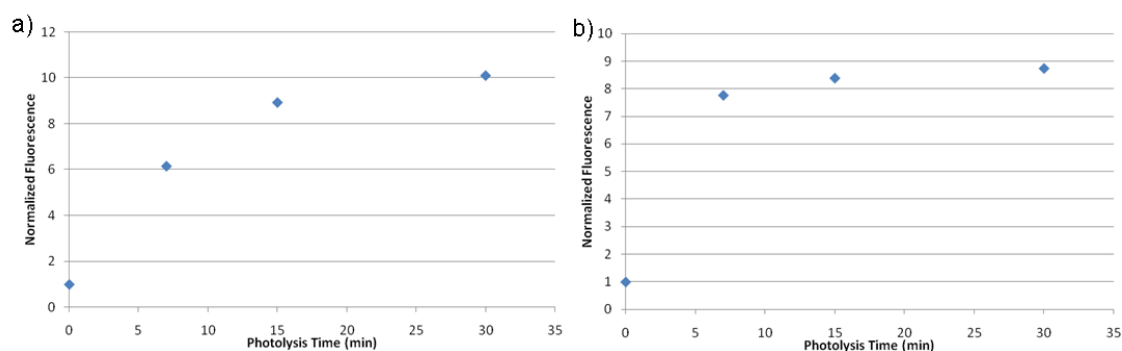


Figure 2.11 Photolysis of erythrocytes loaded with a photolabile cassette. a) Fluorescence increase of erythrocytes loaded with cassette b) fluorescence increase of erythrocytes cleared of hemoglobin and subsequently loaded with cassette. Photolysis was performed using a mercury arc lamp and fluorescence of the erythrocytes was subsequently measured using a plate reader.

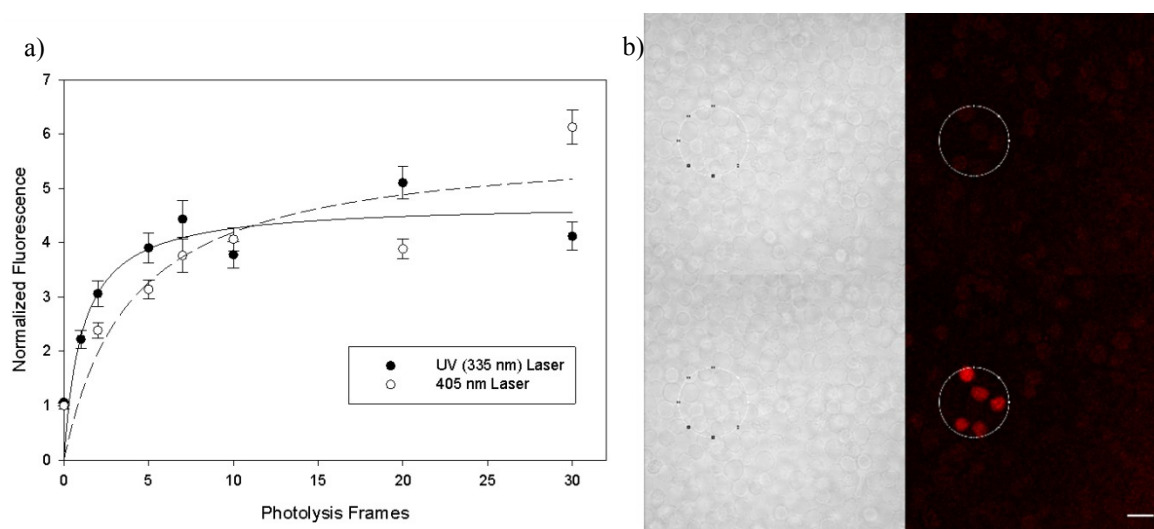


Figure 2.12 Erythrocytes loaded with cassette and imaged using confocal microscopy. After erythrocytes were loaded with the photolabile cassette, the resultant light-dependent fluorescence increase was monitored using confocal microscopy. Photolysis was performed using a UV and a 405 nm laser. a) Quantitation of fluorescence increase after photolysis and b) an example of erythrocyte fluorescence before and after photolysis (white bar indicates 10 μ M)

Demonstration of biological activity in loaded erythrocytes. We next sought to determine if erythrocyte biological activity could be monitored within loaded erythrocytes. We utilized a membrane anchored peptide protease substrate that, upon photolysis with UV light, releases from the membrane and is able to be recognized and cleaved by proteases.^[70] Erythrocytes were loaded

using hypotonic dilution and imaged using confocal microscopy. As depicted in **Figure 2.13**, erythrocytes display large increases in fluorescence after photolysis. Furthermore, in the presence of the protease inhibitor MG-132, or metal chelator EDTA, protease activity is inhibited, providing support that protease activity is responsible for the fluorescence increase (**Figure 2.14**).

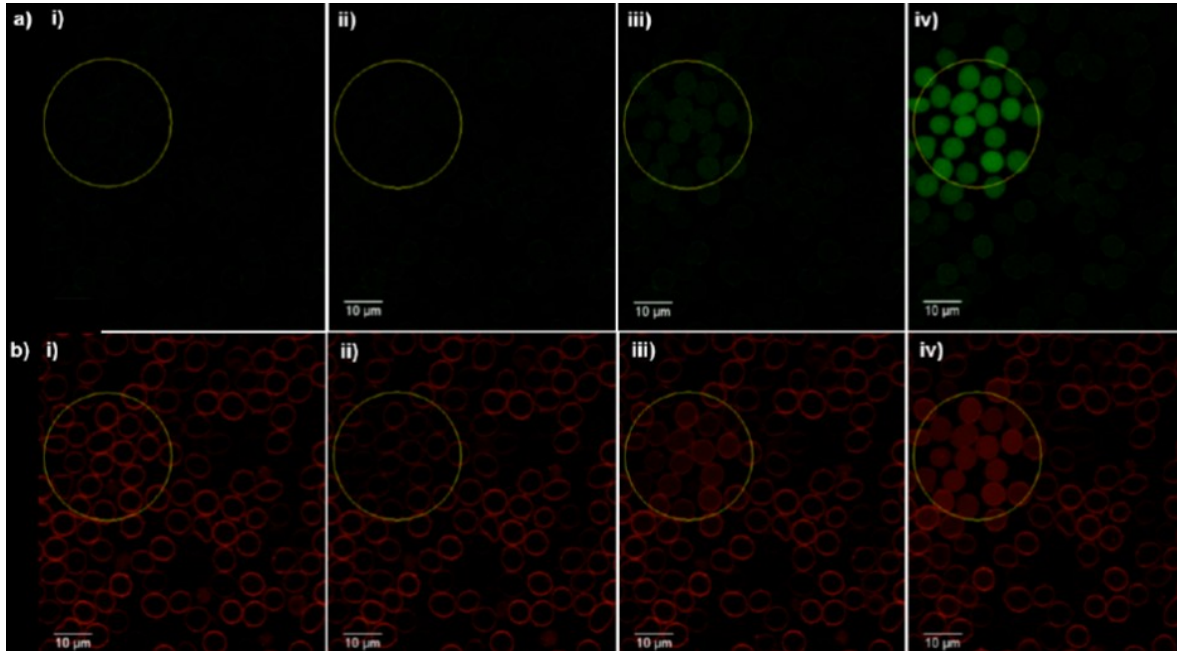


Figure 2.13 Confocal images of erythrocytes loaded with membrane anchored photocleavable protease substrate. a) Monitoring 5-Fam fluorescence (i) before, (ii) immediately after, (iii) 1.5 min after, (iv) and 13 min after photolysis and b) monitoring TAMRA fluorescence (i) before, (ii) immediately after, (iii) 1.5 min after, (iv) and 13 min after photolysis. Reprinted with permission from publisher^[70].

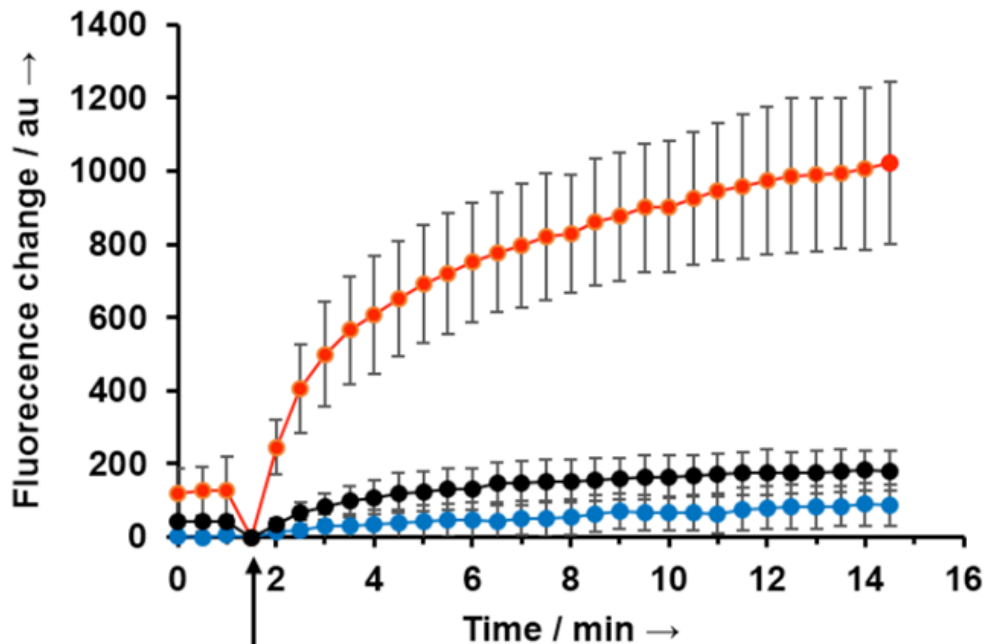


Figure 2.14 Fluorescence fold change of protease substrate loaded into erythrocytes. Fold increase of membrane anchored protease substrate in photolyzed (red), non photolyzed (blue), and photolyzed cells loaded with protease inhibitor cocktail (black). Arrow indicates first frame after photolysis. Reprinted with permission from publisher^[70].

Discussion

Erythrocytes currently represent one of the most interesting methods of drug delivery.^[18] Loading erythrocytes with exogenous small molecules for therapeutic delivery and/or loading erythrocytes with fluorescent reporters that can be used to monitor enzymatic activity represents a simple method to enhance delivery of therapeutic agents or diagnostic tools. More so, entrapping molecules in erythrocytes acts to prevent their interaction with the biological milieu and can protect the molecules from modification and clearance, thus expanding *in vivo* longevity in comparison to free-form (oral) therapeutic agent delivery methods. We explored three primary modes of erythrocyte loading: hypotonic dilution, hypotonic dialysis, and electroporation, for the development

and optimization of an efficient, versatile loading method. Of the three tested, hypotonic dialysis provided the highest ratio of fluorophore loaded to non-loaded cells; however, the uniformity of loading was poor. Electroporation represents an alternative option since every cell was loaded. However, this loading method elicited increased spontaneous erythrocyte membrane lysis and the loaded cargo appeared punctate (**Figure 2.13**). In contrast, hypotonic dilution provided robust substrate loading with comparable loading efficiency (percent of cells loaded) to hypotonic dialysis, as well as limited to no spontaneous erythrocyte lysis. Therefore, the hypotonic dilution loading method was used to determine whether peptides and proteins may also be loaded individually and co-loaded together. Indeed, our results revealed exogenous materials, specifically fluorophore labeled PKA, a 10,000 MW dextran, and substrates could be co-loaded into “carrier” erythrocytes and utilized for further investigations

Currently, nitrobenzyl groups represent an excellent method to temporally control an enzymatic reaction by blocking enzymatic processing until UV light mediated photolysis.^[63] However, due to the large extinction coefficient of hemoglobin observed below 500 nm, hemoglobin content in erythrocytes may prevent UV light from photocleaving the nitrobenzyl group. We addressed this concern by loading erythrocytes containing hemoglobin and erythrocytes depleted of hemoglobin with a cassette (Fig 2.9a) containing fluorophore and a quencher linked together via 4,5 dimethoxynitrobenzyl. Upon photolysis, our cassette produces a greater than 45-fold fluorescent enhancement (**Figure 2.9**). After confirming photolysis of the cassette can be observed under microscopy

conditions (**Figure 2.10**) we loaded the cassette in erythrocytes and demonstrated photolysis using a UV-laser and a 405 laser. A fluorescence increase was observed in both hemoglobin and hemoglobin free erythrocytes. In the presence of hemoglobin, photolysis is likely to occur due to the relatively high power of light supplied and low cross section width of the erythrocytes.

As loading of erythrocytes results in pore formation and possible leakage of proteins, we wanted to validate that enzymatic activity could be monitored. To demonstrate retention of enzymatic activity after loading, we loaded erythrocytes with a membrane anchored protease substrate. A protease peptide substrate containing TAMRA and 5-FAM is linked to a C18 via a 4,5 dimethoxynitrobenzyl group. The C18 group localizes the substrate to the membrane until photolysis.^[70] After photolysis, the substrate dissociates from the membrane and the peptide is thus free to be recognized by proteases and subsequently degraded.^[70] The degradation results in a fluorescent increase as the TAMRA and FAM fluorophores are separated. The protease substrate was loaded into erythrocytes and photolyzed using confocal microscopy. The observed fluorescent increase and subsequent inhibition with proteases inhibitors demonstrates that loaded erythrocytes retain enzymatic activity.

In summary, we demonstrated that erythrocytes can be loaded using hypotonic dilution with small molecules (such as TAMRA), peptides, and a quenched photolabile cassette as well as a 10,000 MW dextran that mimics protein size. Furthermore, we showed loaded erythrocytes retain enzymatic activity, as determined by our protease activity assay. Our work suggests

erythrocytes loaded in such a manner can be used to monitor intracellular activity of not only exogenously loaded enzymes, but also other endogenous erythrocyte enzymes. Our loading method and ability to temporally initiate enzymatic activity may prove a beneficial method to further elucidate the role of other endogenous erythrocyte enzymes and with the potential to be used as a diagnostic assay where aberrant erythrocyte enzymatic activity occurs.

CHAPTER 3: Monitoring Endogenous Erythrocyte PKA Activity

Overview

We demonstrate, utilizing a recently developed assay and the loading method developed in Chapter 2, that erythrocyte PKA activity can be monitored in real time with a far-red fluorophore labeled peptide substrate (Ex. 635 nm Em. 655 nm). We opted to use a long wavelength fluorophore as the sensor as studying the real time activity of kinases in tissue is challenging in large part due to the narrow optical window. Hemoglobin is responsible for a majority of this interference, blocking visualization below 600 nm. As such, the strong inner filter effect interferes with commercially available assays that utilize wavelengths shorter than 600 nm. Using our developed peptide substrate we showed that erythrocyte PKA is inhibited by PKA inhibitors H89 and KT5720 in lysates. We extended this assay to temporally monitor PKA activity inside erythrocytes using confocal microscopy. Temporal control was achieved using a photolabile small molecule (nitrobenzyl) covalently attached to the substrate serine residue. The reaction is subsequently initiated by light.

Introduction

Serine/Threonine (S/T) kinases are a group of tightly regulated proteins that play critical roles in many different cellular signaling cascades. Upon binding to specific peptide motifs, S/T kinases catalyze the transfer of the γ -phosphoryl group of ATP to the hydroxyl group of a serine or threonine. This post-translation modification impacts a myriad of cellular behaviors ranging from apoptosis to motility and proliferation.^[71] As S/T kinases are so vital to cellular behavior, it is not surprising that aberrant kinase activity is observed in many different diseases.^[72] PKA is an example of a S/T kinase that is tightly regulated. PKA is a tetramer containing two regulator subunits and two catalytic subunits. Upon binding of cAMP to PKA holoenzyme, the regulatory subunits undergo a conformational change disrupting the protein-protein interface,^[73] causing release of the catalytic subunit. This disruption allows for phosphorylation of PKA recognition motifs. PKA is a critical S/T kinase that is found in nearly all mammalian cells including erythrocytes. Indeed, even in erythrocytes, aberrant PKA activity has been linked to several diseases including; sickle cell disease, erythrocyte aging, and *P. falciparum* (malaria) invasion and infection.^[1, 74, 75] Interestingly, H89, a PKA inhibitor, has been shown to be a potent inhibitor of malarial reproduction.^[76] Although H89 is not specific to *P. falciparum* PKA (*PfPKA*), this suggests the importance of studying the role PKA plays in *P. falciparum* as a means to develop new therapeutic strategies.^[77] Furthermore,

monitoring erythrocyte PKA activity could provide a diagnostic for the previously mentioned diseases or conditions where aberrant PKA activity is found.

Although the value of studying S/T kinases cannot be overstated, the tools available to monitor the activities of S/T kinases in a biological system in a temporal manner are rare. Furthermore, current biochemical methods do not allow for the monitoring of real time endogenous kinase activity in erythrocytes. Developing a temporally controlled molecular reporter to monitor protein kinase activity in a cellular environment is challenging as many aspects must be considered including physiological conditions (high salt and other proteins), establishing a time zero, and proteolysis. Many current probes used to study protein kinase activity rely on fluorescent proteins, FRET mechanisms, or fluorophore labeled peptide substrates to produce a fluorescent response. However, many of these substrates cannot be used to study activity in real time because they produce minimal fluorescent changes, often times as low as 10%.^[78, 79] Furthermore, probes that use fluorescent proteins and require transfection of plasmids to study activity cannot be used in cells that do not contain replicative machinery such as erythrocytes.^[79] Although many kinase reporters are limited to minimal fluorescent changes, protease reporters do not suffer from this flaw and often produce dramatic fold changes, enabling real time activity monitoring.^[70, 80-82] The ability of a protease to cleave a unimolecular substrate to form a bimolecular species allows for dramatic fold changes to be observed as fluorescent quenching can be relieved or, through cleavage, reporters are transformed from a non-fluorescent to a highly fluorescent state.

The comprehensive tool kit available to monitor protease activity has allowed for successful monitoring in animal models, a feat that has not been replicated to the same degree with kinases.^[83-85] We have sought to address this limitation by constructing (1) temporally controlled substrates that (2) contain far-red fluorophores, thereby furnishing the means to monitor protein kinase activity in cell-based systems.

To address the need for monitoring kinase activity in real time, we report the improvement of a system developed in the Lawrence lab to monitor endogenous PKA activity in a light dependent manner using far-red fluorophores. Our system utilizes a peptide substrate labeled with various different red to far-red fluorophores (492 nm to 670 nm) and a paired small molecule quencher to produce dramatic fluorescent responses upon substrate phosphorylation by PKA.

The kinase assay currently reported by our group relies on a three component system containing peptide, quencher, and a protein based recognition binding motif.^[78] In this system, the quencher interacts with the peptide in the unphosphorylated state. After phosphorylation the peptide is then recognized by the binding motif and the quencher is no longer able to interact with the fluorophore giving rise to dramatic fold changes.^[78] The improvements we have made to this system are four fold. 1) We have eliminated the need for the binding protein, thereby reducing our assay to a two component system. 2) By attaching our peptide sequence to multiple different far-red fluorophores we have increased the utility of our assay allowing for substrates to be tuned to desired wavelengths making our assay compatible with samples that contain

high concentrations of hemoglobin or melanin such as erythrocytes or tissue. 3) We have identified quenchers that are able to significantly reduce fluorescence in biologically relevant solutions at equal molar ratios indicating tight binding. 4) We have established temporal control by modifying the serine in the peptide with a dimethoxynitrobenzyl moiety which prevents phosphorylation until the peptide is exposed to UV light.^[86] A schematic representation of the kinase assay is shown in **Figure 3.1**.

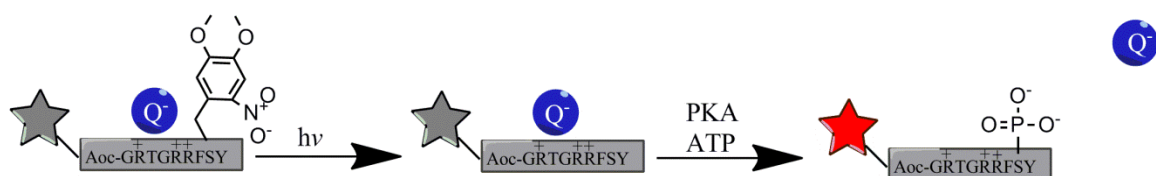


Figure 3.1 Schematic diagram of erythrocyte kinase activity. In the absence of light PKA is unable to phosphorylate the modified serine. After light stimulation the nitrobenzyl group is removed. In the absence of ATP and/or PKA the negatively charged quencher binds tightly to the peptide substrate. After phosphorylation the net charge on the peptide is reduced, resulting in quencher release and an increase in fluorescence.

Materials and Methods

Commercial Sources of Chemicals and Erythrocytes Unless otherwise stated, general reagents and solvents were purchased from Fisher or Sigma-Aldrich. O-(6-chlorobenzotriazol-1-yl)-N,N,N',N'-tetramethyluronium hexafluorophosphate (HCTU), 5-carboxyfluorescein (5-Fam), 5-carboxytetramethylrhodamine (TAMRA), Fmoc protected amino acids, and NovaSyn TGR resin were purchased from Chempep, Inc (Wellington, FL) and NovaBiochem. Fmoc-8-aminooctanoic acid (Fmoc-Aoc-OH) was purchased from Advanced Chemtech (Louisville, KY). All fluorophores, other than Cy3 and Cy5,

were purchased from Sigma-Aldrich as either the free-carboxylic acid or as the NHS ester pre-activated form. Cy3 and C5 carboxylic acids were purchased from Lumiprobe. All reagents for the synthesis of the 4,5-dimethoxy-2-nitrobenzyl ether of FmocSer [Fmoc-Ser(DMNB)-OH] were purchased from Sigma-Aldrich. PKA inhibitors H89 and KT5720 were purchased from Sigma-Aldrich and Calbiochem (EMD) respectively. Peripheral red blood cells were purchased from AllCells. 8-(4-chlorophenylthio) adenosine-3',5'-cyclic monophosphorothioate (CPT-cAMP), ATP, and cAMP were purchased from Sigma-Aldrich. Halt Protease and Phosphatase inhibitors were obtained from Thermo Scientific. PKA, and IgG antibodies as well as secondary goat anti-rabbit antibodies were obtained from Abcam. GAPDH antibody was purchased from Sigma-Aldrich.

Synthesis (*all compounds were synthesized by Luong T. Nguyen or Finith Jernigan. Syntheses are reported here for clarity and in Oien et. al.*)

Synthesis of fluorophore-labeled peptides. Peptides were synthesized using solid phase peptide synthesis. Synthesis was performed on a Prelude automatic peptide synthesizer from Protein Technology using Fmoc protected amino acids (amino acids 3 eq, HCTU 2.95 eq, DIPEA 10 eq in DMF, double coupling in 20 and 40 min). The 4,5-dimethoxy-2-nitrobenzyl (DMNB) modified Ser residue was double-coupled to resin as follows: Fmoc-Ser(DMNB)-OH (3.2 eq.), HCTU (3 eq.), DIPEA (10 eq.) for 30 min and then Fmoc-Ser(DMNB)-OH (1.5 eq.), HCTU (1.5 eq.), DIPEA (10 eq.) for 40 min. Fmoc deprotection was

performed using 25% piperidine in DMF (3 times, 10 min each). Pre-activated fluorophores were coupled to peptides on resin for 4 h using 1 eq. of the pre-activated fluorophore, 10 eq. DIPEA, and an excess amount of peptide.

Fluorophores with a free carboxylic acid moiety were coupled to the peptides on resin for 4 h using 1 eq. of the fluorophore, 1.1 eq. of HCTU, 10 eq. DIPEA, and an excess amount peptide. 5-Fam was coupled to peptides on resin using 1.5 eq. of 5-Fam, 1.7 eq. of diisopropylcarbodiimide, and 10 eq. of HOBt in DMF for 2 h followed by 30 min treatment with 25% piperidine in DMF (2 times). Labeled peptides were cleaved with trifluoroacetic acid (TFA):H₂O:triisopropylsilane in a ratio of 95:2.5:2.5, and purified by HPLC using H₂O: CH₃CN with 0.1 % TFA.

Syntheses of Fmoc-Ser(DMNB)-OH

Fmoc-L-serine allyl ester. DI Water (150 mL) containing N- α -Fmoc-L-serine (10.22 g, 31.2 mmol) and NaHCO₃ (14.36 g, 31.8 mmol) were combined with CH₂Cl₂ (60 mL) containing tricaprylmethylammonium chloride (~11 g) and allyl bromide (16 mL, 184.89 mmol), and the suspension was vigorously stirred at room temperature for 24 h. Water (300 mL) was added to the reaction mixture, and the suspension was extracted with CH₂Cl₂ (3 x 200). The combined organics were dried (Na₂SO₄) and the solvent was removed under reduced pressure. The crude residue was purified by silica flash chromatography (65:35 hexanes:ethyl acetate) to yield Fmoc-L-serine allyl ester as a white solid: ¹H NMR (400 MHz, CDCl₃) δ = 7.77 (d, J = 7.3 Hz, 2 H), 7.62 (br.d., J = 4.6 Hz, 2 H), 7.41 (t, J = 7.5

Hz, 2 H), 7.32 (t, J = 7.5 Hz, 2 H), 5.92 (tdd, J = 5.6, 11.0, 16.9 Hz, 1 H), 5.84 (d, J = 7.8 Hz, 1 H), 5.35 (d, J = 17.1 Hz, 1 H), 5.27 (dd, J = 1.1, 10.4 Hz, 1 H), 4.69 (d, J = 5.4 Hz, 2 H), 4.53 - 4.46 (m, 1 H), 4.46 - 4.37 (m, 2 H), 4.23 (t, J = 7.0 Hz, 1 H), 4.04 (dd, J = 3.1, 11.1 Hz, 1 H), 3.94 (dd, J = 2.9, 11.2 Hz, 1 H), 2.37 (br. s., 1 H). Exact mass calculated for $C_{21}H_{21}NO_5$ 367.14; found (ESI+) 368.1 (M + H)⁺, 390.1 (M + Na)⁺.

4,5-dimethoxy-2-nitrobenzyl trichloroacetimidate. To anhydrous CH_2Cl_2 ; 4,5-dimethoxy-2-nitrobenzyl alcohol (8.97 g, 42.08 mmol) and anhydrous K_2CO_3 (14.2 g, 102.74 mmol) were added and stirred (120 mL) under N_2 atmosphere. To the above mixture, trichloroacetonitrile (10 mL, 99.73 mmol) and anhydrous triethylamine (6 mL, 43.01 mmol) were added and the reaction mixture stirred at room temperature for 24 h. CH_2Cl_2 (300 mL) was added to the reaction mixture. The organic layer was collected and washed with 0.5 N HCl followed by solvent removal. The dried crude residue was purified by silica flash chromatography (75:25 hexanes:ethyl acetate) to give 4,5-dimethoxy-2-nitrobenzyl trichloroacetimidate: 1H NMR (400 MHz, $CDCl_3$) δ = 8.51 (s, 1 H), 7.75 (s, 1 H), 7.23 (s, 1 H), 5.78 (s, 2 H), 3.97 (s, 3 H), 3.96 (s, 3 H). Exact mass calculated for $C_{11}H_{11}Cl_3N_2O_5$ 355.97; found (ESI+) 374.9 (M + H_3O)⁺.

N-(9-fluorenylmethyloxycarbonyl)-o-(4,5-dimethoxy-2-nitrobenzyl)-L-serine allyl ester. Fmoc-serine allyl ester 4 (1.74 g, 4.75 mmol) and the 4,5-dimethoxy-2-nitrobenzyl trichloroacetimidate (3.22 g, 9.04 mmol) were dissolved in CH_2Cl_2 (40 mL) and mixed under nitrogen atmosphere at room temperature. To the above solution was slowly added a solution of triflic acid in CH_2Cl_2 (75 μ L

triflic acid in 5 mL CH₂Cl₂). The reaction mixture was stirred at room temperature for 30 min after the completion of the triflic acid addition. N,N-diisopropylethylamine (DIPEA, 150 µL) in CH₂Cl₂ (10 mL) and silica gel were added to the reaction mixture and then concentrated under reduced pressure. The crude residue, adsorbed on silica, was purified by silica flash chromatography (67:33 hexanes:ethyl acetate) to afford N-(9-fluorenylmethyloxycarbonyl)-o-(4,5-dimethoxy-2-nitrobenzyl)-L-serine allyl ester: ¹H NMR (400 MHz, CDCl₃) δ= 7.77 (d, J = 7.5 Hz, 2 H), 7.72 (s, 1 H), 7.61 (t, J = 6.7 Hz, 2 H), 7.41 (t, J = 7.3 Hz, 2 H), 7.31 (t, J = 6.6 Hz, 2 H), 7.18 (s, 1 H), 5.97 - 5.82 (m, 1 H), 5.71 (d, J = 8.4 Hz, 1 H), 5.33 (d, J = 17.1 Hz, 1 H), 5.23 (d, J = 10.4 Hz, 1 H), 4.98, 4.92 (ABq, JAB = 15.4 Hz, 2 H), 4.71 (d, J = 5.1 Hz, 2 H), 4.68 - 4.62 (m, 1 H), 4.48, 4.39 (ABXqd, JAB = 10.5 Hz, JAX = 6.8 Hz, JBX = 6.9 Hz, 2 H), 4.24 (t, J = 7.1 Hz, 1 H), 4.18 - 4.04 (m, 2 H), 3.96 (s, 3 H), 3.95 (s, 3 H), 3.94 - 3.89 (m, 1 H). Exact mass calculated for C₃₀H₃₀N₂O₉ 562.20; found (ESI+) 563.2 (M + H)⁺, 585.2 (M + Na)⁺.

N-(9-Fluorenylmethyloxycarbonyl)-O-(4,5-dimethoxy-2-nitrobenzyl)-L-serine. The DMNB modified serine allyl ester 6 (1.00 g, 1.78 mmol) was dissolved in CHCl₃ (40 mL) containing acetic acid (21 mL) and N-methylmorpholine (3 mL). To the above solution was added Pd(Ph₃P)₄ (0.97 g, 0.84 mmol). The reaction mixture was stirred for 4 h at room temperature and neutralized by the addition of 0.1 N HCl until pH 4 and then the suspension was extracted with CH₂Cl₂ (twice) and ethyl acetate (three times). The organic extracts was dried (Na₂SO₄), and concentrated under reduced pressure. The

crude residue was purified by silica flash chromatography (CH_2Cl_2 and then 48:2 $\text{CH}_2\text{Cl}_2:\text{CH}_3\text{OH}$) to yield N-(9-Fluorenylmethyloxycarbonyl)-O-(4,5-dimethoxy-2-nitrobenzyl)-L-serine: ^1H NMR (400 MHz, CDCl_3) δ = 7.76 (d, J = 7.6 Hz, 2 H), 7.66 (s, 1 H), 7.60 (t, J = 5.9 Hz, 2 H), 7.40 (t, J = 7.5 Hz, 2 H), 7.31 (dt, J = 1.2, 6.4 Hz, 2 H), 7.10 (s, 1 H), 5.69 (d, J = 8.3 Hz, 1 H), 4.97, 4.87 (ABq, $J_{\text{AB}} = 15.29$, 2 H), 4.68 (br.s., 1 H), 4.53 - 4.37 (m, 2 H), 4.23 (t, J = 6.7 Hz, 1 H), 4.12 (d, J = 9.2 Hz, 1 H), 3.93 (s, 3 H), 3.90 (s, 3 H), 3.89 - 3.83 (m, 1 H). ^1H NMR (400 MHz, acetone- d_6) = 7.86 (d, J = 7.6 Hz, 2 H), 7.73 (dd, J = 3.8, 7.4 Hz, 2 H), 7.70 (s, 1 H), 7.44 - 7.37 (m, 3 H), 7.35 - 7.28 (m, 2 H), 4.98, 4.92 (ABq, $J_{\text{AB}} = 15.7$ Hz, 2 H), 4.58 (t, J = 4.5 Hz, 1 H), 4.41 - 4.29 (m, 2 H), 4.28 - 4.21 (m, 1 H), 4.09 (dd, J = 4.9, 9.6 Hz, 1 H), 3.98 - 3.94 (m, 1 H), 3.93 (d, 6 H). Exact mass calculated for $\text{C}_{27}\text{H}_{26}\text{N}_2\text{O}_9$ 522.16; found (ESI+) 523.2 ($\text{M} + \text{H}$) $^+$, 545.1 ($\text{M} + \text{Na}$) $^+$.

Peptide purification. A Waters HPLC instrument was used to purify all peptides. Flash chromatography purification was performed using an Isolera One instrument (Biotage) equipped with a silica or C18 column (Biotage). Peptides were either purified using C18 flash chromatography or C18 HPLC (Apollo C18, 5 μm , 250 x 22 mm column). LC-MS analytical characterizations were run on an Agilent instrument equipped with UV-VIS and quadrupole mass detectors using either a Viva C4 column (5 μm , 50 x 2.1 mm) from Restek or a Prevail C18 column (3 μm , 50 x 2.1 mm) from Alltech Associates, Inc. All LC-MS experiments were conducted using $\text{H}_2\text{O}-\text{CH}_3\text{CN}$ solvents with 0.1% formic acid.

Absorbance measurements. Absorbance measurements were performed using a Perkin Elmer Lambda 25 UV/Vis spectrophotometer. Data was collected using UV WinLab. To collect erythrocyte lysate absorbance, washed erythrocytes were lysed using mechanical shearing. The lysed erythrocytes were then centrifuged at 10,000 rpm for 3 min and the supernatant collected. The supernatant was then diluted 100-fold and the absorbance measurements collected between 450 - 700 nm. The absorbance spectra were also collected for 5-Fam, Atto620, TAMRA, Red681, and Atto633 (Fluorophore-Aoc-GRTGRRFSY) peptides at 2 μ M. The absorbance maxima between 475 and 700 for each sample were normalized to 1.

Fluorescence measurements. 200 μ L 96 well plate fluorescence assays were performed using a Molecular Devices SpectraMax Gemini EM Dual-Scanning Microplate Spectrofluorometer. Data was collected using SoftMax Pro Software. Alternatively, protein kinase activities were monitored using a PTI Technologies QuantMaster-40 equipped with cooled PMT housing. The data was collected using FelixGX Software. Sensor monitoring studies were performed using a plate reader in a 96 well format (200 μ L/well) in Tris-HCl (25 mM, pH 7.5), MgCl₂ (1 mM), PKA (10 nM), peptide (1 μ M) and quencher concentrations mentioned in the figures. Reactions were initiated with the addition of ATP (final concentration of 1 mM). Excitation and emission wavelengths are reported in Table 1.1.

Screening of the dye library. 200 μ L kinase buffer containing Tris-HCl (25 mM, pH 7.5), $MgCl_2$ (1 mM), ATP (1 mM) and fluorophore-peptide (2.5 or 5 μ M) were added to wells of a 96-well plate. Dyes (Table 3.1, concentration ranging from 5 μ M to 60 μ M) were then added to each well and the initial fluorescence recorded. Phosphorylation was initiated by the addition of PKA (10 nM) into each well and fluorescence was monitored over time. Dyes that produced a fluorescent increase upon the PKA addition were selected for further confirmation by replication in the plate reader or spectrofluorometer. Phosphorylation products were confirmed by LC-MS.

Comparison of kinase reporter assay using various salt concentrations. Fluorophore-labeled peptides were added to 200 μ L of either “no salt” buffer containing Tris-HCl (25 mM, pH 7.5), $MgCl_2$ (1 mM), ATP (1 mM) or “with salt” buffer containing Tris-HCl (25 mM, pH 7.5), $MgCl_2$ (1 mM), ATP (1 mM), and NaCl (150 mM) followed by incubation (5 min at 30 °C). Various quenchers were then added to the solutions followed by incubation (5 min at 30 °C) and the addition of PKA (to 10 nM) to initiate phosphorylation. Fluorescence fold change = F_f/F_q , and fluorescent quenching = $100 \times (F_i - F_q)/F_i$, where F_i , F_q , F_f are the fluorescence of the reaction mixture in the absence of quencher, in the presence of quencher, and after the phosphorylation reaction is completed, respectively.

Job plots. Various ratios of peptide (TAMRA-Aoc-GRTGRRFSY) and quencher dye (Acid Blue 80 1 or Evans Blue 2) at a fix total concentration of peptide and quencher dye (5 μM) were added to 200 μL kinase buffer containing Tris-HCl (25 mM, pH 7.5), MgCl_2 (1 mM), ATP (1 mM), and NaCl (150 mM). Mixtures were then incubated at room temperature for 10 min before the absorbance measurements were taken.

Determination of dye concentrations that generate a 50% loss in fluorescence (EQ_{50}) of fluorophore-labeled peptides. The contribution to signal loss due to the inner filter effect of the dye was subtracted during the EQ_{50} determination. In the rear chamber of a two chamber cuvette (Precision Cells, LT125ES10), peptide (1 μM) was added to PBS buffer [sodium phosphate (8.06 mM), potassium phosphate (1.94 mM), KCl (2.7 mM), and NaCl (137 mM); pH 7.4] and in the front chamber varying concentrations of either Acid Blue 80 1 or Evans Blue 2 (0.1 to 32 μM) was added to PBS buffer. The reduction in fluorescence was calculated as a percent loss in initial fluorescence from the control where $[\text{Dye}] = 0 \mu\text{M}$. This curve was applied to respective samples. EQ_{50} 's were determined by adding peptide (1 μM) and varying concentrations of quencher (0.1 to 32 μM) in PBS buffer and after removing the contribution due to the inner filter effect. EQ_{50} 's were determined by fitting the data to Equation 3.1.

$$\% \text{ Fluorescent Quench} = \frac{B_{\text{max}} [\text{Dye}]}{\text{EQ}_{50} + [\text{Dye}]} \quad (\text{Eq. 3.1})$$

Where B_{max} is the maximum amount of fluorescent quenching observed (100%), $[Dye]$ is the quencher dye concentration, and EQ_{50} is the concentration at which 50% quenching is observed.

IC₅₀ determinations of PKA inhibitors KT5720 and H89. Assays were set up with 200 μ L of PBS buffer containing, Atto633-Aoc-GRTGRRFSY (1 μ M) Evans Blue 2 (2 μ M) was allowed to equilibrate at 25 °C in a spectrofluorometer. The PKA-catalyzed reaction was initiated by adding a stock solution of ATP and cAMP (100 mM each, pH 7.4) to give a final concentration of 500 μ M of ATP and of cAMP. Relative initial rates were determined (relative to no inhibitor control) in triplicate in the presence of H89 or KT5720 (50 nM to 5 μ M). Relative rates were plotted vs H89 or KT5720 concentration and the IC₅₀ value determined using GraphPad Prism 5 software.

Erythrocyte lysates: 200 μ L of PBS containing lysed erythrocytes (10%), Atto633-Aoc-GRTGRRFSY (1 μ M), Evans Blue 2 (2 μ M), and Halt protease and phosphatase inhibitor cocktail (1x) was allowed to equilibrate at 25 °C in a spectrofluorometer. The PKA-catalyzed reaction was initiated by adding a stock solution of ATP and cAMP (100 mM each, pH 7.4) to give a final concentration of 500 μ M of ATP and of cAMP. Relative initial rates were determined in triplicate in the presence of H89 or KT5720 (50 nM to 5 μ M). Relative rates were plotted vs H89 or KT5720 concentration and the IC₅₀ value determined using GraphPad Prism 5 software.

PKA activity in erythrocyte lysates. Peripheral erythrocytes were washed three times in PBS by centrifuging at 1400 g for 10 min. After each centrifugation the supernatant was removed by aspiration and replaced with PBS buffer. After the final wash, erythrocytes were suspended to 50% hematocrit levels and lysed in the presence of DTT (20 mM) with mechanical shearing. The lysed erythrocytes were then centrifuged at 10,000 rpm for 3 min and the subsequent supernatant was used for assay measurements.

Kinase assays were performed in a 200 μ L cuvette using a PTI spectrofluorometer. Solutions contained PBS buffer with fluorophore labeled peptide (1 μ M), MgCl₂ (5 mM), Halt protease and phosphatase inhibitor (1x), and lysed erythrocytes (10%). Reactions were initiated with the addition of cAMP and ATP to a final concentration of 1 mM each.

Fluorescence signal loss study due to erythrocyte lysates. A two-chambered cuvette (Precision Cells, LT125ES10) was filled with PBS or PBS and 10% lysate in one chamber and PBS containing 5-Fam, TAMRA, or Atto633 Aoc-GRTGRRFSY (1 μ M) in the second chamber. The fluorescence spectrum was measured for each peptide using their corresponding maximum excitation and emission wavelengths.

PKA clearing and western blot analysis. Erythrocyte PKA clearing was performed using erythrocyte lysates (see above). Erythrocyte lysates (500 μ L) were incubated with antibody (10 μ L) (anti-PKA C subunit or anti-rabbit IgG) at

4 °C overnight. Protein A agarose was then added to the samples and incubated at 4 °C for 4 h. The samples were then placed in Bio-Rad Micro Bio-Spin chromatography Columns and eluted by centrifuging at 1000 g for 4 min. The eluent was then collected and PKA activity was monitored using TAMRA-Aoc-GRTGRRFSY via the aforementioned method and relative PKA levels were quantitated via western blot.

PKA cleared, IgG control, and non-cleared erythrocyte lysate samples were normalized to 550 nm. 20 µL of normalized lysate was loaded onto 4–12% bis-tris polyacrylamide gels, separated by electrophoresis, and electroblotted onto PVDF membranes. The membranes were then blocked in PBS with tween 20 and 0.5% nonfat dry milk followed by incubation with the appropriate primary antibody (PKA C subunit 1:1000,) at 4 °C overnight. The membranes were then washed 3 times with Tween-20 (0.1%) in PBS followed by incubation with a goat anti-rabbit secondary antibody (1:2000) for 2 h at RT. Subsequent washes with Tween-20 (0.1%) in PBS (three times), PBS (three times), and 0.5% NaCl (three times) were performed prior to detection with GE Amersham ECL Western blotting detection reagent. After image acquisition the membrane was stripped using Restore™ PLUS Western Blot Stripping Buffer (Thermo) and subsequently blotted with rabbit Anti-GAPDH via the aforementioned protocol. Images were analyzed using Image J; PKA levels were quantitated relative to GAPDH levels.

Photoconversion of inactive sensor (DMNB protected Att633-Aoc-GRTGRFSY) to active sensor for erythrocyte lysate studies. Photolysis experiments on Atto633-Aoc-GRTGRRFS(DMNB)Y were performed in PBS or in

PBS buffer containing 10% erythrocyte lysate, DTT (20 mM), and Halt protease and phosphatase inhibitors (1x). Photolysis was performed using a Zeiss Colibri 1 LED light source (365 nm light at 100% power) for 5 min or using a mercury arc lamp for 2 min. PBS containing Atto633-Aoc-GRTGRRFSY (1 μ M), Evans Blue (2 μ M), and PKA (10 nM) was photolyzed. Following photolysis, activity was monitored using fluorescence by the addition of ATP (1 mM) to initiate the phosphorylation.

Erythrocyte integrity assessment in the presence of dye fluorescence quenchers and UV/405 nm light. Erythrocytes were washed three times in PBS. Packed erythrocytes were then diluted to 10% in PBS. Erythrocytes were then exposed to dye fluorescent quencher (Acid Blue 80 [1] or 30 μ M Evans Blue [2]) and 405 nm or UV light for 5 min. Loss of erythrocyte integrity as assessed by lysis was determined by spinning the treated erythrocyte solution at 2000 g for 5 min and monitoring the supernatant absorbance at 414 nm. Experimental results were compared to controls: (1) no dye quencher, (2) in the dark, and (3) sonication for 30 s (resulting in 100%).

Loading kinase assay into erythrocytes. Erythrocytes were loaded with peptide and dye quencher via a hypotonic dilution method. Whole peripheral erythrocytes were washed three times in PBS. Erythrocytes were then stored overnight at 4 °C to deplete any remaining ATP. Washed erythrocytes (50 μ L,

50%) were added to a solution containing Atto633-Aoc-GRTGRRFS(DNMB)Y (1 μ M), Evans Blue (2) (2 μ M), ATP (5 mM), CPT-cAMP (1 mM), Tris-HCl (10 mM, pH 7.5), and Halt protease and phosphatase inhibitor cocktail (1x) to a final volume of 500 μ L. The solution was incubated on ice (10 min) and turned a transparent red. 52.7 μ L of 10x buffer [KCl (1.22 M), MgCl₂ (180 mM), glucose (100 mM), and Tris-HCl (100 mM, pH 7.5)] was then added to the erythrocyte solution, which changed from transparent to opaque. At this point erythrocytes were allowed to recover at 4 °C for 30 min. 5 μ L of DTT (1 M) and 5 μ L of Evans Blue (2) (400 μ M) were then added to the erythrocyte solution. Several studies have demonstrated that, upon resealing, erythrocytes are unable to completely reseal the membrane. To prevent loss of smaller molecules (ATP, cAMP, or quencher) the erythrocytes were not washed.^[11, 87, 88] For microscopy experiments, 7 μ L of the final erythrocyte solution was placed between two cover slips. Erythrocytes added to the cover slips were allowed to rest for 10 min, and subsequently imaged using confocal microscopy. For flow cytometry experiments, the same solution was washed once in PBS buffer and re-suspended in PBS containing Evan's Blue (2) (10 μ M). The erythrocyte solution was then filtered through Partec CellTrics® filters and analyzed by flow cytometry.

Flow cytometry. Erythrocytes loaded with (1) Atto633-Aoc-GRTGRRF(DMNB)SY (1 μ M) alone, (2) Atto633-Aoc-GRTGRRF(DMNB)SY (1 μ M) and Evans Blue (2) (2 μ M), and (3) neither were analyzed using flow

cytometry. Flow cytometry was performed on a BD LSR II flow cytometer in UNC Flow Cytometer Core Facility in the Department of Microbiology and Immunology.

Confocal microscopy. All microscopy experiments were performed at room temperature on an Olympus FV1000 scanning confocal with an IX81 microscope base. Laser and region of photolysis were controlled via Fluoview software. Photolysis was performed using the stimulation mode with images collected before and after stimulation. A photolytic dwell time of 20 μ s/pixel in tornado mode was employed for the defined region of interest using 25 frames with the 405 nm laser at 2% power level. All imaging was performed with a 100X objective using a 635 laser nm at 2% power. The Atto-633 peptide, in the absence of dye quencher, was used to generate a photobleaching curve. ImageJ software was employed for image analyses. Final fluorescence intensity changes of Atto-633 were corrected for photobleaching effect by equation 3.2.

$$F_t \text{ (corrected)} = F_t \times f_0/f_t \quad (\text{Eq. 3.2})$$

Where F_t are fluorescence values measured at time t , f_0 and f_t are fluorescence values of bleaching curve at $t = 0$ and at t .

Western blot analysis of CPT-cAMP stimulated erythrocytes. Western blot analysis was performed using erythrocyte lysates (see above) that had been

stimulated with 1 mM CPT-cAMP, DMSO (Control), or 1 mM CPT-cAMP and 10 μ M H89. PKA stimulated erythrocyte lysate samples were normalized to 550 nm. 20 μ L of normalized lysate was loaded onto 4–12% bis-Tris polyacrylamide gels, separated by electrophoresis, and electroblotted onto PVDF membranes. The membranes were then blocked in PBS + tween containing 0.5% nonfat dry milk followed by incubation with the appropriate primary antibody (PAN p-PKA-substrate subunit 1:1000,) at 4 °C overnight. The membranes were then washed 3 times with Tween-20 (0.1%) in PBS. followed by incubation with a goat anti-rabbit secondary antibody (1:2000) for 2 h at RT. Subsequent washes with Tween-20 (0.1%) in PBS (three times), PBS (three times), and 0.5% NaCl (three times) were performed prior to detection with GE Amersham ECL Western blotting detection reagent. After image acquisition the membrane was stripped using Restore™ PLUS Western Blot Stripping Buffer (Thermo) and subsequently blotted with rabbit Anti-GAPDH via the aforementioned protocol.

Results

Identification of quencher-fluorophore pairs for monitoring PKA

activity. Two peptide sequences that are phosphorylated by PKA were selected based on prior literature sources.^[89, 90] Red to far-red fluorophores were appended to the N-termini of the peptides and each peptide-fluorophore conjugate was incubated with each of the 48 quenchers. All 18 fluorophore labeled peptides were screened against the 48 quenchers (**Table 3.1 and 3.2**). PKA was added to initiate the assay to screen the quencher library. Fluorophore-quencher pairs that produced the brightest fluorescent responses are reported. The quenchers that were identified in the screen had similar characteristics. The quencher's maximum absorbance occurs between 550 and 650 nm and the quenchers that produced the brightest responses are negatively charged. This implies that the mechanism of the fluorescence response is primarily based on a charge interaction between the negatively charged quencher and the positively charged peptide. Peptide-quencher pairs were then tested in the presence of salt. Our results showed (**Table 3.3**) that salt reduces the ability of the quenchers, Acid Blue 80 and Acid Blue 27, to quench fluorescence. Evans Blue was also tested in the presence of salt, and was identified to show larger increases (**Table 3.4**). Generally, the ability of the quencher to reduce fluorescence was strongly correlated with the fluorescence fold change after addition of PKA. We showed (**Figure 3.2**) that the greater the percentage of

fluorescent quenching, the greater the fluorescent fold change upon phosphorylation.

Table 3.1 Quenchers used in PKA assay screen. Quenchers most often identified in the kinase screen are bolded.

λ_{max} (nm)	<500	501-550	551-600	601-650	651-700
Dyes	Disperse Yellow 3 Acid Alizarin Violet N Acridine Orange Acridine Yellow G Bismark Brown Y Brilliant Yellow Carminic Acid Chrysoidine Y Cresol Red Ethyl Orange Methylthymol Blue N,N-dimethylnitrosoaniline Rosolic Acid Tartrazine	Acid Fuchsin Acid Red 27 Basic Fuchsin Eriochrome Black T Erythrosin Methyl Orange Nuclear Fast Red Ponceau S Rose Bengal	Acid Green 25 Brilliant Blue R Bromocresol Purple Bromophenol Blue Chlorazol Black E Chlorophenol Red Ethyl Violet Methyl Violet Phenol Red Phenolphthalein Safranin O	Acid Blue 129 Acid Blue 40 Acid Blue 80 Acid Green 27 Alizarin Red Aniline Blue WS Azure A Evans Blue Malachite Green oxalate Naphthol Blue Black Trypan Blue Xylene Cyanol FF	Azure B bromide Methylene Blue

Table 3.2 Fluorescent increase of peptides associated with quenchers after addition of PKA. Each of the following fluorophore labeled peptides were screened against the 48 quenchers in **Table 3.1**. The hits that produced the best fluorescent fold changes after reaction initiation are reported below with the concentration of quencher. Numbers in parentheses represent concentrations in μM . Reprinted with permission from publisher.^[63]

Peptide	Quencher	Fluorescent fold change \pm sd
5-Fam-KRRRLASLAA (2.5)	Acid green 27 (30)	3.70 \pm 0.8
Cy3-KRRRLASLAA (2.5)	Bromophenol Blue (20)	5.05 \pm 0.12
TAMRA-KRRRLASLAA (2.5)	Acid Blue 80 (15)	24.50 \pm 1.4
Atto610-KRRRLASLAA (2.5)	Bromophenol Blue (35)	5.47 \pm 0.15
Atto620-KRRRLASLAA (2.5)	Acid Blue 80 (7.5)	21.85 \pm 0.47
Red630-KRRRLASLAA (2.5)	Bromophenol Blue (30)	3.97 \pm 0.54
Atto635-KRRRLASLAA (2.5)	Bromophenol Blue (35)	4.19 \pm 0.18
Cy5-KRRRLASLAA (2.5) *	Bromophenol Blue (20)	5.82 \pm 0.23
Atto655-KRRRLASLAA (2.5)	Acid Blue 80 (10)	16.71 \pm 0.51
Atto680-KRRRLASLAA (2.5)	Acid Blue 80 (15)	22.54 \pm 2.67
Red681-KRRRLASLAA (2.5)	Acid Blue 80 (5)	13.83 \pm 0.67
NIR700-KRRRLASLAA (2.5)	Bromocresol Purple (80)	2.73 \pm 0.05
NIR730-KRRRLASLAA (2.5)	Bromocresol Purple (80)	2.59 \pm 0.19
5-Fam-Aoc-GRTGRRFSY (2.5)	Acid green 27 (30)	21.19 \pm 0.41
TAMRA-Aoc-GRTGRRFSY (2.5)	Acid Blue 80 (15)	100.68 \pm 27.5
Atto620-Aoc-GRTGRRFSY (2.5)	Acid Blue 80 (7.5)	31.36 \pm 1.04
Red681-Aoc-GRTGRRFSY (2.5)	Acid Blue 80 (5)	11.18 \pm 0.57
Atto633-Aoc-GRTGRRFSY (2.5)	Acid Blue 80 (5)	30.93 \pm 4.89

Table 3.3 Effect of salt on the fluorescent response of PKA sensors upon phosphorylation. The addition of 10 nM PKA was used to initiate phosphorylation. Fold change = F_f/F_q , Fluorescent quenching = $(F_i - F_q)/F_q$, where F_i , F_q , F_f were the fluorescence of the reaction mixture in the absence of quencher, in the presence of quencher, and after phosphorylation reaction completed, respectively. Reprinted with permission from publisher.^[63]

Buffer condition	Peptide (2.5 μM)	Quencher (concentration/ μM)	Fluorescent quenching (%)	Fold change after phosphorylation
No salt	5Fam-Aoc-GRTGRRFSY	Acid green 27 (30)	97.2 \pm 0.3	18.5 \pm 3.4
With salt	5Fam-Aoc-GRTGRRFSY	Acid green 27 (30)	97.0 \pm 0.1	3.5 \pm 0.5
No salt	TAMRA-Aoc-GRTGRRFSY	Acid Blue 80 (15)	99.8 \pm 0.1	103.7 \pm 24.4
With salt	TAMRA-Aoc-GRTGRRFSY	Acid Blue 80 (15)	99.7 \pm 0.0	41.0 \pm 1.2
No salt	Atto620-Aoc-GRTGRRFSY	Acid Blue 80 (7.5)	99.1 \pm 0.1	16.6 \pm 0.8
With salt	Atto620-Aoc-GRTGRRFSY	Acid Blue 80 (7.5)	98.6 \pm 0.0	18.2 \pm 0.1
No salt	Atto633-Aoc-GRTGRRFSY	Acid Blue 80 (5)	99.4 \pm 0.3	30.2 \pm 9.1
With salt	Atto633-Aoc-GRTGRRFSY	Acid Blue 80 (5)	98.6 \pm 0.2	23.6 \pm 3.0

Table 3.4 Effect of salt on the fluorescent response upon phosphorylation of peptides with Evans Blue. Either “no salt” buffer (200 μ L) containing tris-HCL (25 mM, pH 7.5), MgCl₂ (1 mM), ATP (1 mM) or “with salt” buffer (200 μ L) containing tris chloride (25 mM, pH 7.5), MgCl₂ (1 mM), ATP (1 mM), and 150 mM NaCl were added peptides followed by 5 min incubated at 30 °C. To the reaction mixture were then added evan blue (2.5 μ M) followed by 5 minute incubation at 30 oC and the addition of 10 nM PKA to initiate the phosphorylation. Fold change and fluorescent quenching were calculated as previously described. Reprinted with permission from publisher.^[63]

Buffer condition	Peptide (2.5 μ M)	Fluorescent quenching (%)	Fold change after phosphorylation
No salt	5Fam-Aoc-GRTGRRFSY	80.9 \pm 1.5	2.9 \pm 0.5
With salt	5Fam-Aoc-GRTGRRFSY	62.1 \pm 1.1	1.4 \pm 0.0
No salt	TAMRA-Aoc-GRTGRRFSY	99.8 \pm 0.0	20.6 \pm 2.9
With salt	TAMRA-Aoc-GRTGRRFSY	99.8 \pm 0.0	34.6 \pm 14.5
No salt	Atto633-Aoc-GRTGRRFSY	98.0 \pm 0.4	2.0 \pm 0.3
With salt	Atto633-Aoc-GRTGRRFSY	94.6 \pm 1.3	3.0 \pm 0.5

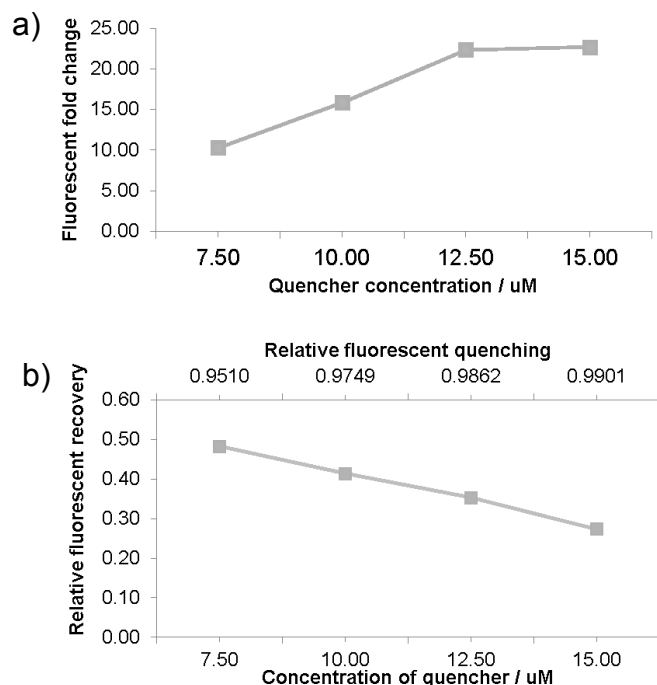


Figure 3.2 Fluorescent fold increase of Atto680-KRRRLASLAA (2.5 μ M) due to PKA phosphorylation with various Acid Blue 80 concentrations. Relative fluorescent quenching = $(1 - F_i/F_o)$ (a), relative fluorescent recovery = $(F_f - F_i)/F_o$ (b). Fluorescent fold change = F_f/F_i , where F_i and F_o were the fluorescence in the presence and absence of quencher respectively; F_f was the final fluorescence after the phosphorylation has completed in the presence of quencher. Reprinted with permission from publisher.^[63]

Quencher compatibility with erythrocytes. Quenchers Acid Blue 80 and Evans Blue were mixed with intact erythrocytes and tested in the presence and absence of UV and 405 nm light (as it is known that both UV light and 405 nm

light can induce photocleavage of the nitrobenzyl-serine C-O bond). Erythrocyte lysis was determined by measuring hemoglobin release in the supernatant (**Figure 3.3**). Evans Blue was determined to be well tolerated and exposure of erythrocytes to 405 nm light had minimal impact on erythrocyte viability. Erythrocytes exposed to Acid Blue 80 experienced dramatic lysis.

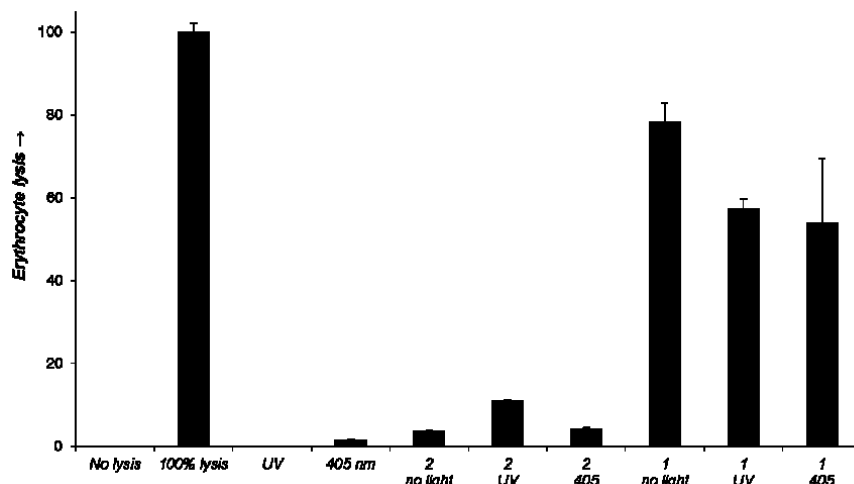


Figure 3.3 Percent erythrocyte lysis from exposure to quenchers. Evans Blue is labeled 1, and Acid Blue 80 is labeled 2. Reprinted with permission from publisher.^[63]

Measuring affinity for quenchers to Atto633-peptide. To assess the ability of the quencher to interact with the peptide we measured the binding affinity. A high binding affinity is necessary as the higher the binding affinity the more specifically the quencher will interact with the peptide. A 1:1 binding is determined by a Job Plot containing a single maximum peak. As the Job Plots depicted in **figure 3.4**, each contain more than one maximum peak the relative affinity of quenchers Acid Blue 80 and Evans Blue toward the fluorophore labeled peptide was measured by calculating the concentration required to quench 50% of the fluorescence (EQ_{50}). **Figure 3.5** shows that Evans Blue has a greater apparent affinity for the peptide than Acid Blue 80. Next we increased the salt

concentration and demonstrated that salt decreases the affinity (**Figure 3.6**).

Finally, we measured the change in apparent affinity of Evans Blue in the presence of lysate and determined the affinity was reduced (**Figure 3.7**).

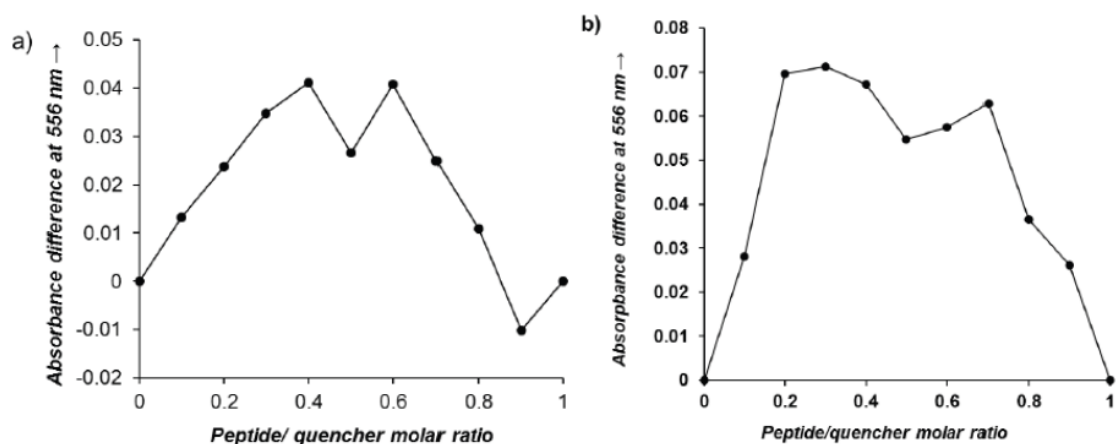


Figure 3.4 Job plot analysis of a) Acid Blue 80 and b) Evans Blue. Job plots were determined for both quenchers using Atto633-Aoc-GRTGRRFSY at 556 nm. Reprinted with permission from publisher.^[63]

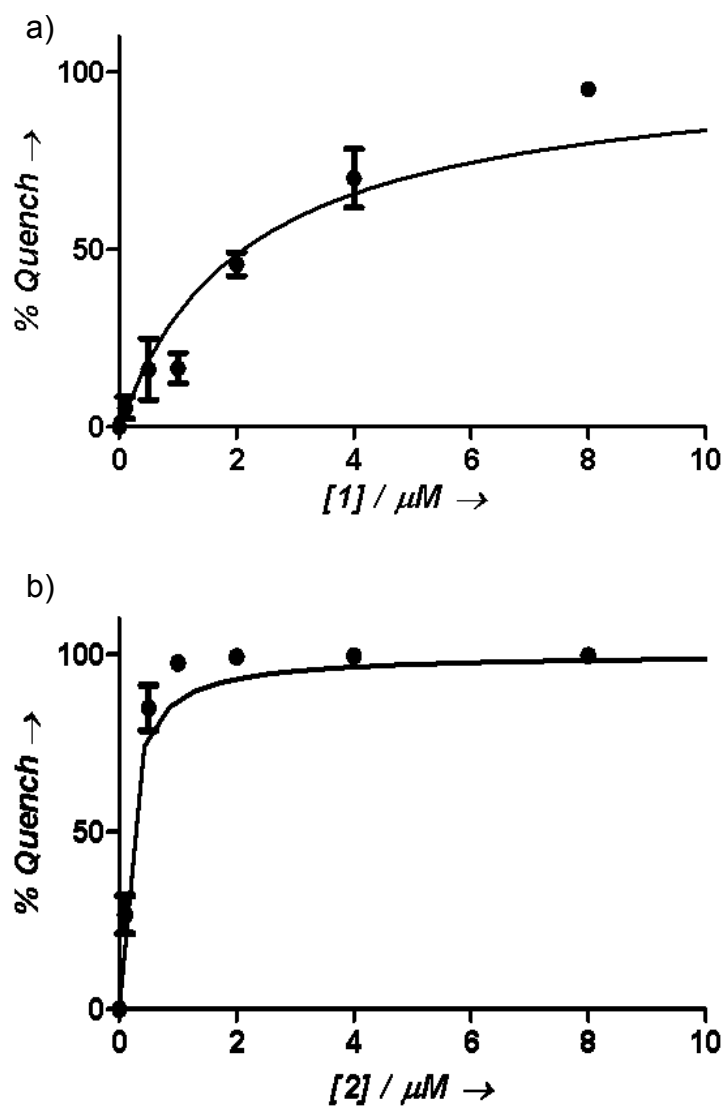


Figure 3.5 EQ_{50} of Acid Blue 80 (a) and Evans Blue (b) for Atto633-Aoc-GRTGRRFSY. 1 indicates Acid Blue 80 and 2 indicates Evans Blue. Reprinted with permission from publisher.^[63]

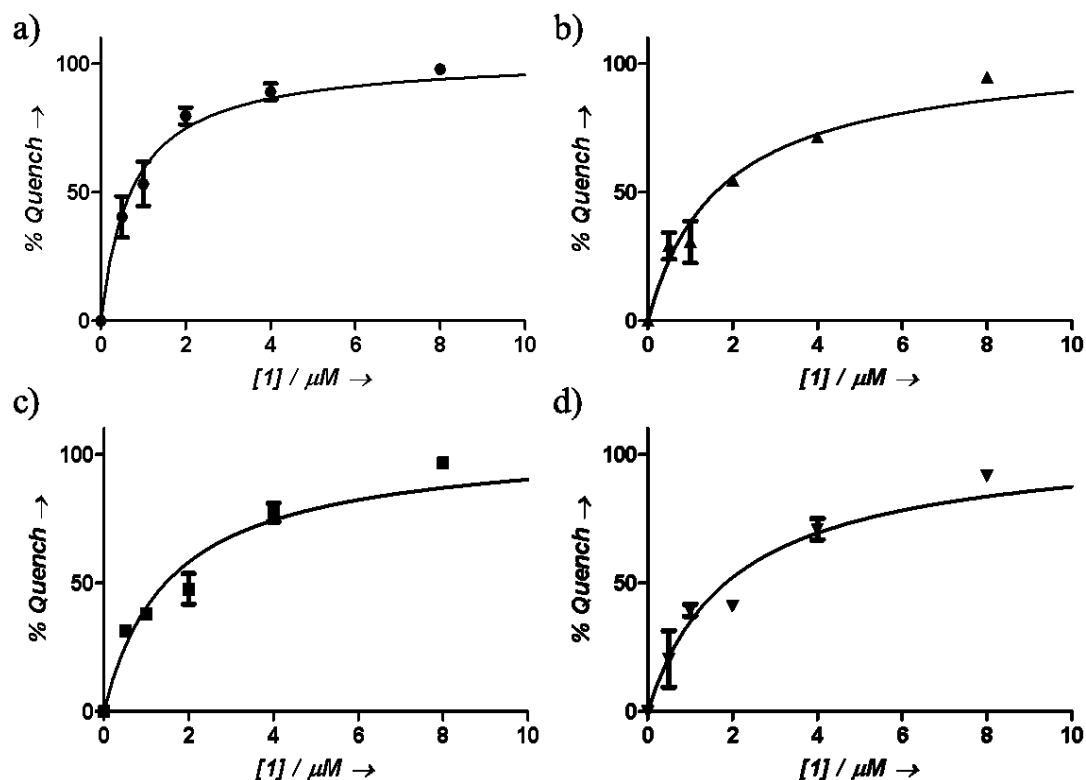


Figure 3.6 Effect of salt on EQ₅₀ of Atto633-Aoc-GRTGRRFSY. Quenching of Atto633-Aoc-GRTGRRFSY (1 μ M) fluorescence as a function of Acid Blue 80 (1) at various NaCl concentrations, where (a) [NaCl] = 0 mM (circles, EQ₅₀ = 0.69 \pm 0.07 μ M), (b) 50 mM (squares, EQ₅₀ = 1.5 \pm 0.14 μ M), (c) 100 mM (triangles, EQ₅₀ = 1.6 \pm 0.16 μ M), and (d) 150 mM (inverted triangles, EQ₅₀ = 1.9 \pm 0.2 μ M). Reprinted with permission from publisher Reprinted with permission from publisher.^[63]

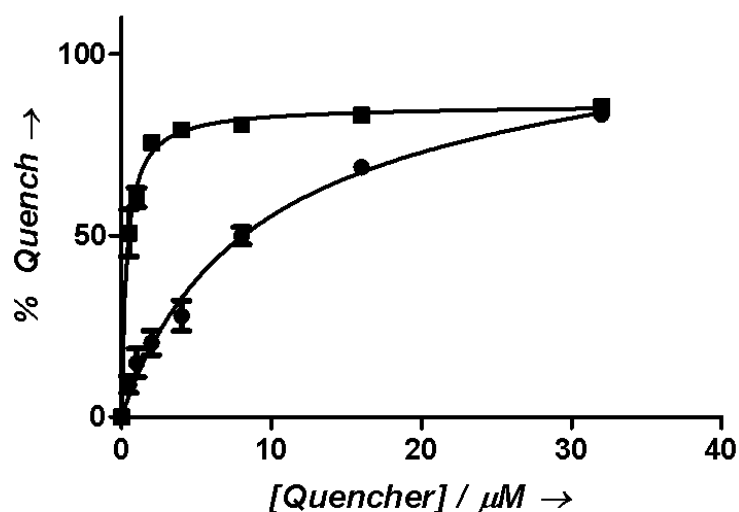


Figure 3.7 Effect of lysates on quenching of Atto633-Aoc-GRTGRRFSY. Fluorescence Quenching of Atto633-Aoc-GRTGRRFSY (1 μ M) by Acid Blue 80 (1) (circles, EQ₅₀ = 8.1 \pm 1.7 μ M) and Evans Blue (2) (squares, EQ₅₀ = 0.35 \pm 0.03 μ M) in the presence of 10% erythrocyte lysate. Reprinted with permission from publisher.^[63]

Selection of fluorophore for lysate and cellular assays. Erythrocytes have a strong absorbance band below 550 nm. Therefore, the fluorophores used to monitor PKA activity were chosen with this in mind. Atto633 and TAMRA labeled peptides were used to measure activity in erythrocyte lysates. We demonstrated (**Figure 3.8**) that PKA activity can be monitored in 10% hematocrit erythrocyte lysates using either fluorophore, but increasing the hematocrit completely abolished the TAMRA labeled peptide signal. Although the fold change is reduced for the Atto633-Aoc-GRTGRRFSY, this may be due to a reduction in the quencher's interaction with the peptide, Atto633-Aoc-GRTGRRFSY was used for future studies as the signal to noise is better.

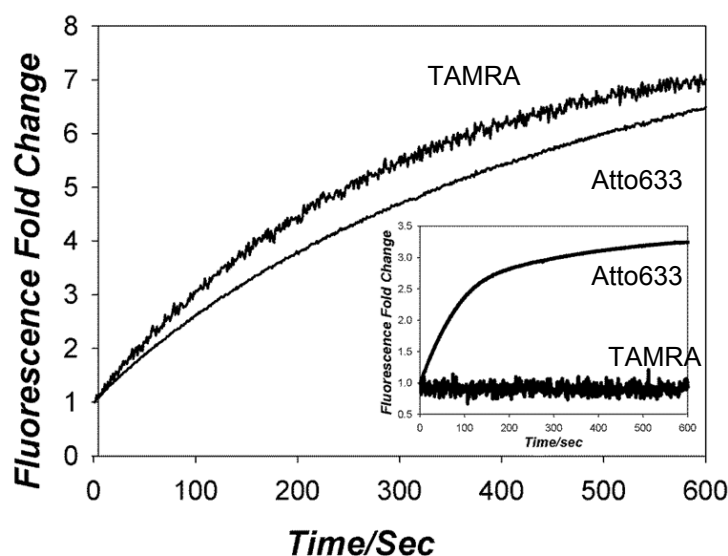


Figure 3.8 Fluorescence increase of Atto633-Aoc-GRTGRRFSY and TAMRA-Aoc-GRTGRRFSY in 10% erythrocyte lysates and in 100% erythrocyte lysates (inset) Reprinted with permission from publisher.^[63]

Demonstrating PKA specificity. PKA inhibitors H89 and KT5720 were used to demonstrate that PKA activity was specifically monitored using our assay. Both H89 and KT5720 inhibit PKA activity in buffer and erythrocyte lysates (**Figure 3.9**). Furthermore, kinase inhibitors not specific to PKA (all used

at 1 μM) did not inhibit activity in lysates (**Figure 3.10**). Gö6938 is known to be a potent PKC inhibitor, but has also been shown to have some ability to inhibit PKA (IC_{50} of 9 μM) which may explain the partial inhibition observed. Lastly, erythrocyte lysates cleared of PKA demonstrated reduced rate of phosphorylation as evidenced by the reduce fluorescence signal. Furthermore, the reduced rate of phosphorylation correlates to the amount of PKA cleared (**Figure 3.11**).

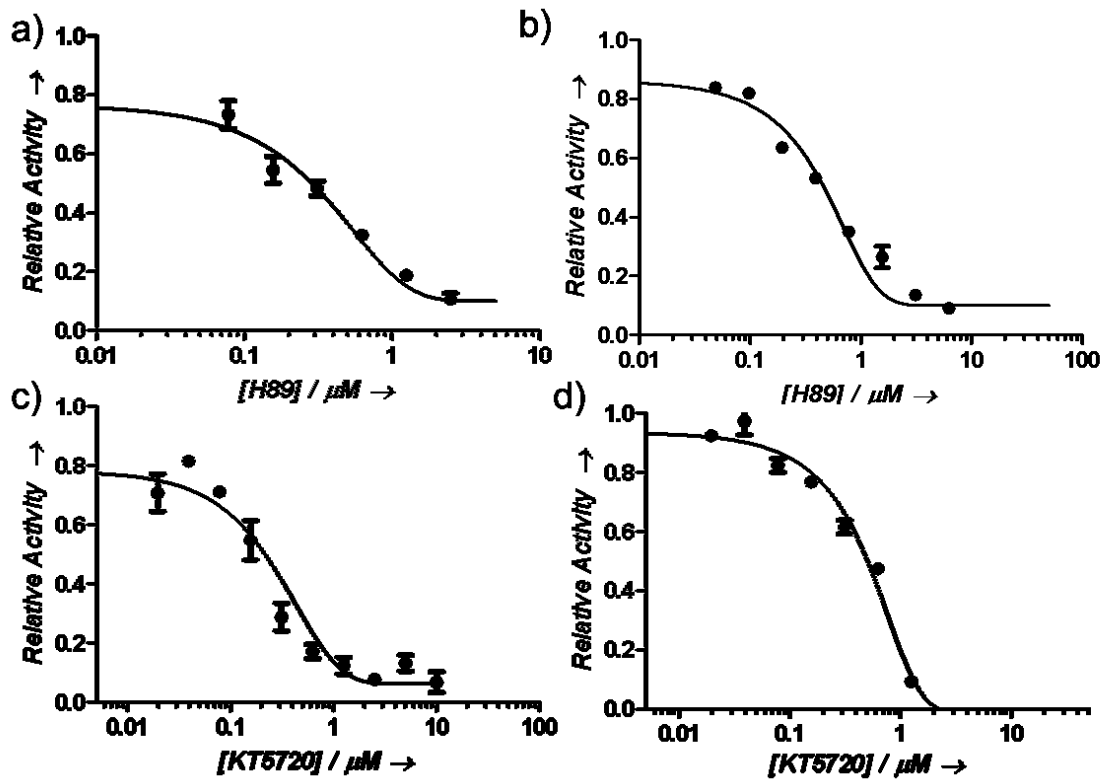


Figure 3.9 Inhibition of PKA activity by specific inhibitor H89 in buffer by (a) H89 and (b) KT5720. IC_{50} (H89) = 430 ± 150 nM; IC_{50} (KT5720) = 610 ± 250 nM. In 10% erythrocyte lysates by (c) H89 and (d) KT5720. 200 μL buffer containing PBS, MgCl_2 (1 mM), ATP (100 μM) 10% erythrocyte lysates IC_{50} (H89) = 1.14 ± 0.17 μM ; IC_{50} (KT5720) = 1.59 ± 0.36 μM . Reprinted with permission from publisher.^[63]

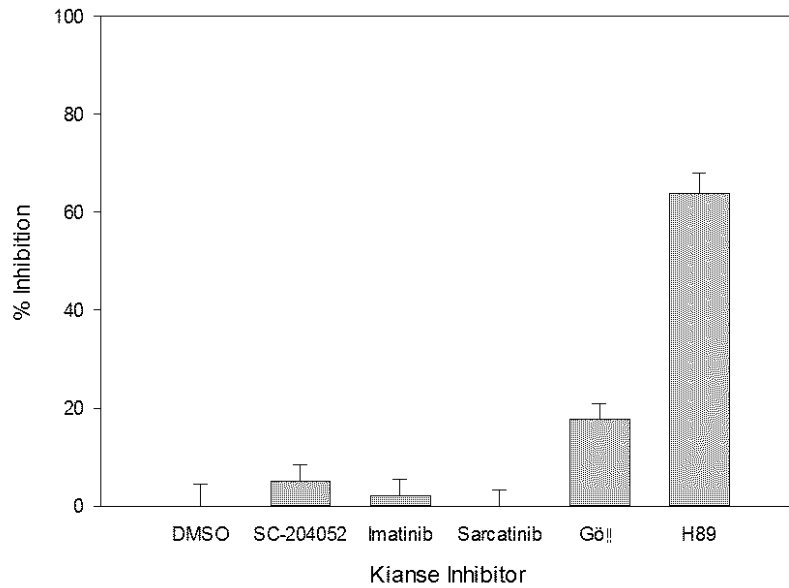


Figure 3.10 Inhibition of erythrocyte PKA activity in lysates using non-specific PKA inhibitors. Reprinted with permission from publisher.^[63]

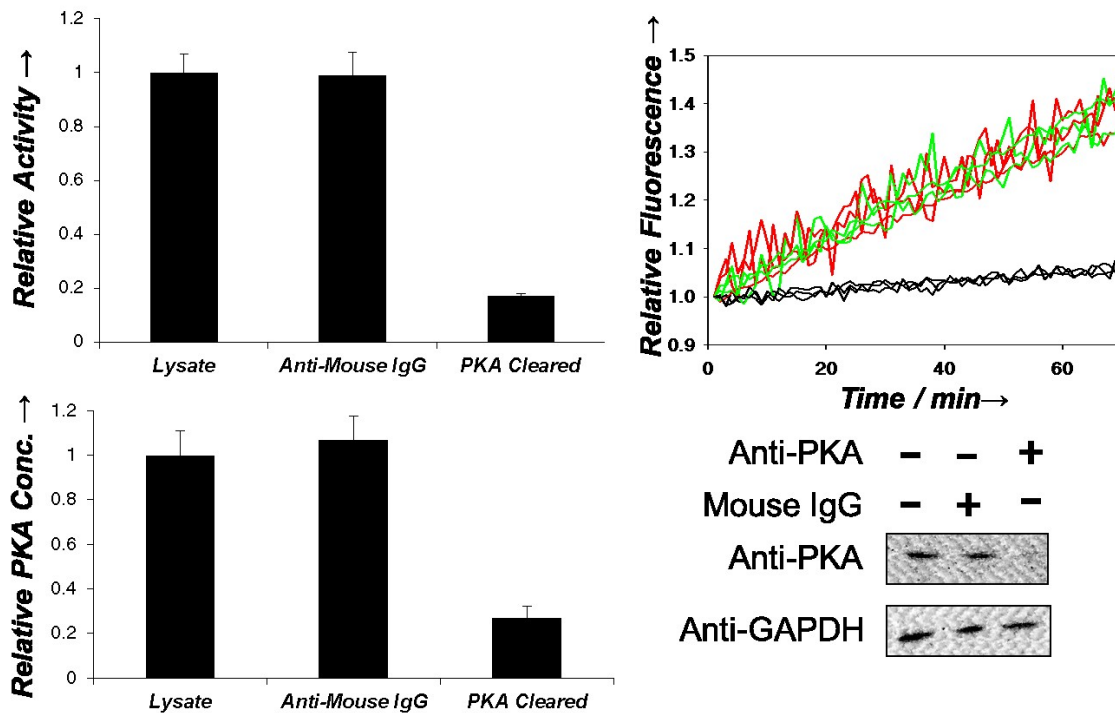


Figure 3.11 Immunodepletion of PKA from erythrocyte lysates. Activity of erythrocytes pre-cleared with a control anti-mouse IgG and lysates pre-cleared with an antibody against the catalytic subunit of PKA (a-b). Erythrocyte PKA levels (c-d) in lysates, lysates pre-cleared with a control anti-mouse IgG, and lysates pre-cleared with an antibody against the catalytic subunit of PKA. Reprinted with permission from publisher.^[63]

Temporal control using DMNB Atto-633 peptide. The GRTGRRFSY peptide was modified to contain a DMNB light cleavable group on the serine hydroxyl moiety, which prevents the serine from being phosphorylated until the DMNB is photocleaved by UV or 405 nm light. The light sensitive compound was determined to not be phosphorylated by PKA until illuminated with light both in buffer and in erythrocyte lysates (**Figure 3.12**).

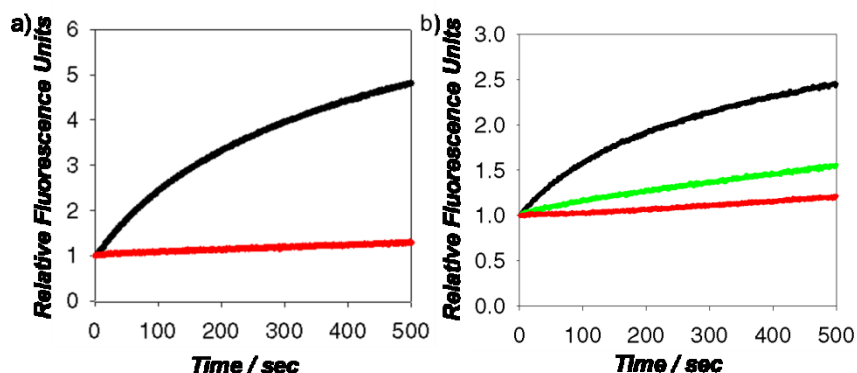


Figure 3.12 Photorelease of Atto633-Aoc-GRTGRRFS(DMNB)Y. (a) Atto633-Aoc-GRTGRRFS(DMNB)Y (1 μ M) and Evans Blue (2 μ M) in PBS buffer in the presence (black, 5 min) and absence (red) of illumination (365 nm for 10 min). PKA-catalyzed phosphorylation was initiated following illumination by the addition of PKA (10 nM). (b) Atto633-Aoc-GRTGRRFS(DMNB)Y (1 μ M) and Evans Blue (2 μ M) in 10% erythrocyte lysate/PBS buffer upon illumination (365 nm, 5 min) in the absence (black, 5 min) and presence of KT5720 (green, 5 μ M) and in the absence of illumination (red). PKA-catalyzed phosphorylation was initiated following illumination by the addition of ATP (1 mM). Reprinted with permission from publisher.^[63]

Loading peptide and quencher into erythrocytes. To determine if PKA activity can be monitored within intact erythrocytes, the light-responsive peptide and quencher were loaded into erythrocytes. As described in Chapter 2 (**Figure 2.7a**) and **Figure 3.13** peptides can be loaded into erythrocytes and microscopy can be used to image fluorescence. Erythrocytes were subsequently loaded with peptide (Atto633-Aoc-GRTGRRFSY) and quencher (Evans Blue) and fluorescence was monitored by flow cytometry (**Figure 3.14**). Erythrocytes

loaded with peptide (Atto633-Aoc-GRTGRRFSY) display a bright fluorescence signal, while erythrocyte loaded with peptide (Atto633-Aoc-GRTGRRFSY) and quencher (Evans Blue) show reduced fluorescent signal indicating quencher and peptide associate in the erythrocytes.

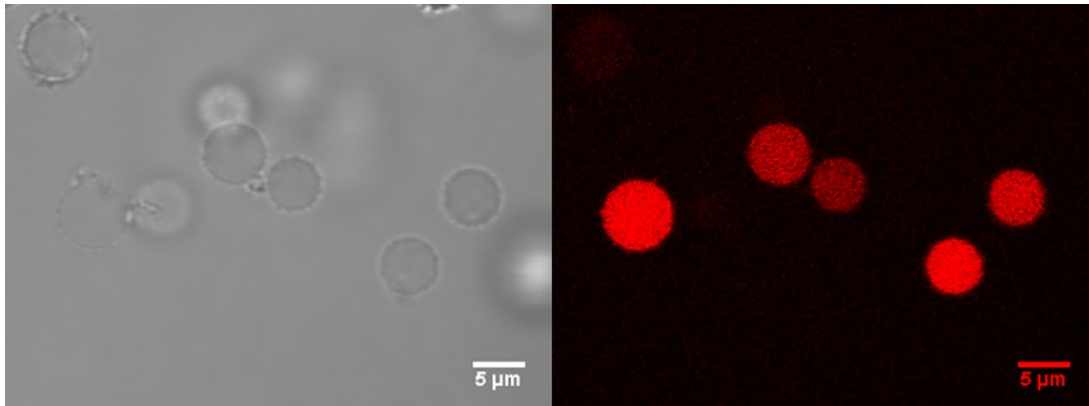


Figure 3.13 Confocal fluorescence images of Atto633-Aoc-GRTGRRFSY loaded peptides. Erythrocyte were loaded with Atto633-Aoc-GRTGRRFSY and imaged by confocal microscopy. Reprinted with permission from publisher.^[63]

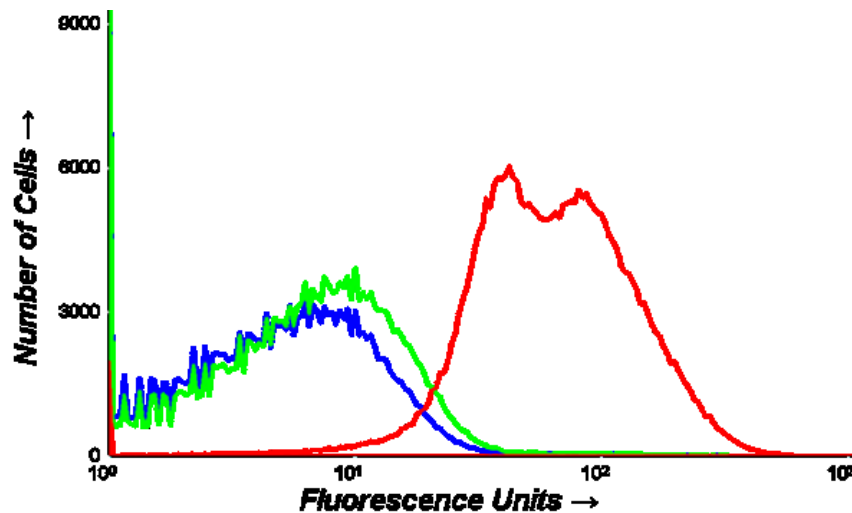


Figure 3.14 Flow cytometry analysis of erythrocytes loaded with Atto633-Aoc-GRTGRRFSY peptide (red), Atto633-Aoc-GRTGRRFSY peptide and Evans Blue (green), and no loading control (blue). Reprinted with permission from publisher.^[63]

Monitoring endogenous PKA activity in erythrocytes. Atto-633

GRTGRRF(DMNB)SY (1 μ M) was loaded into erythrocytes with Evans Blue (2 μ M). Activity was monitored by confocal fluorescence microscopy. 405 nm light was used to initiate the reaction in select cells. **Figure 3.15a** demonstrates that loaded erythrocytes display a fluorescent increase after photolysis, indicating phosphorylation. Similarly, in the presence of PKA inhibitor KT5720 or EDTA no fluorescence change is observed (**Figure 3.15b**). The fluorescent rings around the erythrocytes are most likely due to the negative charge associated with the erythrocyte membranes. The negatively charged quencher is unable to interact with the positively charged peptide at the erythrocyte membrane.

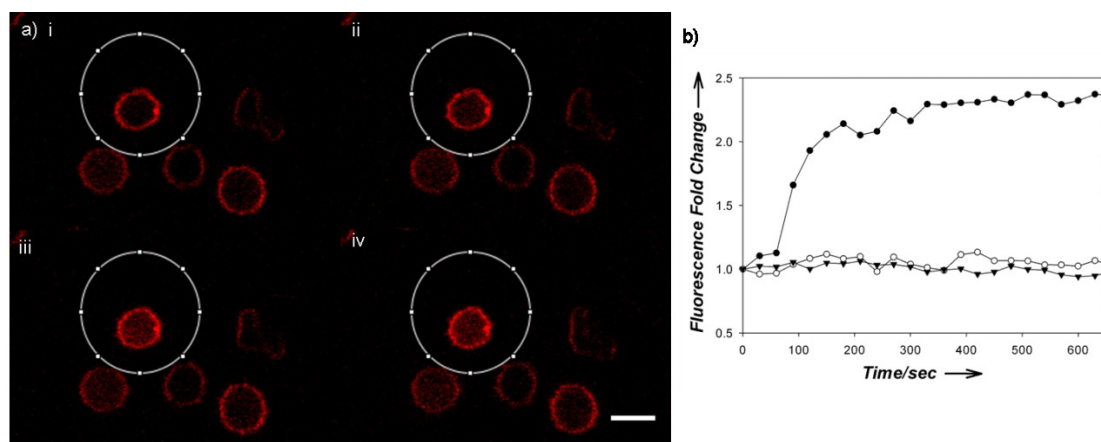


Figure 3.15 Confocal images of Atto633-Aoc-GRTGRRFSY and Evans Blue loaded erythrocytes. Confocal images Atto633-Aoc-GRTGRRFSY and Evans Blue loaded erythrocytes (a) i before photolysis and ii 0.5, iii, 5 and iv 10 min after photolysis. Photolysis was performed with 50 mW, 405 nm laser (2% power level) in tornado mode using a dwell time of 20 μ s/pixel and 25 frames. Imaging was performed with a 100X objective using 635 nm at 4% laser power. Bar = 5 μ m. (b) fluorescence fold change quantitated in confocal images black circles indicate peptide and quencher, white circles indicate not photolysis and black triangles indicate in the presence of cell permeable PKA inhibitor KT5720. Reprinted with permission from publisher.^[63]

Discussion and Future Directions

Assays to monitor erythrocyte kinase activity could be used to elucidate erythrocyte signaling and potentially be used as a diagnostic disease marker. However, the ability to monitor kinase activity in erythrocytes is hindered due to the strong inner filter effect associated with high intracellular concentrations of hemoglobin, which while not evident through small cross sections such as a single red blood cell becomes exceedingly apparent in erythrocytes suspensions (figure 1.9). In order to overcome the inner filter effect we developed a fluorescent assay that uses red-shifted fluorophores (**Figure 1-8**). The developed assay uses a positively charged peptide that interacts with negatively charged quenchers. Upon PKA mediated phosphoryl transfer to the serine in the peptide, the overall charge of the peptide is decreased and the negatively charged quencher no longer interacts with the peptide, and a fluorescent increase is observed. The method should be adaptable to other kinases as a sensor, provided that the recognized peptide sequence is positively charged. We initially screened a 48 member dye library, which covers a wide absorbance range, against two peptide sequences appended with various fluorophores on the N-termini. The two peptide sequences selected were both previously reported to be recognized by PKA. ^[89, 90] All of the peptides we screened identified quenchers that provided robust fluorescent responses. The sequence GRTGRRFSY was selected for further optimization as the hits generally returned higher fluorescence increases after phosphorylation. The quencher that provided the most robust response in the absence of salt was Acid Blue 80, while in the

presence of salt, Evans Blue yielded better results. As a result, both quenchers were tested in the presence of erythrocytes to ensure the quenchers did not induce erythrocyte lysis. Evans Blue was selected as the quencher to use in further studies, as Acid Blue 80 induced significant lysis and had a lower affinity for the peptide. Erythrocytes have been previously demonstrated to contain significant amounts of PKA and its role PKA in erythrocytes has been implicated in controlling localized vasodilation through ATP release and also has been suggested to be important in erythrocyte phosphatidylserine (PS) flipping. With this in mind we first set about determining if erythrocyte PKA activity could be monitored in erythrocyte lysates. **Figure 3.7** demonstrates that PKA activity can be monitored. Furthermore, as previously suggested, fluorophores that have excitation maximum that overlap with the hemoglobin absorbance experience a reduced signal. Atto633-Aoc-GRTGRRFSY was selected to be used in combination with Evans Blue for all PKA activity monitoring. As erythrocytes contain many other kinases, we set about demonstrating that our assay was specifically monitoring PKA activity in lysates. Inhibition of activity in the presence of PKA inhibitors H89 and KT5720 provided strong support that kinase activity is responsible for the fluorescence increase (**Figure 3.9**). Furthermore, activity was not inhibited in the presence of inhibitors that are not specific to PKA (**Figure 3.10**). Lastly, clearing erythrocyte lysates of PKA using anti-PKA reduced the activity by an equal amount (**Figure 3.11**). These results provide strong evidence that the fluorescence activity observed in erythrocyte lysates is a result of PKA phosphorylation. In order to accomplish our goal of monitoring erythrocyte kinase

activity within loaded erythrocytes, we needed to establish control over when the substrate is susceptible to phosphorylation. Having previously demonstrated that light dependent photolysis of a nitrobenzyl group can be accomplished using confocal microscopy (Chapter 2), we modified the peptide serine hydroxyl group with a dimethoxynitrobenzyl (DMNB) group. This group blocks phosphoryl transfer to the hydroxyl group. Indeed, in buffer and in lysates, no phosphorylation is observed in the absence of light (**Figure 3.12**). Lastly, we demonstrated that our system can be loaded into erythrocytes using the method optimized in Chapter 2, and that upon illumination with 405 nm light, fluorescence activity is observed. By contrast, in the presence of KT5720, no fluorescence change is observed.

PKA activity is highly regulated and well understood in nucleated cells. However, PKA activity in erythrocytes remains largely under-studied. The assay developed in this chapter provides a way to fluorescently monitor real-time PKA activity in erythrocyte lysates. We found that erythrocytes stimulated with CPT-cAMP, a cell permeable cAMP analog, contain many downstream proteins that experience dramatic increase in phosphorylation (**Figure 3.14**). Furthermore, PKA has been demonstrated to be localized to the membrane and the cytosol. Other stimulators of erythrocyte kinase activity such as sheer force, epinephrine, norepinephrine, or acetyl salicylic acid may provide selective stimulation to PKA activity.^[91, 92] Our assay combined with proteomic and other physiological studies could be utilized to elucidate the role of PKA in erythrocytes.

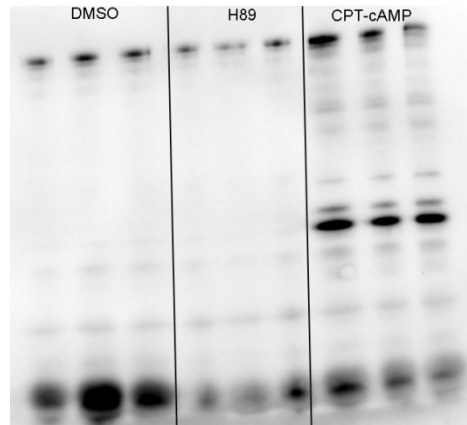


Figure 3.14 Erythrocytes stimulated with DMSO H89 or CPT-cAMP then analyzed by western blot for phosphorylated PKA substrates.

CHAPTER 4: Erythrocyte Mediated Delivery of Anti-inflammatory Therapeutics

OVERVIEW

Controlling drug release with light provides a means of spatial and temporal control of its' pharmacological activity. This, in turn, may help reduce unintended side effects associated with non-selective treatment.^[2, 93] However, current technologies are limited to short wavelength (<450 nm) light or two photon absorption. Short wavelength light is unable to sufficiently penetrate tissue (see Chapter 1), while two photon technology can only release drugs in a very small cross section and requires highly specialized equipment. We have developed a strategy that utilizes cobalamin and a far-red fluorophore as an antenna for light capture and energy transfer to cobalamin. This enables the release of drugs from carriers within the optical window of tissue. Cobalamin-drug conjugates and far-red fluorophores are appended to an octadecyl (C18) which acts to anchor the Cobalamin-drug conjugates to erythrocyte membranes. Analytical and cell based methods were used to demonstrate methotrexate, colchicine, and dexamethasone can be released from erythrocytes in a light dependent manner.

INTRODUCTION

Currently, there are more than 1,500 FDA approved drugs.^[2] However, this seemingly large number of therapeutics is not adequate to treat all known diseases. Recently, it was estimated that there currently exist approximately 555 genes in the human genome that encode proteins that could potentially serve as therapeutic drug targets. Furthermore, clinical trials are currently involved in targeting more than 85% of the known aforementioned targets. However, many of these clinical candidates will not pass efficacy and toxicity studies. When evaluating 108 failed clinical candidates 51% failed due to efficacy and 19% failed due to safety concerns.^[94] Therapeutic efficacy and safety of these drugs can sometimes be improved by utilizing different delivery techniques. Improving drug delivery techniques has the potential to reduce side effects, undesirable immune responses, degradation and elimination while simultaneously improving bioavailability and targeted delivery.^[2, 93] Encapsulation of drugs within liposomes, micelles, nanoparticles, and erythrocytes has been purposed as a possible mechanism to improve bioavailability. Erythrocytes represent one of the most promising tools for reasons discussed in Chapter 1 and have been described as “champions of drug delivery”.^[18]

Using light to activate therapeutic agents is another method that can be used to reduce unintended side effects. Light dependent activation of these agents allows for temporal and spatial control. The therapeutic agents of interest

(photosensitizing agents) are targeted to cells of interest. Upon stimulation with light the photosensitizing agents produce cytotoxic reactive oxygen species that result in cell death.^[41] One of the benefits of this procedure is that cells not targeted with light are not destroyed thereby reducing side effects. This minimally invasive procedure has been demonstrated to be successful in treating cancer while simultaneously reducing side effects.^[41] However, this method is limited in scope to killing cells. Developing a general method to spatially control the release of drugs could provide a new line of treating cancer and other diseases such as diabetes, autoimmune diseases, or vascular diseases by targeting the specific site of disease. One of the largest hurdles in developing a therapy that can be released in a light dependent manner is developing a system that responds to light within the optical window of tissue. However, light between 600 and 950 nm is not able to provide enough energy to activate the pro-drugs described to date.^[64] Others have attempted to circumvent this limitation by using two-photon technology or up converting nanoparticles (particles that absorb longer wavelength light and emit shorter wavelength light), but the challenges associated with these technologies (both have small absorption cross sections) hinder the extent of their current therapeutic applications.^[95-97]

We developed a method using alkylcobalamins that release anti-inflammatory therapeutics using long wavelength light (>600 nm).^[98] Cobalamins do not naturally absorb light above 570 nm. However, covalent modification of these species with far-red and near-IR fluorophores generates cobalamin derivatives that can both capture long wavelength light and use it to release

molecules from the weak Co-alkyl bond (<30 kcal/mol). We demonstrate using C18 modified far-red fluorophores and C18 modified cobalamin-drug conjugates localized to erythrocyte membranes, that transfer energy between the fluorophore and the cobalamin is sufficient to induce drug release.

Our initial efforts have focused on photo-releasing anti-inflammatory agents. The treatment of inflammation in a localized region has the potential for excellent therapeutic enhancement over the current standard of care. Furthermore, erythrocytes are able to readily access areas of inflammation which will increase effectiveness of the drug release. Inflammation results in the destruction of tissue and involves migration of plasma, proteins, fluid, and leukocytes within the diseased area. Migration of proteins and small molecules leads to vasodilation and consequently an increased blood flow.^[99] The aforementioned disruption in tissue homeostasis can result from bacterial infection or exposure to foreign particles.^[100] Alternatively, altered immune response can lead to recognition of endogenous proteins and this can also lead to inflammation. We utilized three commonly prescribed anti-inflammatory compounds; methotrexate (rheumatoid arthritis), colchicine (gout), and dexamethasone (steroid based rheumatoid arthritis treatment) to demonstrate light dependent release of therapeutics from erythrocytes. The three drugs were appended to the lipidated cobalamin and similarly a series of lipidated fluorophores were generated (**Figure 4-1**). The C18 moieties were appended to the 5' ribose –OH of Cbl and drugs or fluorophores were attached to the Co via an amine or carboxylic acid handle. The synthesized compounds were then

added to erythrocytes and demonstrated, via analytical and cell based assays, to be inactive until the appropriate wavelength of light was used to photo release the anti-inflammatory drugs.

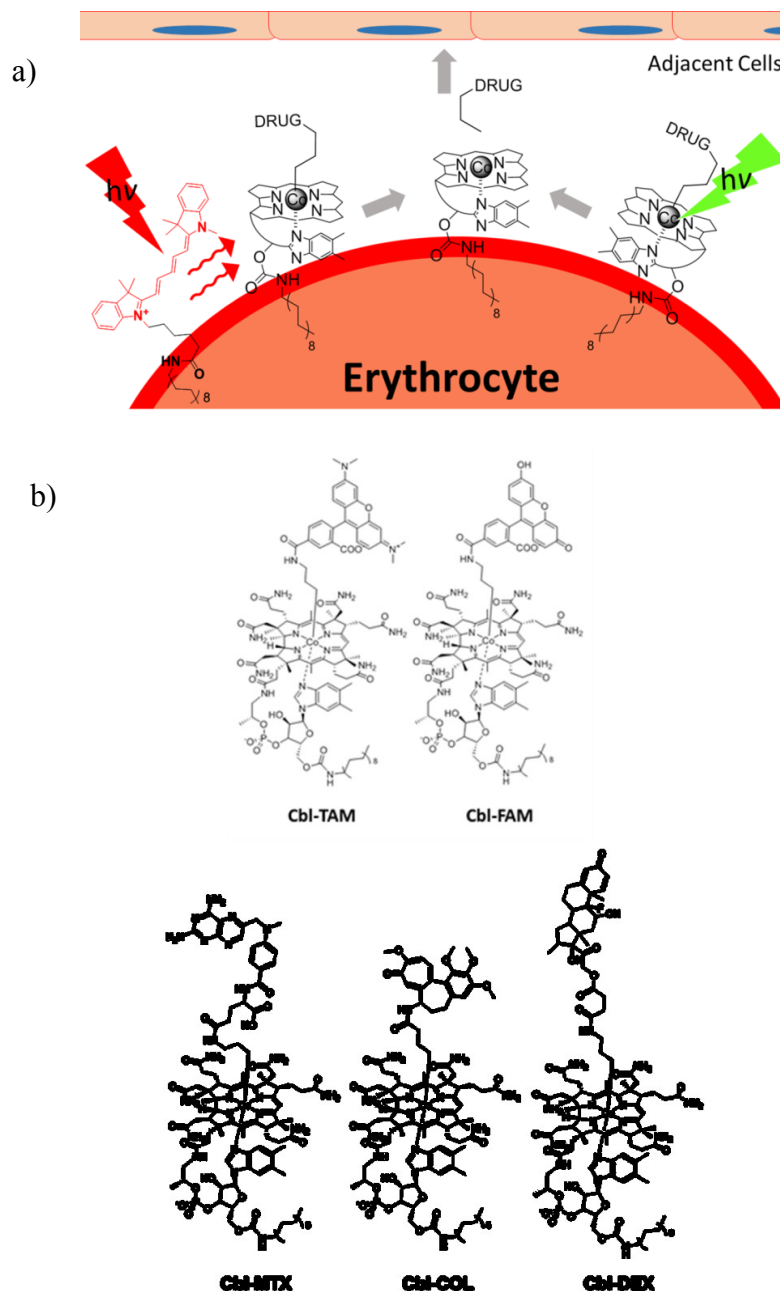


Figure 4.1 Wavelength-encoded drug release strategy. a) Anti-inflammatory drugs are covalently appended to cobalamin (Cbl) via a weak photolabile Co-C bond. Lipidated Cbl and far-red/near-IR fluorophore constructs assemble on the plasma membrane of human erythrocytes. The fluorophore

serves as an antenna, capturing long wavelength light and transmitting it to the Cbl-drug, resulting in drug release from the erythrocyte carrier. b) Cbl-C18 derivatives anchored to erythrocyte membranes

MATERIALS AND METHODS

Materials. Cyanocobalamin was purchased from Lalilabs Inc. Alexa Fluor 700 carboxylic acid, succinimidyl ester was purchased from Life Technologies. All other chemical reagents were purchased from Sigma Aldrich. 8x10 Color Film Gels were manufactured by MacNan and supplied by Amazon. 525 nm and 660 nm LEDs were purchased from LED Supply. 725 nm and 780 nm LEDs were purchased from Techmark. Erythrocytes were purchased from Allcells.

Synthesis (*all compounds were synthesized by Zach Rodgers or Weston Smith. Synthetic steps have been included for clarity*)

Octadecylaminylcyanocobalamin. Cyanocobalamin (200 mg, 148 μmol , mw = 1355) was dissolved in 10 mL anhydrous DMSO and CDT (121 mg, 740 μmol , mw = 164) was added. The solution was stirred for 45 min. To this solution octadecylamine (398 mg, 1.48 mmol, mw = 269) was added to the rapidly stirring solution. The resulting mixture was stirred for 1 h before being added to 90 mL ether/chloroform. The resulting precipitate was collected by centrifugation and decantation. The pellet was dried under vacuum and 10 mL EtOH was added. Dimerized octadecylamine formed a white precipitate which was removed by centrifugation and the cobalamin was precipitated in 40 mL ether/chloroform and collected by centrifugation and decantation. The pellet was dissolved in EtOH

and purified on a 100 g Biotage KP-C18-HS flash column with a linear gradient an H₂O:MeOH gradient from 0 – 100% in 8 column volumes.

Octadecylaminylcyanocobalamin eluted at 100% MeOH. Red solid, 75%, ESI MS calculated for C₈₂H₁₂₅CoN₁₅O₁₅P⁻ (M₂⁺): m/z = 825.98, found 826.81.

3-aminopropyloctadecylaminylcobalamin. The previous compound (100 mg, 61 μmol, mw = 1651) was dissolved in 10 mL of EtOH and degassed under nitrogen. NH₄Br (500 mg, 5% w/v) and Zn powder (200 mg, 3 mmol) were added and the solution was stirred for 20 min under nitrogen. To this slurry 3-chloropropylamine hydrochloride (40 mg, 305 μmol, mw = 130) was added. The resulting mixture was stirred for 3 h under continuous nitrogen flow. A color change from red to orange was observed. Zinc was removed by centrifugation, and the cobalamin was recrystallized twice in ether/chloroform (50 mL). The resulting precipitate was collected by centrifugation and decantation. The pellet was dried under vacuum and 10 mL EtOH was added. UV-Vis analysis revealed the alkylation went to completion. 3-aminopropyloctadecylaminylcobalamin was purified on a 100 g Biotage KP-C18-HS flash column with a linear H₂O:MeOH (0.1% TFA) gradient from 0 – 100% in 8 column volumes. 3-aminopropyloctadecylaminylcobalamin eluted at 100% MeOH. Orange solid, ESI MS calculated for C₈₄H₁₃₃CoN₁₅O₁₅P⁻ (M₂⁺): m/z = 842.96, found 842.2.

Octadecylaminocobalaminbutyrate. Octadecylaminylcyanocobalamin (100 mg, 61 μmol, mw = 1651) was dissolved in 10 mL of EtOH and degassed under nitrogen. NH₄Br (500 mg, 5% w/v) and Zn powder (200 mg, 3 mmol) were added and the solution was stirred for 20 min under nitrogen. To this slurry 4-

chlorobutryic acid (30 μ L, 305 μ mol, mw = 122, d = 1.24) was added. The resulting mixture was stirred for 3 h under continuous nitrogen flow. A color change from red to orange was observed. Zinc was removed by centrifugation, and the cobalamin was recrystallized twice in ether/chloroform (50 mL). The resulting precipitate was collected by centrifugation and decantation. The pellet was dried under vacuum and 10 mL EtOH was added. UV-Vis analysis revealed the alkylation went to completion. Octadecylaminocobalaminbutyrate was purified on a 100 g Biotage KP-C18-HS flash column with a linear gradient an $\text{H}_2\text{O}:\text{MeOH}$ (0.1% TFA) gradient from 0 – 100% in 8 column volumes. Octadecylaminocobalaminbutyrate eluted at 100% MeOH. Orange solid, 82% yeild, ESI MS calculated for $\text{C}_{85}\text{H}_{133}\text{CoN}_{14}\text{O}_{17}\text{P}^-$ (M_2^+): m/z = 855.95, found 856.7.

Methotrexate Octadecylaminylcobalamin (Cbl-MTX). Methotrexate (30 mg, 66 μ mol, mw = 454), N,N,N',N'-tetramethyl-O-(1H-benzotriazol-1-yl)uronium hexafluorophosphate (HBTU, 25 mg, 66 μ mol, mw = 379), and N,N-diisopropylethylamine (DIPEA, 58 μ L, 332 μ mol, mw = 129, d = 0.74) were dissolved in 5 mL of DMF and stirred for five min. 3-aminopropyloctadecylaminylcobalamin (120 mg, 71 μ mol, mw = 1681) was added and the solution was stirred overnight. Because 3-aminopropyloctadecylaminylcobalamin and Cbl-MTX cannot be separated by HPLC, 1,4,5,6,7,7-Hexachloro-5-norbornene-2,3 dicarboxylic anhydride (37 mg, 185 μ mol, mw = 370) was added. The solution was stirred for 30 min and then frozen at -80 $^{\circ}\text{C}$ being careful not to thaw until just before purification. Cbl-MTX

was purified on a Viva C4 preparative column 5 μm , 250 x 21.2 mm from Restek, $\text{H}_2\text{O}:\text{ACN}$, 0.1% TFA, using a gradient elution (elution time 46 min), Orange solid, 37%, ESI MS calculated for $\text{C}_{104}\text{H}_{153}\text{CoN}_{23}\text{O}_{19}\text{P}^-$ (M_2^+): $m/z = 1059.7$, found 1060.3; (M_3^+): $m/z = 706.5$, found 707.2.

Synthesis of Colchicine octadecylaminylcobalamin (Cbl-COL).

Octadecylaminylcyanocobalamin (63 mg, 37 μmol , $\text{mw} = 1681$), HBTU (10 mg, 26 μmol , $\text{mw} = 379$), and DIPEA (15 μL , 86 μmol , $\text{mw} = 129$, $d = 0.74$) were dissolved in 2 mL of DMF and stirred for 5 min. Colchicine (10 mg, 28 μmol , $\text{mw} = 1386$) was added and the solution and was stirred overnight. Cbl-COL was purified on a Viva C4 preparative column 5 μm , 250 x 21.2 mm) from Restek, $\text{H}_2\text{O}:\text{ACN}$, 0.1% TFA, gradient elution (elution time 35 min). Orange solid, ESI MS calculated for $\text{C}_{105}\text{H}_{153}\text{CoN}_{15}\text{O}_{21}\text{P}^-$ (M_2^+): $m/z = 1025.0$, found 1026.5; (M_3^+): $m/z = 683.3$, found 684.5.

Synthesis of Dexamethasone succinyloctadecylaminylcobalamin

(Cbl-DEX). Dexamethasone (6 mg, 12 μmol , $\text{mw} = 492$), HBTU (5 mg, 12 μmol , $\text{mw} = 379$), and TEA (10 μL , 57 μmol , $\text{mw} = 129$, $d = 0.74$) were dissolved in 1 mL of DMF and stirred for 5 min. 3-aminopropyloctadecylaminylcobalamin (30 mg, 18 μmol , $\text{mw}=1681$) was added and the solution was stirred overnight. Cbl-DEX was purified on a Viva C4 preparative column 5 μm , 250 x 21.2 mm) from Restek, $\text{H}_2\text{O}:\text{ACN}$, 0.1% TFA, using a gradient elution (elution time 62 min). Orange solid, ESI MS calculated for $\text{C}_{110}\text{H}_{164}\text{CoN}_{15}\text{O}_{22}\text{P}^-$ (M_2^+): $m/z = 1078.1$, found 1079.3.

Synthesis of 5-TAMRA Octadecylaminylcobalamin (Cbl-TAM).

Tetramethylrhodamine (TAMRA) (5 mg, 12 μ mol, mw = 430), HBTU (4.5 mg, 12 μ mol, mw = 379), and DIPEA (8.3 μ L, 48 μ mol, mw = 129, d = 0.74) were dissolved in 5 mL of DMF and stirred for 5 min. 3-aminopropyloctadecylaminylcobalamin (20 mg, 12 μ mol, mw=1681) was added and the solution was stirred overnight. Cbl-TAM was purified on a Viva C4 preparative column (5 μ m, 250 x 21.2 mm) from Restek, H₂O:ACN, 0.1% TFA, using a gradient elution (elution time 46 min). Red solid, ESI MS calculated for C₁₀₉H₁₅₄CoN₁₇O₁₉P⁻ (M₂⁺): m/z = 1047.5, found 1048.7; (M₃⁺): m/z = 698.3, found 699.3.

Syntheseis of 5-FAM Octadecylaminylcobalamin (Cbl-FAM).

carboxyfluorecein (5-FAM, 5 mg, 12 μ mol, mw = 430), TSTU (3.6 mg, 12 μ mol, mw = 301), and DIPEA (8.3 μ L, 48 μ mol, mw = 129, d = 0.74) were dissolved in 5 mL of DMF and stirred for 5 min. 3-aminopropyloctadecylaminylcobalamin (20 mg, 12 μ mol, mw = 1681) was added and the solution was stirred overnight. Cbl-FAM was purified on a Viva C4 preparative column (5 μ m, 250 x 21.2 mm) from Restek, H₂O:ACN, 0.1% TFA, using a gradient elution (elution time 46 min). Orange solid, ESI MS calculated for C₁₀₄H₁₄₃CoN₁₅O₁₉P⁻ (M₂⁺): m/z = 1020.0, found 1021.5; (M₃⁺): m/z = 680.0, found 681.2.

Synthesis of C18-AF700. Alexa Fluor 700 NHS Ester (1 mg, 1 μ mol, mw = 1086), DIPEA (5 μ L, 29 μ mol, mw = 129, d = 0.74), and C18 (5 mg, 19 μ mol, mw = 269) were dissolved in 500 μ L DMF and mixed by agitation overnight. The resulting mixture was poured into 5:1 H₂O:DCM mixture (5 mL). The DCM layer

was washed with 4 mL H₂O 3x. Purified by flash chromatography silica column (30g). MeOH:DCM (0.1% TFA) linear gradient 0-80%. The purified lipidated fluorophore was concentrated by rotary evaporation.

Synthesis of Cy5 and Cy7 dyes. Cy 5, Cy 7, N-(5-carboxypentyl)-2,3,3-trimethyl indolium-5-sulfonate, and N-(3-sulfopropyl)-2,3,3-trimethyl indolium-5-sulfonate were synthesized as previously described.^[101]

Synthesis of C18-Cy5. Cy 5 (6.2 mg, 12.8 μ mol) and di-isopropyl carbodiimide (2.5 mg, 19.2 μ mol) were dissolved in DCM (320 μ L) and mixed for 5 min. A solution of octadecylamine (6.9 mg) in chloroform (100 μ L) was then added and the solution was allowed to react for 1 h. The solution was diluted with additional DCM (2 mL) and purified via silica gel elution using a binary solvent system (A: DCM, B: MeOH) with an initial A:B ratio of 90:10, gradually increasing to 1:4. Removal of solvent by rotary evaporation yielded a blue-viscous oil (74%, calculated from absorption, λ_{max} : 646 nm) LC-MS ESI MS calculated for C₅₀H₇₆N₃O⁺ (M₂⁺): m/z = 735.16, found 734.6

Synthesis of C18-Cy7. Cy 7 (5.0 mg, 9.8 μ mol) was coupled to octadecylamine similarly to the synthesis of Cy5-C18. Silica gel chromatography using the same A:B solvent gradient afforded a blue-green oil (95.2%, calculated from absorption, λ_{max} : 760 nm) LC-MS ESI MS calc. for C₅₂H₇₈N₃O⁺ (M₂⁺): m/z = 760.61, found 760.6.

Synthesis of Chloro-DY800. N-(5-carboxypentyl)-2,3,3-trimethyl indolium-5-sulfonate (300 mg, 850 μ mol) and 3-chloro-2,4-trimethyleneglutacondianil hydrochloride (305 mg, 850 μ mol) were refluxed in a

solution of acetic acid/acetic anhydride (4 mL, 1:1 ratio) for 2 h. The solvent was then removed under reduced pressure and the residue was re-dissolved in a mixture of pyridine and acetic acid (4 mL, 1:1 ratio). N-(3-sulfopropyl)-2,3,3-trimethyl indolium-5-sulfonate (325 mg, 850 μ mol) was added and the solution was heated to 80 °C for 1 h. The product was then precipitated and washed thrice with ethyl acetate (100 mL). The blue precipitate was dissolved in water and eluted on a Biotage KP-C18-HS column using a binary solvent A:B solvent system (A: Water .1 v/v% TFA, B: CH₃CN .1 v/v% TFA). The A:B ratio was gradually increased from an initial ratio of 19:1 to 2:3. Removal of the solvent by lyophilization yielded a green solid (180 mg, 25% yield, λ_{max} : 794 nm) LC-MS ESI MS calculated. for C₃₉H₄₅ClN₂O₁₁S₃₂⁻ (M2⁺): m/z = 848.43, found 851.3

Synthesis of DY800. Chloro-DY800 (100 mg, 120 μ mol) was dissolved in anhydrous DMF (18 mL) to which was added a solution of sodium phenoxide (139 mg, 1.2 mmol) in DMF (1mL). The solution was stirred for 1 h, and then poured into a vigorously stirring solution of diethyl ether (250 mL). The precipitate was collected and then purified with a Biotage KP-C18-HS column using a binary solvent A:B solvent system (A: Water .1 v/v% TFA, B: CH₃CN .1 v/v% TFA). The A:B ratio was gradually increased from an initial ratio of 19:1 to 2:3. Lyophilization provided the product as a green solid (86 mg, 79% yield, λ_{max} : 774 nm). LC-MS ESI MS calculated for C₄₅H₄₉N₂O₁₂S₃₃⁻ (M2⁺): m/z = 906.07, found 909.2

Synthesis of C18-DY800. DY800 (2.0 mg, 2.2 μ mol) and HCTU (1.4 mg, 3.3 μ mol) were dissolved in anhydrous DMF (500 μ L) and allowed to activate for

5 min. A 500 μ L solution of octadecylamine in chloroform (1 mg/mL) was added and the solution was then mixed for 1 h. The product was extracted into aqueous solution by washing of the organic solution with water (2 x 1 mL). The aqueous phase was then purified by HPLC using a stationary C4 phase with a A:B solvent system (A: Water .1 v/v% TFA, B: CH₃CN .1 v/v% TFA). The A:B ratio was gradually increased from 10:1 to 1:19. The solvent was removed by rotary evaporation to give a blue-green oil (35% yield, λ_{max} : 776 nm in ethanol). LC-MS ESI MS calculated for C₆₃H₈₇N₃O₁₁S₃₂⁻ (M2⁺): m/z = 1158.57, found 1160.6

Quantitation of methotrexate release. 75 μ L samples of MTX suspended in 1x PBS containing 1 mM MgCl₂ were injected onto an 1200 series Agilent HPLC with a UV-Vis detector, 1260 infinity fluorescent detector, and 6110 quadrapole mass spectrometer from a 384 well plate. The mobile phase consisted of H₂O:ACN (0.1% FA) (gradient provided in the following table). The column used was a Viva C4 analytical column 5 μ m, 50 x 21.2 mm from Restek. Concentrations were determined by taking the area under UV absorbance trace at 300 nm from 3.1-3.7 min where the Cbl-MTX cleavage products were shown to elute and this integration was compared to known standards. Mass cutoff was 450 daltons. Fluorescent detector λ_{ex} 365 nm λ_{em} 470 nm to detect known products of light degradation.

Quantitation of colchicine release 75 μ L samples of colchicine suspended in 1x PBS containing 1 mM MgCl₂ were injected onto an 1200 series

Agilent HPLC with a UV-Vis detector, 1260 infinity fluorescent detector, and 6110 quadrupole mass spectrometer from a 384 well plate. The mobile phase consisted of H₂O:ACN (0.1% FA) (gradient provided in the following table). The column used was a Viva C4 analytical column 5 µm, 50 x 21.2 mm from Restek. Concentrations were determined by taking the area under UV absorbance trace at 365 nm from 4.3-4.8 min where the Cbl-COL cleavage products were shown to elute and this integration was compared to known standards. LC gradient is given in the MTX LC-MS Assay.

Quantitation of dexamethasone release. 120 µL samples of dexamethasone suspended in 1x PBS containing 1 mM MgCl₂ were boiled for 10 min to denature and precipitate any protein and lipids in solution. Protein was then pelleted by centrifugation at 21,000 rcf. Samples of 75 µL were injected onto a 1200 series Agilent HPLC with a UV-Vis detector, 1260 infinity fluorescent detector, and 6110 quadrupole mass spectrometer from a 384 well plate. The mobile phase consisted of H₂O:ACN (0.1% FA) (gradient provided in Table S2). The column used was a Viva C4 analytical column 5 µm, 50 x 21.2 mm from Restek. Concentrations were determined by taking the area under UV absorbance trace at 239 nm from 4.5-4.9 min where the Cbl-DEX cleavage product was shown to elute and this integration was compared to known standards. LC gradient is given in the MTX LC-MS Assay.

Octanol / water partition MTX. Cbl-MTX was added to 100 μ L octanal to a final concentration of 5 μ M and was thoroughly mixed with 1x PBS (500 μ L) in a 1.5 mL clear centrifuge tube and allowed to equilibrate for 30 min in the dark before undergoing centrifugation for 10 min at 21,000 g. Samples were photolyzed with a 525 nm LED for 0 min, 1 min, 2 min, 5 min, 10 min, and 20 min before being mixed by shaking and allowed to equilibrate for 15 min. This was followed by a 10 min centrifugation at 21,000 g. The octanol layer was removed and 100 μ L aliquots were taken from the remaining aqueous layer and loaded onto a 384 well plate. The concentrations of was determined by the MTX LC-MS assay.

Octanol / water partition TAMRA. Cbl-TAM was added to 100 μ L octanal to a final concentration of 10 μ M and was thoroughly mixed with 1x PBS (300 μ L) in a 1.5 mL clear centrifuge tube and allowed to equilibrate for 30 min in the dark before undergoing centrifugation for 10 min at 21,000 g in a quartz fluorescence cuvette with a 200 μ L viewing window. The fluorescence of the aqueous layer was measuring using a PTI Model 710 LPS-220 (ex: 555 nm em: 570-600 nm). The solution was transferred to a clear 1.5 mL centrifuge tube and photolyzed using a 525 nm centered LED array for 0 min, 1 min, 2 min, 3 min, and 10 min. The solutions were transferred back to the cuvette for 10 min centrifugation at 21,000 g and the fluorescence was measured again. All samples were measured in triplicate.

Erythrocyte sample preparation and storage. Erythrocytes were washed 3x in 1x PBS containing 1 mM MgCl_2 and diluted to 10% hematocrit. Storage was in RBC Buffer (1x PBS, 1mM MgCl_2) for one no more than month at 4°C.

Erythrocyte loading procedure. To 10% hematocrit erythrocytes, lipidated compounds were added at various loading concentrations (depending on the assay). The erythrocytes were then incubated at RT for 20 min and subsequently washed 3x in 1x PBS containing 1 mM MgCl_2 and then stored at 10% hematocrit in RBC buffer. RBCs were used within 48 h.

Widefield microscopy with Cbl-TAM loaded erythrocytes. 10% hematocrit erythrocytes were loaded with 10 μM Cbl-TAM using the erythrocyte loading procedure. 2 μL of loaded erythrocytes were then added to 200 μL RBC buffer and imaged using widefield microscopy. Images were taken using 20 μs exposure times and a Cy3 filter cube 333 ms apart.

Erythrocyte lysis assay. To a 1.5 mL centrifuge tube containing 100 μL of a cobalamin drug complex (Cbl-MTX, Cbl-COL, or Cbl-DEX) in PBS at various concentrations (5 μM , 10 μM , 20 μM , and 40 μM) was added 100 μL RBCs in RBC buffer (10% hematocrit). Three additional samples contained 100 μL RBCs treated with 100 μL PBS. Three samples contained 0.1% SDS before RBCs were added. Final concentrations were 0.05% SDS; 0 μM , 2.5 μM , 5 μM , 10 μM ,

and 20 μM lipidated complex. Cells were mixed by flicking before centrifugation at 300 g for 30 min. Samples were re-homogenized and allowed to incubate at 4 $^{\circ}\text{C}$ overnight. Samples were pelleted at 1000 g for 5 min. 150 μL of the supernatant was plated on a 96 well plate and analyzed at 550 nm by UV Vis. SDS samples had to be diluted 10 fold to be measured accurately. SDS absorbance multiplied by 10 was considered to be complete hemolysis and PBS treated blood was considered to be completely intact and the absorbance from those samples was subtracted from the background of the rest.

Erythrocytes drug loading capacity. Using the erythrocyte loading procedure different concentration of Cbl-MTX, Cbl-COL, and Cbl-DEX were added to 10% hematocrit RBCS. Cbl-MTX was loaded at 6 μM , 4 μM , 2 μM , and 1 μM . Cbl-COL was loaded at 10 μM , 8 μM , 6 μM , 4 μM , and 2 μM . The cells were diluted to 5% hematocrit and photolyzed for 2 h under 525 nm centered LEDs and then spun down at 1000 g. Concentration was quantitated by LC-MS.

DHFR inhibition assay. Dihydrofolate reductase activity was monitored using the Sigma Dihydrofolate Reductase Assay Kit. This kit was used to monitor conversion of NADPH to NADP^{+} . Briefly, assay buffer was prepared containing 1.5 mU DHFR, 100 μM NADPH, and 1x assay buffer (provided with kit). Inhibition of DHFR activity at various concentrations MTX or photolyzed Cbl-MTX (between 100 nm and 5 μM) was monitored using a fluorescent plate reader (Ex: 340 nm Em: 450 nm).

(Cell work completed by Robert Hughes)

Colchicine HeLa cell assay. HeLa cells were plated in a 6-well glass bottom plate (Mattek) at a density of 1.5×10^5 cells per well and maintained at 37 °C in a humidity-controlled incubator with a 5% CO₂ atmosphere in DMEM (10% FBS, 1% Pen-Strep). The following day, cells were treated with colchicine (Sigma C9754; 1 mM stock in DMSO) or DMSO for either 30 min or 1 h at 37 °C in a humidity-controlled incubator. At the conclusion of the incubation period, cells were fixed with 1 mL of methanol at room temperature for 10 min. Cells were washed 2x 1 mL with PBS and blocked for 1 h in 5% Donkey Serum. Blocking was followed by overnight incubation at 4 °C with mouse anti-tubulin antibody (Cell Signaling 3873S) at 1:100 dilution in antibody dilution buffer (1% BSA; 0.3% Triton-X-100; PBS). Cells were then washed with PBS (3x 5 min) before incubation with anti-mouse AlexaFluor 488 secondary antibody (Life Technologies A21202) at 1:500 dilution in antibody dilution buffer. After washing cells with PBS (3x 5 min), images were acquired with an inverted Olympus IX81 microscope equipped with a Hamamatsu C8484 camera, 40X phase contrast objective and a FITC filter cube (Semrock). Metamorph software was employed for imaging analysis.

Treatment of HeLa cells with Cbl-COL loaded erythrocytes. HeLa cells were plated in 24-well glass bottom plates (Mattek) at a density of 3.3×10^4 cells per well and maintained at 37 °C in a humidity-controlled incubator with a 5% CO₂ atmosphere in DMEM (10% FBS, 1% Pen-Strep). The following day, cells

were washed 2x with PBS, followed by the addition of 100 μ L of L-15 media. Cells were then treated with 250 μ L of a suspension of Cbl-COL loaded red blood cells in PBS (6 μ M loading concentration at 5% hematocrit) or 250 μ L PBS (control cells). Cells were then either kept in the dark at 37 °C in a humidity-controlled incubator, or exposed to 530 nm LED flood light (PAR38; 500 – 570 nm emission; 5 mW power) for 5, 10, or 20 min at room temperature. All cells incubated for 1 h in a 37 °C in a humidity-controlled incubator post-photolysis. At the conclusion of the incubation period, cells were washed 3 x 1 mL with PBS and then fixed with 1 mL of methanol at room temperature for 10 min. Cells were washed 2 x 1 mL with PBS and blocked for 1 h in 5% Donkey Serum. Blocking was followed by overnight incubation at 4 °C with mouse anti-tubulin antibody (Cell Signaling 3873S) at 1:100 dilution in antibody dilution buffer (1% BSA; 0.3% Triton-X-100; PBS). Cells were then washed with PBS (3 x 5 min) before incubation with anti-mouse AlexaFluor 488 secondary antibody (Life Technologies A21202) at 1:500 dilution in antibody dilution buffer. After washing cells with PBS (3x 5 min), images were acquired with an inverted Olympus IX81 microscope equipped with a Hamamatsu C8484 camera, 40X phase contrast objective and a FITC filter cube (Semrock). Metamorph software was employed for imaging analysis.

Treatment of HeLa cells with dexamethasone. HeLa cells were plated in a 6-well glass bottom plate (Mattek) at a density of 7.5×10^4 cells per well and maintained at 37 °C in a humidity-controlled incubator with a 5% CO₂

atmosphere in DMEM (10% FBS, 1% Pen-Strep). The following day, cells were treated with varying concentrations of dexamethasone (1 mM stock in DMSO) or DMSO for 1 h at 37 °C in a humidity-controlled incubator. At the conclusion of the incubation period, cells were fixed with 4% PFA in PBS for 10 min at room temperature, then washed 1x with PBS, and then treated with 1 mL of methanol at room temperature for 5 min. Cells were washed 2 x 1 mL with PBS and subsequently incubated overnight at 4 °C with rabbit anti-GR α antibody (abcam 3580) at 1:100 dilution in antibody dilution buffer (1% BSA; 0.3% Triton-X-100; PBS). Cells were then washed with PBS (3 x 5 min) before incubation with anti-rabbit AlexaFluor 488 secondary antibody (Life Technologies A21206) at 1:500 dilution in antibody dilution buffer for 1 h at room temperature. Cells were washed with PBS (3 x 5 min) and Hoescht 33342 (100 μ g/mL in PBS) applied for 30 min before an additional wash with PBS. Images were subsequently acquired with an inverted Olympus IX81 microscope equipped with a Hamamatsu C8484 camera, 40X phase contrast objective and a FITC filter cube (Semrock). Metamorph software was employed for imaging analysis.

Treatment of HeLa cells with Cbl-DEX loaded erythrocytes. HeLa cells were plated in 12-well glass bottom plates (Mattek) at a density of 2.5×10^4 cells per well and maintained at 37 °C in a humidity-controlled incubator with a 5% CO₂ atmosphere in DMEM (10% FBS, 1% Pen-Strep). The following day, cells were washed 2x with PBS, then treated with 500 μ L of a suspension of Cbl-DEX loaded red blood cells in L-15 media (1 μ M loading concentration at 5%

hematocrit) or 500 μ L L-15 (control cells). Cells were then either kept in the dark at 37 °C in a humidity-controlled incubator, or exposed to 530 nm LED flood light (PAR38; 500 – 570 nm emission; 5 mW power) for 10, 20, or 30 min at room temperature. All cells incubated for 1 h in a 37 °C in a humidity-controlled incubator post-photolysis. At the conclusion of the incubation period, cells were washed 3 x 1 mL with PBS and then fixed with 4% PFA in PBS for 10 min at room temperature, then washed 1x with PBS and treated with 1 mL of methanol at room temperature for 5 min. Cells were subsequently washed 2 x 1 mL with PBS and then incubated overnight at 4 °C with rabbit anti-GR α antibody (abcam 3580) at 1:100 dilution in antibody dilution buffer (1% BSA; 0.3% Triton-X-100; PBS). Next, cells were washed with PBS (3 x 5 min) before incubation with anti-rabbit AlexaFluor 488 secondary antibody (Life Technologies A21206) at 1:500 dilution in antibody dilution buffer for 1 h at room temperature. Cells were finally washed with PBS (3 x 5 min). Images were subsequently acquired with an inverted Olympus IX81 microscope equipped with a Hamamatsu C8484 camera, 40X phase contrast objective and a FITC filter cube (Semrock). Metamorph software was employed for imaging analysis.

Demonstrating TAMRA and fluorescein release from erythrocyte membranes upon photolysis. Erythrocytes were taken from 10% hematocrit stock solutions. RBCs were loaded with 1 μ M Cbl-TAM or Cbl-FAM according to the established procedure. For those experiments requiring lipidated fluorophores, 5 μ M were also loaded from stock solutions in DMSO.

Erythrocytes were re-suspended to 10% hematocrit and exposed to LEDs centered at varying wavelengths for set time points. After photolysis, the erythrocyte solution was centrifuged at 1,000 g and the supernatant was analyzed for TAMRA (Ex: 550 nm Em: 580 nm) or fluorescein (Ex: 492 nm Em: 519 nm) release using a fluorescent plate reader.

Cbl-DEX light independent translocation test. HeLa cells were plated in 6 well glass bottom plates (Mattek) at a density of 8.8×10^4 cells per well and maintained at 37 °C in a humidity-controlled incubator with a 5% CO₂ atmosphere in DMEM (10% FBS, 1% Pen-Strep). The following day, cells were washed 2x with PBS, then treated with 250 µL of a suspension of Cbl-DEX loaded red blood cells in L-15 media (1 µM loading concentration at 5% hematocrit) or 250 µL L-15 (control cells). Cells were then incubated in the dark for 1 h at 37 °C in a humidity-controlled incubator. After the 1 h pre-incubation, cells were washed 3x 1 mL with PBS (dark room; red safe light) and 2 mL of L-15 added to each well. The washed cells were then exposed to a green LED light source (PAR38; 500 – 570 nm emission; 5 mW power) or kept in the dark for 15 min at room temperature. All cells incubated for 1 h in a 37 °C in a humidity-controlled incubator post-photolysis. At the conclusion of the second incubation period, cells were washed 3x 1 mL with PBS and then fixed with 4% PFA in PBS for 10 min at room temperature, then washed 1x with PBS and treated with 1 mL of methanol at room temperature for 5 min. Cells were subsequently washed 2x 1 mL with PBS and then incubated overnight at 4 °C with rabbit anti-GRα

antibody (abcam 3580) at 1:100 dilution in antibody dilution buffer (1% BSA; 0.3% Triton-X-100; PBS). Next, cells were washed with PBS (3 x 5 min) before incubation with anti-rabbit AlexaFluor 488 secondary antibody (Life Technologies A21206) at 1:500 dilution in antibody dilution buffer for 1 h at room temperature. Cells were finally washed with PBS (3x 5 min). Images were subsequently acquired with an inverted Olympus IX81 microscope equipped with a Hamamatsu C8484 camera, 40X phase contrast objective and a FITC filter cube (Semrock). Metamorph software was employed for imaging analysis.

Determining the ratio of Cbl-TAM to C18-Cy5 for optimal release of Tetramethylrhodamine. To 10% hematocrit erythrocytes, various concentrations of Cbl-TAM (0 to 10 μ M) and various concentrations of C18-Cy5 were added (0 to 20 μ M). Erythrocytes were photolyzed using a 660 nm LED board for 30 min. After photolysis, erythrocytes were spun down at 1,000 g for 3 min and the supernatant was analyzed for tetramethylrhodamine (Ex: 550 Em: 580) release using a fluorescent plate reader.

$$Photon\ Flux\ \left\langle \frac{\mu mol\ photons}{m^2 s} \right\rangle = \frac{\left\langle \frac{P}{m^2} \right\rangle}{h\nu \times 6.022 \times 10^{17}}$$

Light power measurements. All light measurements were recorded with a Coherent Field Max II. Each measurement is reported as the average of 10 readings and the error is reported as the standard deviation. The measurements were recorded using the same distance and light configurations as the samples.

Confocal images of erythrocytes loaded with C18-Cy5. To 10% hematocrit erythrocytes C18-Cy5 was loaded at a concentration of 5 μ M using the erythrocyte loading procedure. 2 μ L of loaded erythrocytes were then added to 200 μ L RBC buffer and imaged using confocal microscopy. Images were taken using 4% laser power, 1000 hv, and 10 μ s/pixel in line scan mode and a 635 nm laser.

Methotrexate NIR photolysis from erythrocyte membranes. Cbl-MTX and either C18-Cy5, C18-AF700, C18-Cy7, C18-DY800 were loaded with a concentration of 1 μ M and 5 μ M respectively to 10% hematocrit erythrocytes. After the loading erythrocytes were re-suspended to 5% hematocrit and exposed to 660 nm, 725 nm, or 780 nm centered LEDs 30 min. Other loaded erythrocytes were photolyzed for 2 h using 525 nm LEDs to free all bound MTX to assess the total amount of drug loaded. After photolysis, the erythrocyte solution was centrifuged at 1,000 g and the supernatant was analyzed for by the methotrexate LC/MS assay.

Dexamethasone and colchicine NIR photolysis from erythrocyte membranes. Cbl-COL (loading concentration of 5 μ M) or Cbl-DEX (final concentration of 0.5 μ M) were loaded with either C18-DY800 or C18-Cy5 fluorophore to 10% hematocrit erythrocytes. C18-DY800 was added to a final concentration of 5 and 2.5 μ M for the Cbl-COL and Cbl-DEX erythrocytes respectively. C18-Cy5 was added to a final concentration of 25 and 2.5 μ M for

the Cbl-COL and Cbl-DEX erythrocytes respectively. Erythrocytes were re-suspended to 5% hematocrit. The C18-DY800 samples were exposed to 525 nm LEDs for 2 h or 780 nm LEDs for 0 and 30 min and the C18-Cy5 were exposed to 525 nm and 660 nm LEDs in similar fashion. After photolysis, the erythrocyte solution was centrifuged at 1,000 g and the supernatant was analyzed for Col or Dex release by LC/MS. Baseline was determined by analyzing erythrocyte lacking the cobalamated drugs.

Treatment of HeLa cells with Cbl-DEX /C18-Cy5 loaded erythrocytes.

HeLa cells were plated in 35 mm glass bottom dishes (Mattek) at a density of 1.0×10^5 cells per well and maintained at 37 °C in a humidity-controlled incubator with a 5% CO₂ atmosphere in DMEM (10% FBS, 1% Pen-Strep). The following day, cells were washed 3x with PBS, then treated with 200 μ L of a suspension of Cbl-DEX /C18-Cy5 (0.5 μ M / 2.5 μ M) loaded red blood cells in L-15 media (5% hematocrit) or 200 μ L L-15 (control cells). The cells were either kept in the dark or exposed to a 660 nm LED array for 10, 20, or 30 min using the appropriate filter sets. All cells were placed in a 37 °C in a humidity-controlled incubator post-photolysis until harvest 1 h after the end of the last photolysis interval. Cells were washed 3 x 1 mL with PBS and then fixed with 4% PFA in PBS for 10 min at room temperature, then washed 1x with PBS and treated with 1 mL of methanol at room temperature for 5 min. Cells were subsequently washed 2 x 1 mL with PBS and then incubated overnight at 4 °C with rabbit anti-GR α antibody (abcam 3580) at 1:100 dilution in antibody dilution buffer (1% BSA; 0.3% Triton-

X-100; PBS). Next, cells were washed with PBS (3x 5 min) before incubation with anti-rabbit AlexaFluor 488 secondary antibody (Life Technologies A21206) at 1:500 dilution in antibody dilution buffer for 1 h at room temperature. Cells were finally washed with PBS (3 x 5 min). Images were subsequently acquired with an inverted Olympus IX81 microscope equipped with a Hamamatsu C8484 camera, 60X oil objective and a FITC filter cube (Semrock). Metamorph software was employed for imaging analysis.

Treatment of HeLa cells with Cbl-COL /C18-Cy5 loaded erythrocytes.

HeLa cells were plated in 35 mm glass bottom dishes (Mattek) at a density of 1.0×10^5 cells per well and maintained at 37 °C in a humidity-controlled incubator with a 5% CO₂ atmosphere in DMEM (10% FBS, 1% Pen-Strep). The following day, cells were washed 3x with PBS, then treated with 200 µL of a suspension of Cbl-COL/C18-Cy5 (5 µM/25 µM) loaded red blood cells in L-15 (5% hematocrit) or 200 µL L-15 (control cells). Cells were then either kept in the dark at 37 °C in a humidity-controlled incubator, or exposed to a 660 nm LED array for 10, 20, or 30 min using the appropriate filter sets. All cells incubated for 1 h in a 37 °C in a humidity-controlled incubator post-photolysis. At the conclusion of the incubation period, cells were washed 3x 1 mL with PBS and then fixed with 1 mL of methanol at room temperature for 10 min. Cells were washed 2x 1 mL with PBS and blocked for 1 h in 5% donkey serum. Blocking was followed by overnight incubation at 4 °C with mouse anti-tubulin antibody (Cell Signaling 3873S) at 1:100 dilution in antibody dilution buffer (1% BSA; 0.3% Triton-X-100; PBS).

Cells were then washed with PBS (3x 5 min) before incubation with anti-mouse AlexaFluor 488 secondary antibody (Life Technologies A21202) at 1:500 dilution in antibody dilution buffer. After washing cells with PBS (3x 5 min), images were acquired with an inverted Olympus IX81 microscope equipped with a Hamamatsu C8484 camera, 60X oil objective and a FITC filter cube (Semrock). Metamorph software was employed for imaging analysis.

Treatment of HeLa cells with Cbl-COL/DY800 loaded erythrocytes.

HeLa cells were plated in 35 mm glass bottom dishes (Mattek) at a density of 1.0×10^5 cells per well and maintained at 37 °C in a humidity-controlled incubator with a 5% CO₂ atmosphere in DMEM (10% FBS, 1% Pen-Strep). The following day, cells were washed 3x with PBS, then treated with 200 µL of a suspension of Cbl-COL/DY800 (5 µM/5 µM) loaded red blood cells in L-15 (5% hematocrit) or 200 µL L-15 (control cells). Cells were then either kept in the dark at 37 °C in a humidity-controlled incubator, or exposed to a 660 nm LED array for 10, 20, or 30 min using the appropriate filter sets. All cells incubated for 1 h in a 37 °C in a humidity-controlled incubator post-photolysis. At the conclusion of the incubation period, cells were washed 3x 1 mL with PBS and then fixed with 1 mL of methanol at room temperature for 10 min. Cells were washed 2x 1 mL with PBS and blocked for 1 h in 5% donkey serum. Blocking was followed by overnight incubation at 4 °C with mouse anti-tubulin antibody (Cell Signaling 3873S) at 1:100 dilution in antibody dilution buffer (1% BSA; 0.3% Triton-X-100; PBS). Cells were then washed with PBS (3 x 5 min) before incubation with anti-mouse

AlexaFluor 488 secondary antibody (Life Technologies A21202) at 1:500 dilution in antibody dilution buffer. After washing cells with PBS (3 x 5 min), images were acquired with an inverted Olympus IX81 microscope equipped with a Hamamatsu C8484 camera, 60X oil objective and a FITC filter cube (Semrock). Metamorph software was employed for imaging analysis.

CETSA assay of HeLa cells treated with Cbl-MTX loaded

erythrocytes. HeLa cells were plated in 12-well tissue culture plates at a density of 9.4×10^4 cells per well and maintained at 37 °C in a humidity-controlled incubator with a 5% CO₂ atmosphere in DMEM (10% FBS, 1% Pen-Strep). The following day, cells were washed 3x with PBS, then treated with 300 µL of a suspension of Cbl-MTX loaded red blood cells in L-15 (5 µM methotrexate loading concentration at 5% hematocrit), 300 µL L-15 (control cells), or 300 µL L-15 with 10 µM methotrexate (positive control). Cells were then either kept in the dark at 37 °C in a humidity-controlled incubator, or exposed to a green LED light source (PAR38; 500 – 570 nm emission; 5 mW power) for 10, 20, or 30 min. At the end of the photolysis interval, all cells were incubated for 1 h in a 37 °C in a humidity-controlled incubator. Next, cells were washed 3x 1 mL with PBS and trypsinized with 300 µL 0.05% Trypsin (Gibco) for 5 min at 37 °C. Trypsinized cells were then pelleted (5 min, 2000 rpm, 4 °C), washed 1 x 300 µL PBS, and then pelleted again. After removal of the supernatant, cell pellets were heated at 52 °C in a temperature controlled heat block for 3 min, and then cooled for 3 min at room temperature. 30 µL of lysis buffer (25 mM Tris HCl/2 mM DTT/1X Pierce

HALT protease and phosphatase inhibitor) was added to each pellet, which were then subjected to 2 freeze-thaw cycles in liquid N₂. The resulting solutions were then spun at 17000 g from 20 min at 4 °C. The resulting supernatants were removed and combined with 6X LSB-BME and boiled for 4 min at 95 °C, then analyzed by western blot (Overnight incubation at 4 °C with Santa Cruz anti-DHFR E18 primary antibody(1:1000 in TBST/5%BSA) and Cell Signaling anti-GAPDH antibody (1:2000), followed by incubation with the appropriate secondary antibodies.

RESULTS

Water-octanol demonstration of release from cobalamin. The water-octanol experiment seeks to mimic the layer between the erythrocyte membrane and the surrounding buffered solution. To demonstrate that the Cbl-C18 derivatives stay in the octanol (lipid-like) layer until illumination, TAMRA-Cbl-C18 and MTX-Cbl-C18 were incubated in octanol and mixed with PBS buffer. After illumination both TAMRA (**Figure 4.2**) and MTX (**Figure 4.3**) were observed in the aqueous layer.

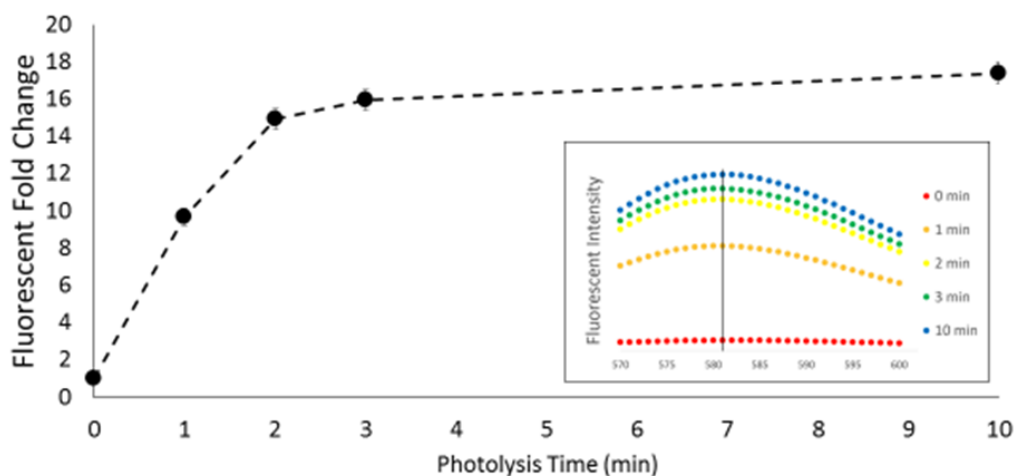


Figure 4.2 Fluorescent fold change in aqueous fraction after photolysis. Fluorescence increase in aqueous fraction after photolysis of TAMRA-Cbl-C18. Reprinted with permission from the publisher.^[102]

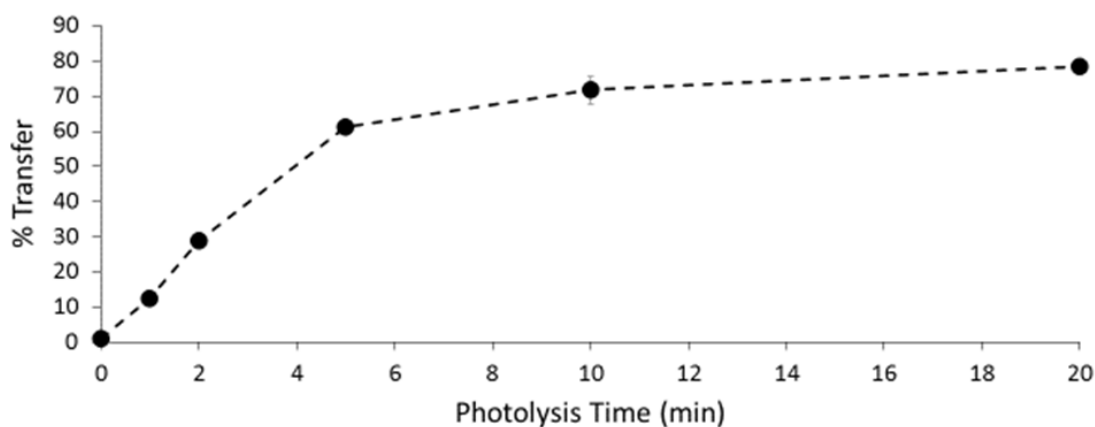


Figure 4.3 Transfer of methotrexate to aqueous layer after photolysis. % transfer of methotrexate after photolysis of MTX-Cbl-C18 to aqueous layer. Reprinted with permission from the publisher.^[102]

Demonstration of TAMRA and FAM release from erythrocyte

membranes. To demonstrate proof of concept that our Cbl-C18 constructs stayed in the erythrocyte membrane until photolysis we used TAM-Cbl-C18 and FAM-Cbl-C18. FAM and TAM are fluorescence reporters that are easily visualized by plate readers. After photolysis with 525 nm light, the samples were centrifuged and the supernatant was monitored for fluorescence of TAM and

FAM respectively. We demonstrated (**Figure 4.4**) that TAM and FAM were released from erythrocyte membranes only upon illumination with 525 nm light. The concentration of TAM and FAM released in the supernatant increased as the photolysis time increased.

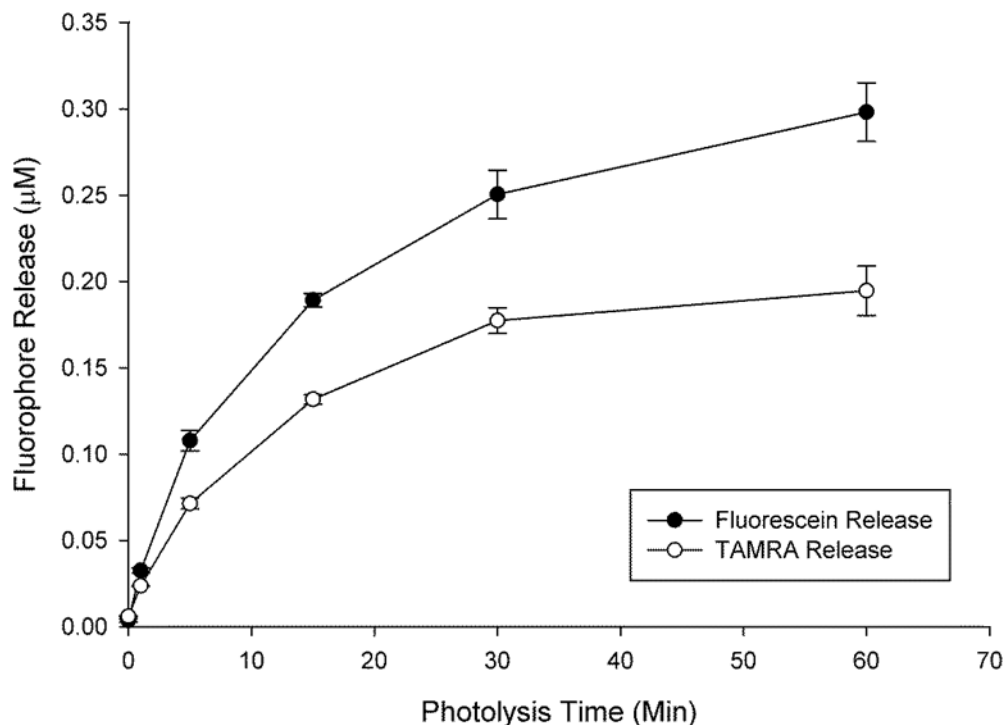


Figure 4.4 Monitoring FAM and TAM release after fluorescence in erythrocyte supernatants. Erythrocytes were loaded with either TAM-Cbl-C18 (open circles) or FAM-Cbl-C18 (closed circles) and photolyzed using 525 nm light. Fluorescence was monitored in the supernatant after centrifuging and reported with the background subtracted of the no loading control.

Optimization of NIR release of TAMRA from erythrocyte membranes.

To determine the optimal ratio of fluorophore-C18 to Drug-Cbl-C18 needed to see sufficient release (as characterized by observed fluorescence signal), various concentrations of TAM-Cob-C18 and Cy5-C18 were incubated with erythrocytes. The erythrocytes were illuminated with 660 nm light the supernatant

was then analyzed for TAMRA release by fluorescence spectroscopy. Although significant release was observed at many ratios (**Figure 4.5** and **Figure 4.6**), 5 μ M fluorophore-C18 and 1 μ M TAM-Cbl-C18 was selected as the optimal ratio for most future studies. The values reported in **Figure 4.5** and **Figure 4.6** represent the concentration of TAMRA released as determined by fluorescence with the background (no loading control) subtracted out. However, where higher concentrations of Drug-Cbl-C18 was needed to see biological activity, the concentration of the fluorophore-C18 were kept constant and only the concentration of the Drug-Cbl-C18 was increased to the necessary levels.

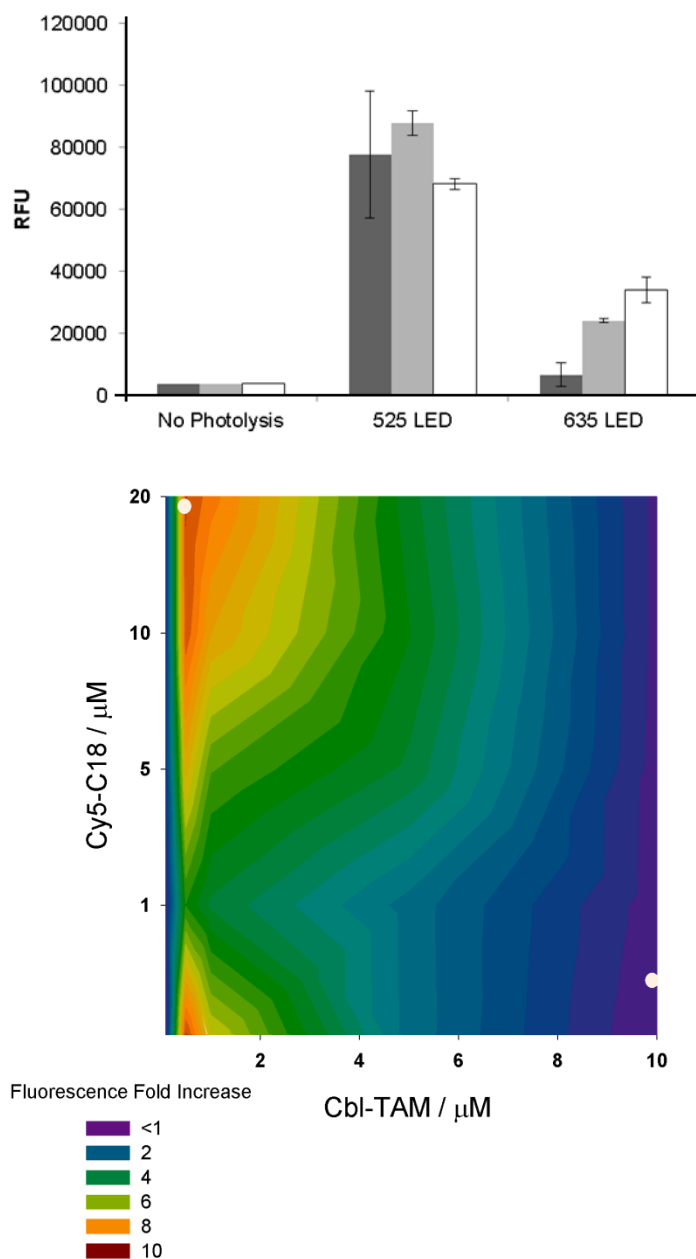


Figure 4.5 TAMRA release (fluorescence fold increase) as a function of Cy5-C18 and TAM-Cbl-C18. TOP: Fluorescence increase in supernatant after photolysis no Cy5-C18 (dark), 10x Cy5-C18 (grey) 100x Cy5-C18 (white). BOTTOM: Erythrocytes were mixed with various concentrations of Cy5-C18 and TAM-Cbl-C18 then washed and illuminated with 660 light. TAMRA release was monitored in the supernatant by fluorescence (Ex 550 nm Em 550 nm). Circles represent maximum (top left) and minimum (bottom right) fluorescence fold changes.

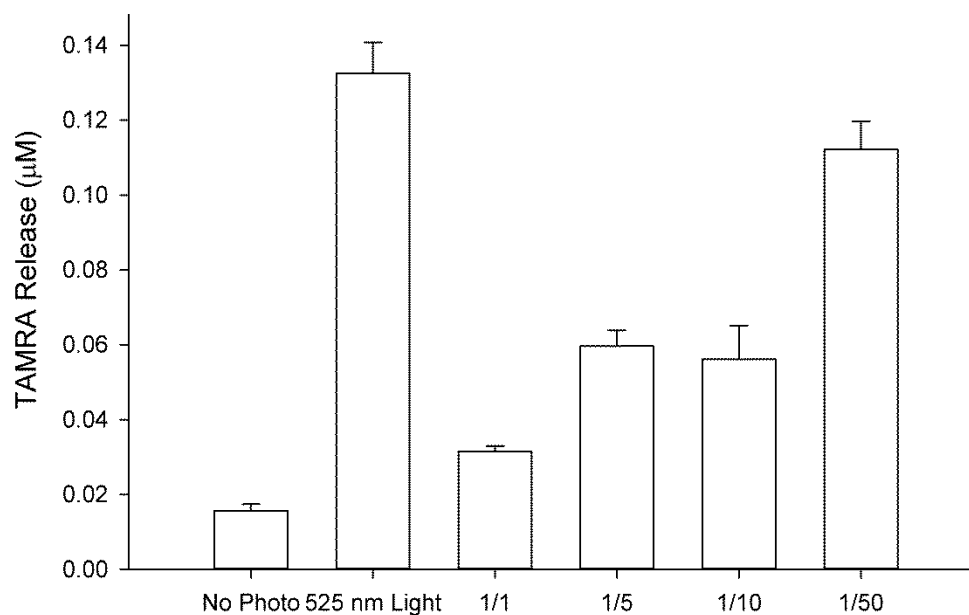


Figure 4.6 Concentration of TAMRA released at 660 nm using various concentrations of Cy-5 C18 and 1 µM TAM-Cbl-C18. Erythrocytes were mixed with various concentrations of Cy5-C18 and 1 µM TAM-Cbl-C18 then washed and illuminated using 660 nm light (525 nm light as a positive control). Concentration of TAMRA released was measured in the supernatant as determined by fluorescence.

Release using NIR light is accomplished using co-localized C18 modified fluorophores. We co-loaded erythrocytes with TAM-Cbl-C18 or FAM-Cbl-C18 and either Cy5-C18, AF700-C18, Cy7-C18, or FL800-C18. Loaded erythrocytes were then illuminated with LED boards corresponding to the excitation of the fluorophore-C18 conjugates. In the absence of Fluorophore-C18 no TAMRA release is observed (**Figure 4.7**). We demonstrated (**Figure 4.8** and **Figure 4.9**) that upon illumination of the ‘antenna’ fluorophore at its excitation wavelength TAM or FAM release from the erythrocyte membrane.

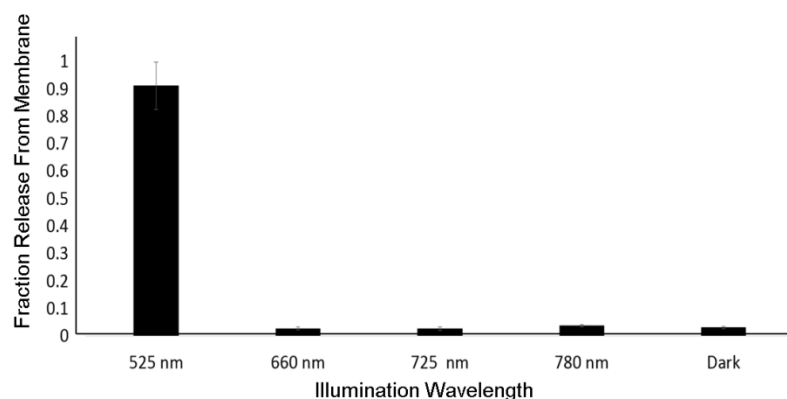


Figure 4.7 Ratio of TAMRA released in the absence of fluorophore-C18 after photolyzing at the fluorophore-C18 corresponding excitation maximum. Erythrocytes were mixed with 1 μ M TAM-Cob-C18 and 5 μ M of the Fluorophore-C18. TAMRA release was quantitated after 30 min photolysis at the corresponding wavelengths.

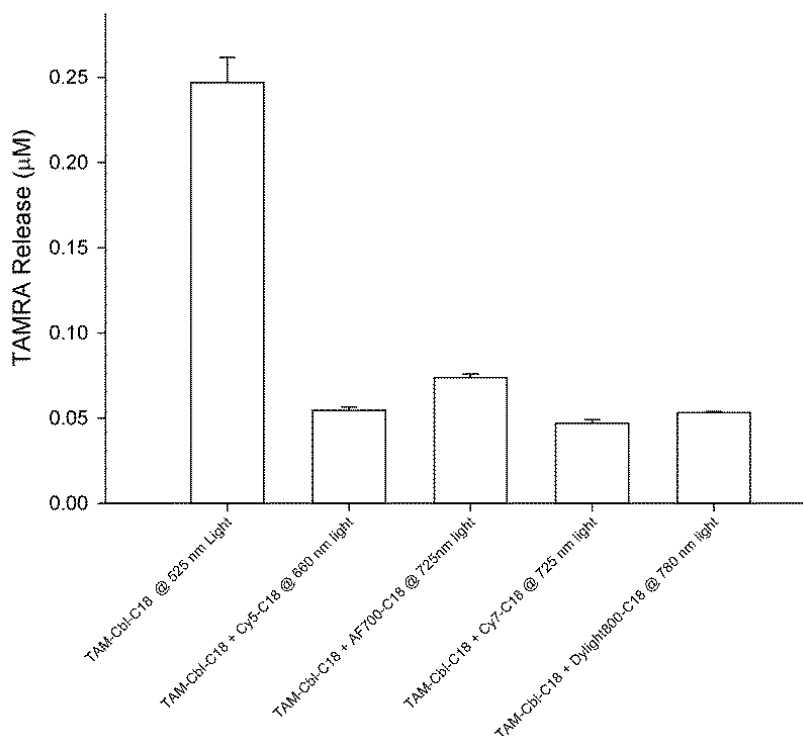


Figure 4.8 Concentration of TAMRA released using various fluorophore-C18 after photolyzing at their corresponding excitation maximum. Erythrocytes were mixed with 1 μ M TAM-Cob-C18 and 5 μ M of the Fluorophore-C18. TAMRA release was quantitated using fluorescence (no loading control as background) after 30 min photolysis at the corresponding wavelengths.

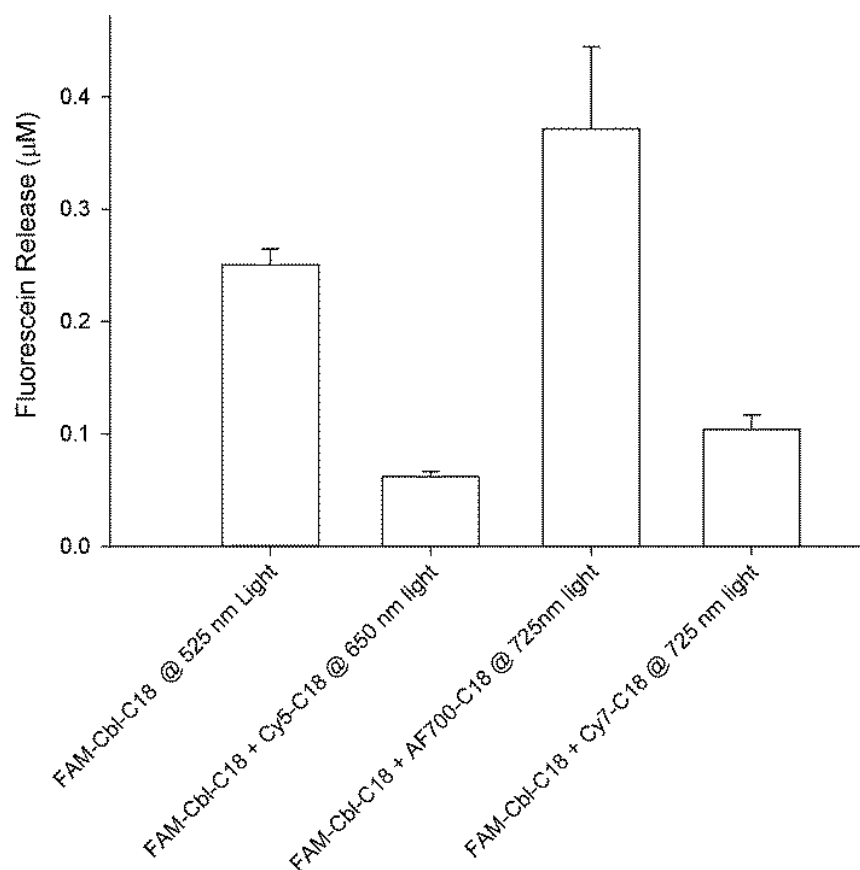


Figure 4.9 Concentration of Fluorescein released using various fluorophore-C18 after photolyzing at their corresponding excitation maximum. Erythrocytes were mixed with 1 μ M FAM-Cob-C18 and 5 μ M of the Fluorophore-C18. Fluorescein release was quantitated after 30 min photolysis at the corresponding wavelengths.

Microscopy imaging of loaded erythrocytes. Confocal microscopy was used to assess the distribution of fluorophore-C18 loaded erythrocytes. The disruption of loading was found to be uniform (**Figure 4.10**). Similarly, widefield microscopy (significantly faster acquisition times) was used to image TAM-Cbl-C18 loaded erythrocytes. Although imaging TAMRA induced rapid release from the erythrocytes, it was determined that the TAMRA is evenly distributed amongst the RBCs (**Figure 4.11**).

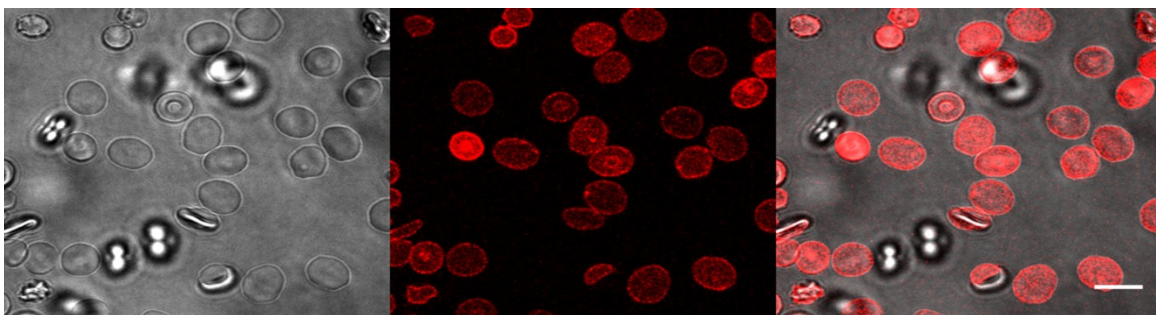


Figure 4.10 Confocal images of erythrocytes loaded with Cy5-C18. Cy5-C18 (5 μM) was added to 10% hematocrit erythrocytes. Following incubation and washing erythrocytes were plated at 0.1% hematocrit and imaged by confocal microscopy. Left; phase contrast, Middle; Cy-5 fluorescence, Right; Overlay, white bar indicates 5 μm . Reprinted with permission from the publisher.^[102]

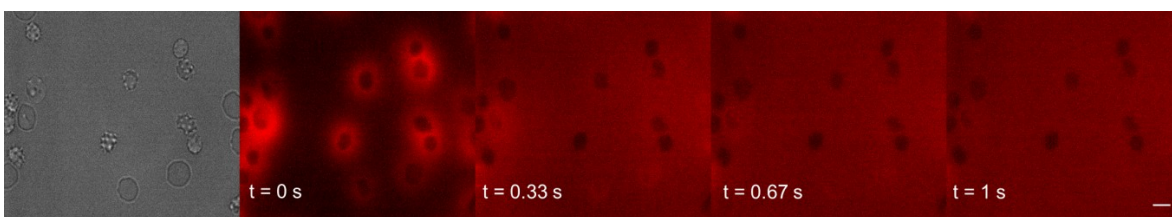


Figure 4.11 Release of TAMRA from the erythrocytes membrane into the surrounding medium visualized by widefield microscopy. TAM-Cbl-C18 (5 μM) was added to 10% hematocrit erythrocytes. Following incubation and washing erythrocytes were plated at 0.1% hematocrit and imaged by confocal microscopy. Left; brightfield, Middle to right; TAM fluorescence, white bar indicates 5 μm . Reprinted with permission from the publisher.^[102]

Anti-inflammatory drug release from erythrocyte membranes. The anti-inflammatories have a minimal impact on erythrocyte lysis as determined by monitoring hemoglobin in the supernatant (<10%) when using 5 μM MTX-CBL-C18, DEX-CBL-C18 or COL-CBL-C18. MTX-CBL-C18, DEX-CBL-C18, and COL-CBL-C18 were loaded onto erythrocytes. Erythrocytes were illuminated with 525 nm light and subsequently the samples were centrifuged and the supernatants analyzed by LC-MS for the presence of the anti-inflammatory agents. The amount of drug release correlated with the amount loaded onto the erythrocytes (Figure 4.12).

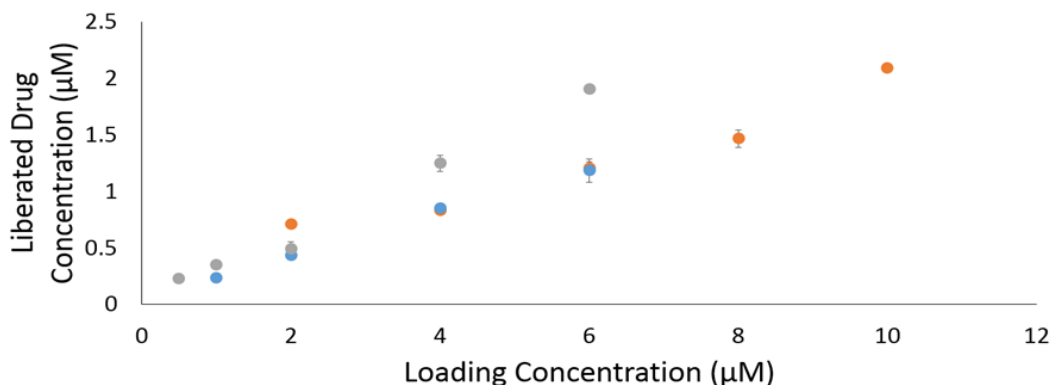


Figure 4.12 Correlation between amount of Drug-Cbl-C18 loaded onto erythrocytes and concentration of Drug released into the supernatant. Erythrocytes were loaded with Col-Cbl-C18 (orange), MTX-Cbl-C18 (blue), and Dex-Cbl-C18) at various concentrations. After loading was completed concentration of release was measured by LC/MS after photolysis. Reprinted with permission from the publisher.^[102]

Testing biological activity of released anti-inflammatories. To

demonstrate the release of drugs has an impact on biological activity MTX-Cbl-C18, and Col-Cbl-C18 were photolyzed independently and tested for biological activity. The photolyzed MTX demonstrated inhibition of DHFR (**Figure 4.13**). Lastly, photolyzed colchicine induced the expected depolymerization of microtubules (**Figure 4.14**).

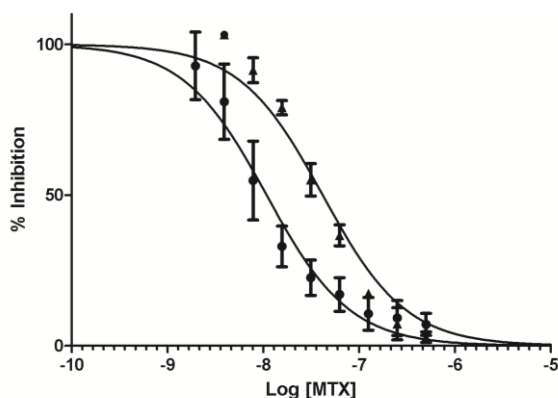


Figure 4.13 Inhibition of DHFR using methotrexate (circles) and photo-MTX (triangles). DHFR inhibition was monitored in the presence of various concentrations of commercially source methotrexate and photolyzed MTX-CBL (photo-MTX refers to the photolyzed cbl-MTX product). Reprinted with permission from the publisher.^[102]

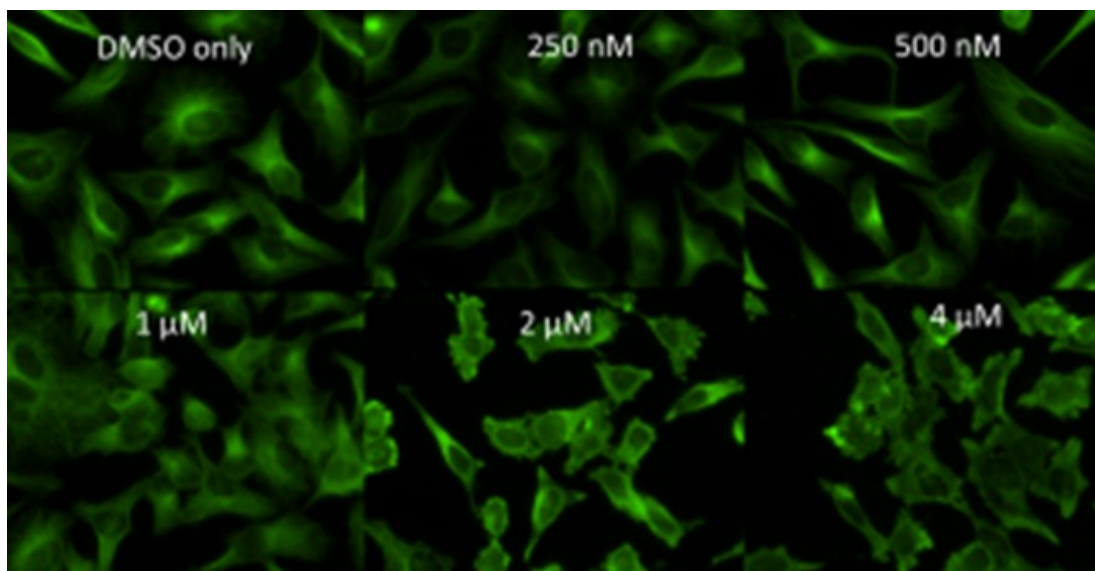


Figure 4.14 Photolyzed colchicine added to HeLa cells. Photolyzed Col-CBL-C18 was titrated into HeLa cell culture before the cells were fixed and stained for tubulin to visualize microtubule networks. At around 2 μM colchicine the networks are disrupted and lamellapodia are truncated as microtubules aggregate chaotically at their fringes. Reprinted with permission from publisher.^[102]

Release of anti-inflammatories from erythrocytes. MTX-Cbl-C18, Dex-Cbl-C18, and Col-Cbl-C18 were individually incubated with erythrocytes. After incubation and washing, the different drug-carriers were exposed to HeLa cells and illuminated (or incubated in the dark) with 525 nm light. As before, GR_α translocation was observed only upon illumination in the presence of Dex-Cbl-C18 (**Figure 4.15**). Depolymerization of microtubules was observed upon illumination with 525 nm light and not observed in the dark samples in the presence of Col-Cbl-C18 (**Figure 4.16**). The CETSA assay (measures amount of drug bound protein by measuring remaining protein in supernatant after heating)^[103] was used to demonstrate methotrexate was delivered to cells and as observed in **Figure 4.17**, methotrexate delivery is only observed in the presence of 525 nm light.

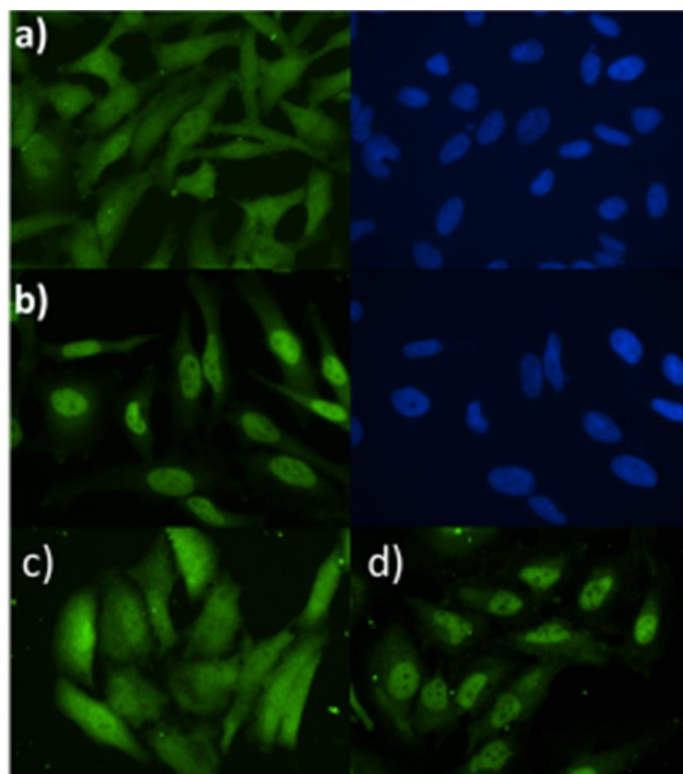


Figure 4.15 HeLa cells exposed to dexamethasone. a) DMSO treated HeLa cells b) HeLa cells treated with 250 nm dexamethasone (commercially sourced). c) HeLa cells were treated with RBCs loaded with 1 μ M Cbl-DEX no photolysis. d) HeLa cells were treated with RBCs loaded with 1 μ M Cbl-Dex-C18 with photolysis. HeLa cells were stained with Alexa488 antiRabbit/anti-Gralpha (green) and DAPI (blue). Reprinted with permission from publisher.^[102]

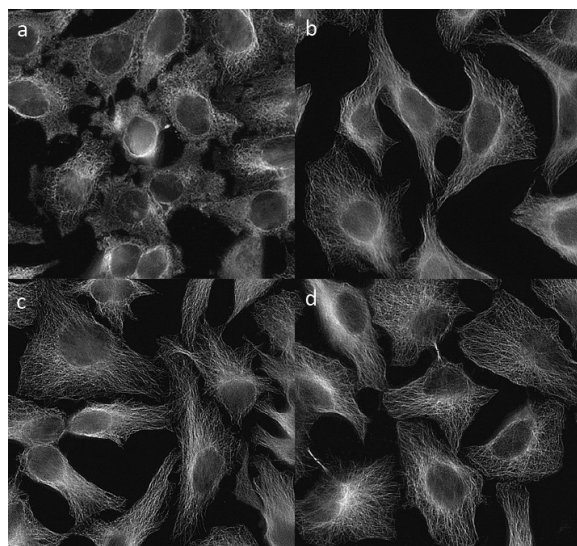


Figure 4.16 HeLa cells exposed to Col-Cbl-C18 loaded erythrocytes. a) 20 min photolysis at 525 nm, b) dark, c) no erythrocytes in the dark, d) no erythrocytes 20 min photolysis 525 nm light. Col-Cbl-C18 loaded erythrocytes were added to HeLa cell culture and photolyzed. The cells were fixed and stained for tubulin to visualize microtubule networks. Reprinted with permission from publisher.^[102]

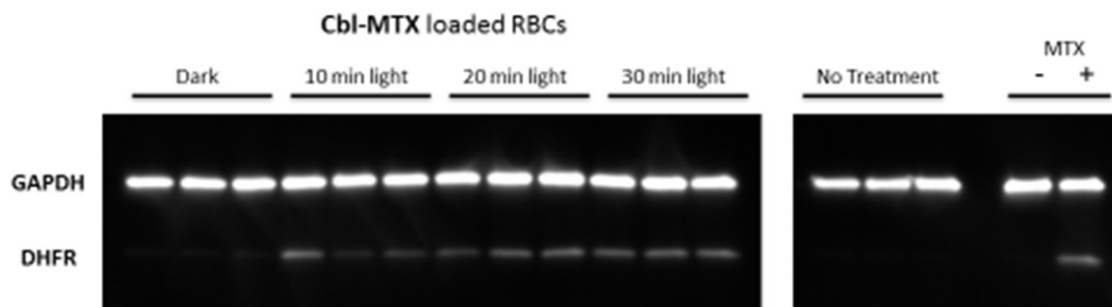


Figure 4.17 Cellular thermal shift assay of HeLa cells treated with MTX-Cbl-C18 loaded erythrocytes. In the absence of MTX no MTX bound DHFR is detected (no treatment). HeLa cells treated with MTX-Cbl-C18 and not exposed to light contain minimal MTX bound DHFR as evidenced by no observable band in the dark lane using anti-DHFR. After 30 min of photolysis significant MTX bound DHFR is present. Photolysis was carried out by 525 nm centered LEDs. Reprinted with permission from publisher.^[102]

NIR light release of anti-inflammatories from erythrocytes. MTX-Cbl-C18, Dex-Cbl-C18, and Col-Cbl-C18 were individually incubated with erythrocytes and Cy7-C18, FL800-C18, and Cy5-C18, respectively. After incubation and washing, each of the erythrocytes were exposed to HeLa cells and illuminated (or incubated in the dark) with 725 nm, 780 nm, 660 nm, light respectively, corresponding to the excitation wavelengths of the antenna. As before, when DexCbl-C18 and Cy5-c18 are introduced to erythrocytes, GR α translocation was observed only upon illumination with 660 nm light (**Figure 4.18**). When Col-Cbl-C18 and FL800-C18 are introduced to erythrocytes, depolymerization of microtubules was observed upon illumination with 780 nm light and not observed in the dark samples (**Figure 4.19**). The CTSA assay was used to demonstrate methotrexate was delivered to cells and as observed in **Figure 4.20**, methotrexate delivery is only observed in the presence of 725 nm light.

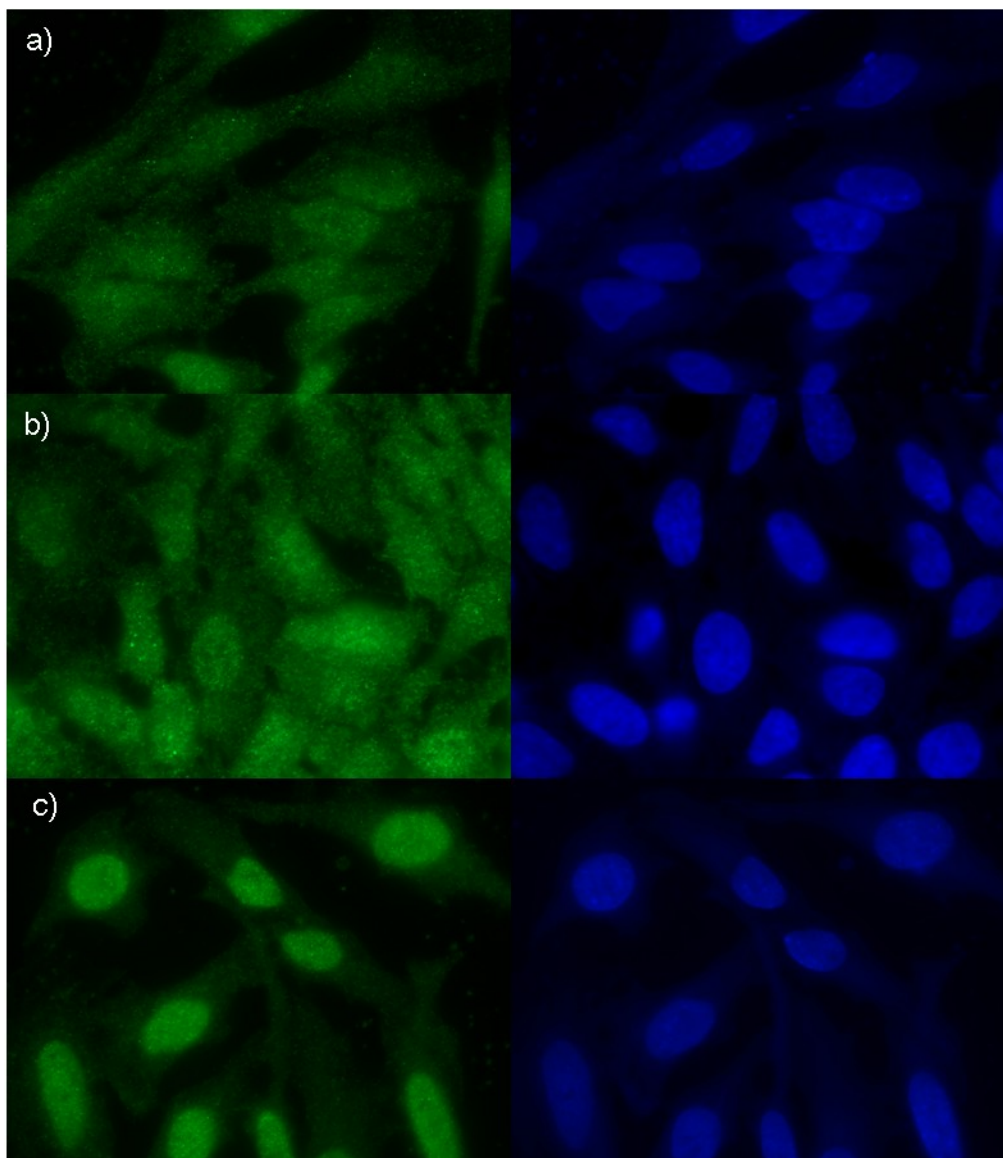


Figure 4.18 Widefield images HeLa cells after dexamethasone release from Dex-Cbl-C18 and Cy5-C18 loaded erythrocytes using 660 nm light. a) Untreated HeLa cells. b) HeLa cells treated with RBCs loaded with 1 μM Dex-Cbl-C18 in the absence of light. c) HeLa cells treated with RBCs loaded with 1 μM Dex-Cbl-C18 and photolyzed at 780 nm for 15 min. Cells were visualized using Alexa488 antiRabbit/anti-GR α (green) and Dapi (blue). Reprinted with permission from publisher.^[102]

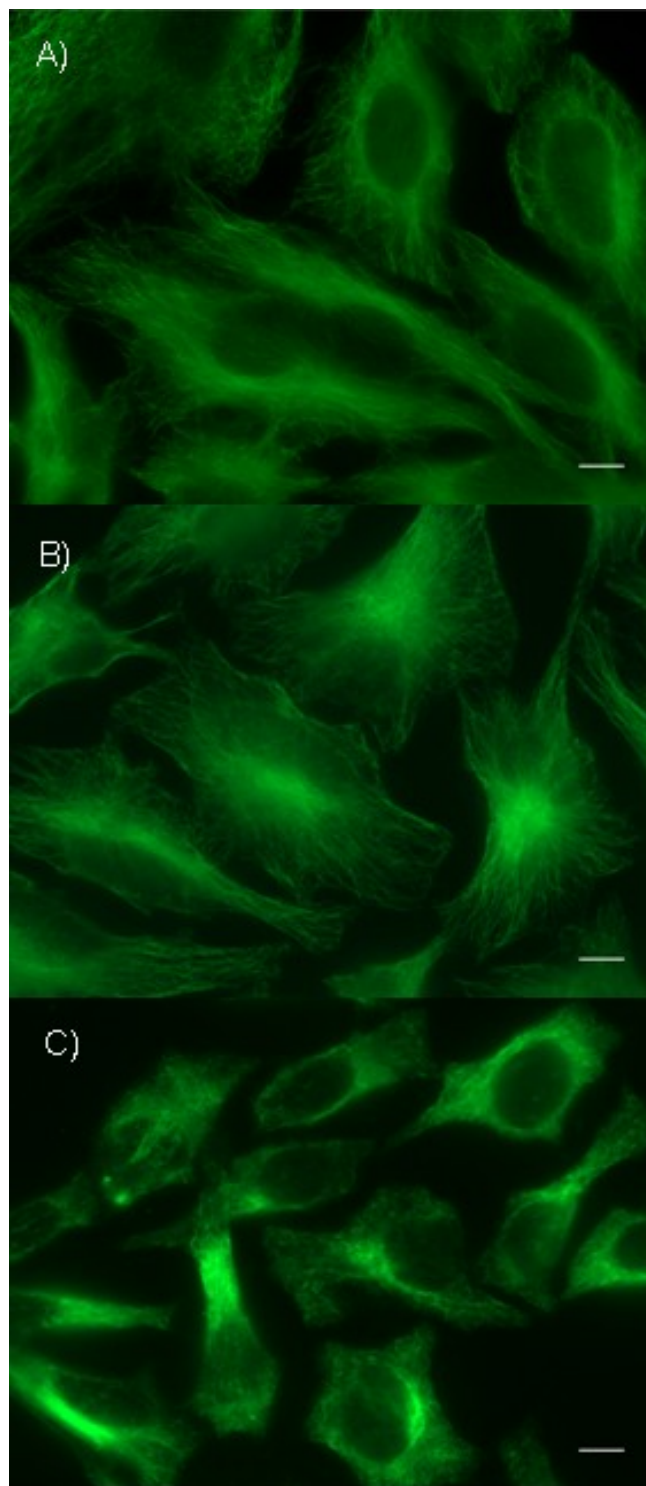


Figure 4.19 Widefield images HeLa cells after colchicine release from COL-Cbl-C18 and FL800-C18 loaded erythrocytes using 780 nm light. a) untreated HeLa cells. b) HeLa cells treated with RBCs loaded with 5 μM Col-Cbl-C18 in the absence of light. c) HeLa cells treated with RBCs loaded with 5 μM Col-Cbl-C18 and photolyzed with 780 nm light for 15 min. The cells were fixed and stained for tubulin to visualize microtubule networks. Reprinted with permission from the publisher.^[102]

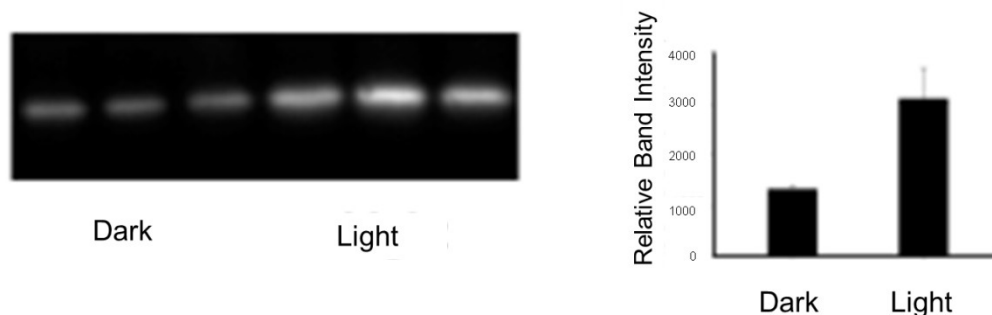


Figure 4.20 Cellular thermal shift assay of HeLa cells treated with MTX-Cbl-C18 and Cy7-C18 loaded erythrocytes HeLa cells treated with MTX-Cbl-C18 in the absence of light have minimal MTX bound DHFR after 30 mins of photolysis with 725 nm light significant MTX bound DHFR is present. Photolysis was carried out by 725 nm centered LEDs. Reprinted with permission from publisher.^[102]

DISCUSSION AND FUTURE DIRECTIONS

A light mediated drug delivery system could provide a general method to reduce side effects due to interactions of therapeutics with unintended targets. As such, we sought to develop a light mediated method for therapeutic agents that operate within the optical window of tissue. Using vitamin B₁₂ derivatives (cobalamin) known to be photoresponsive at wavelengths less than 600 nm, our lab had previously demonstrated that modifying the 5' hydroxyl of ribose with fluorophores that have excitation maximum in the optical window of tissue will induce cleavage of the Co-C bond at the excitation wavelength of the fluorophore. We hypothesized that simply localizing fluorophores and the cobalamin derivatives to membranes would allow for sufficient cross-talk between the fluorophore and the cobalamin to induce release at the fluorophore excitation wavelengths. To test our hypothesis we created a series of lipidated

fluorophores and lipidated cobalamin conjugates. Our initial efforts focused on release of fluorophores TAMRA and Fluorescein from lipidated cobalamin.

Initially we confirmed that following photolysis of TAM-Cbl-C18 and MTX-Cbl-C18 translocation of TAM and MTX from octanol to an aqueous buffer is observed (confirming our C18 derivatives prefer to remain in a non-polar environment until photolysis). We next determined fluorophores could be released in such a manner from erythrocyte membranes. Our results, shown in **Figure 4.4**, demonstrate, using 525 nm light, the release of both TAM and FAM from erythrocyte membranes. Furthermore, in the presence of 660 nm light no fluorophore is released. Next, we wanted to determine if adding a fluorophore with an excitation maximum near 660 would allow for light mediated release at 660 nm. Our results, shown in **Figure 4.5**, demonstrate TAM is released under these conditions. However, the ratio of TAM-Cbl-C18 to Cy5-C18 was unsuitable for general adaptation to other systems. Therefore, we tested a wide range of TAM-Cbl-C18 (0 to 10 μ M) and Cy5-C18 (0 to 20 μ M) concentrations. **Figure 4.5** reveals that although a wide range of ratios induce significant TAM release at 660 nm, using 5 μ M Cy5-C18 and 1 μ M TAM-Cbl-C18 furnishes significant release with a minimal excess of Cy5-C18. We therefore decided that for all future studies 5 μ M fluorophore-C18 would be used to promote the release of drugs of interest to maintain minimal concentration of exogenous lipid added to the membrane, even if excess drug-Cbl-C18 was needed to elicit a response. Cy5-C18 was also shown to promote the release FAM from cobalamin. We next sought to determine if Alexa Fluor 700, Cy7, and a far-red fluorophore we call

FL800 could also induce release of TAM and FAM from Cbl-C18. We demonstrated, **Figure 4.9** and **Figure 4.9**, each fluorophore-C18 induces significant release of TAM and FAM with minimal loss in the absence of light.

Our findings provided us with proof of concept. We subsequently sought to apply the technology toward the release of anti-inflammatory agents. Anti-inflammatory agents are represented by a broad class of chemical entities and often elicit harmful side effects. As inflammation is highly localized, using our system to spatially and temporally deliver anti-inflammatory agents could potentially reduce the side effects associated with systemic delivery. Our choice of anti-inflammatory drugs is more specifically based on their role in the treatment of rheumatoid arthritis (RA). RA therapies generally require frequent and long-term drug systemic administration, which commonly results in increased risk of severe side effects. For example, the nearly 50% of RA patients who are dependent upon glucocorticoids, such as dexamethasone, experience weight gain, osteoporosis, diabetes mellitus, hypertension, skin fragility and infections (infections arising from being systemically immunocompromised).^[104, 105] As a result, there is significant demand for the development of therapeutics that can be selectively delivered to arthritic joints.^[106-108] We tested our technology on commonly used anti-inflammatory agents. We first synthesized methotrexate, dexamethasone, and colchicine Cbl-C18 derivatives. We subsequently determined that Cbl-MTX, Cbl-Col and Cbl-Dex can be loaded onto erythrocyte membranes at concentrations up to 5 μ M with minimal damage to the erythrocyte. Furthermore, the concentration of drug-loaded and subsequent

photolysis released a predictable amount of drug. Photolysis of the Co--
 $\text{CH}_2\text{CH}_2\text{CH}_2\text{Drug}$ bond primarily, but not exclusively, generates the alkyl product
 $\text{CH}_3\text{CH}_2\text{CH}_2\text{Drug}$. We photolyzed MTX-Cbl and demonstrated inhibition of
 dihydrofolate reductase (DHFR) using a commercially available DHFR assay kit
(Figure 4.13). As expected, based on previous reports of the structure activity
 relationship of MTX derivatives, the photolyzed product of Cbl-MTX is an
 effective inhibitor of dihydrofolate reductase.^[109] N-colchicine butyramide as the
 photolyzed erythrocyte-loaded Cbl-COL was identified by LC-MS to be the
 primary product. N-colchicine butyramide was determined to be an inhibitor as
 effective as native colchicine of microtubules in HeLa cells **(Figure 4.14)**.
 Photolysis of Cbl-DEX-loaded erythrocytes produces three products (1, X = CH_3 ,
 CH_2OH , CHO) and are known prodrugs that are hydrolyzed to DEX upon cellular
 uptake.^[110, 111] To demonstrate the impact of dexamethasone on HeLa cells,
 HeLa cells were exposed to commercially available dexamethasone and showed
 the expected nuclear translocation of GR_α **(Figure 4.15)**. Having established
 biological activity of the released anti-inflammatories we wanted to demonstrate
 that our drug-Cbl-C18 derivatives could be released from erythrocytes at 525 nm
 and that release could be tuned to wavelengths in the optical window of tissue.
 As expected, erythrocytes loaded with each individual drug produced the desired
 cellular responses using the dexamethasone and colchicine assays previously
 described and the cellular thermal shift assay (CETSA) was used to determine if
 methotrexate bound DHFR in HeLa cells **(Figure 4.15, Figure 4.16, and Figure**
4.17). We then co loaded erythrocytes with Cy5-C18 and Dex-Cbl-C18 and

demonstrated that photolysis in the presence of 660 nm light led to nuclear translocation of GR_{α} . Furthermore, in the absence of Cy5-C18 migration of GR_{α} did not occur. Similarly, microtubule depolymerization only occurred after illumination by 760 nm light when Col-Cbl-C18 was co-loaded with FL800-C18 into erythrocyte. MTX binding to DHFR, as determined by CTSA, at 725 nm occurred only in erythrocytes co-loaded with Cy7-C18.

We report the development of long-wavelength photo-responsive drug release constructs that are able to be tuned to the optical window of tissue. We demonstrated that anti-inflammatory release is able to be tuned to other wavelengths based on the excitation properties of the fluorophores. Our strategy uses erythrocytes since their long half-life and negligible immunogenic response ideally positions them as carriers. Additionally, this strategy could be extended to other carrier systems such as liposomes or nanoparticles.

CHAPTER 5: Final Thoughts and Future Directions

Overview

My dissertation research has sought to address the utility of erythrocytes for studying intracellular enzymatic activity with potential for use as diagnostic agents and as a tool for localized delivery of anti-inflammatory therapeutics. The key findings of my research are that 1) erythrocytes can be loaded, using hypotonic dilution, with small molecules, peptides, and fluorophore labeled PKA . 2) Erythrocytes can be loaded with UV light response photocleaving groups. 3) Erythrocyte PKA activity can be monitored using confocal microscopy and a light-controlled kinase assay. 4) Erythrocytes can be ‘decorated’ with drug-cobalamin (Drug-Cbl) derivatives that can be tuned to release drugs using light within the optical window of tissue. In the final chapter of this dissertation the focus will be on the future directions in which this technology can be applied.

Erythrocytes as carriers

As discussed throughout this dissertation, erythrocytes represent an excellent prospect for drug and diagnostic agent delivery. This lab’s future

objectives for erythrocyte based drug delivery is to 1) optimize erythrocyte based delivery systems, 2) increase the affinity of the Drug-Cbl conjugates to the membrane by using more hydrophobic anchors and 3) load drug-Cbl into erythrocytes and demonstrate release.

Anchoring therapeutics to erythrocyte membranes. Through our research, it was demonstrated that C18 is sufficient to anchor certain constructs to erythrocyte membranes. However, exchange of lipids between membranes has been demonstrated since the 1960s.^[112] The lipid exchange rate is dependent on the association constant of the lipid with membrane bilayer and is a function of the hydrophobic nature of the lipid. Increasing the lipid hydrophobicity may increase the association of the lipid drug-Cbl conjugates and reduce membrane exchange. As a demonstration of lipid membrane exchange erythrocytes were loaded with either Cy5-C18 or TAMRA-C18 and separately washed as described in Chapter 4. The erythrocytes were then mixed together and imaged using confocal microscopy. As observed in **Figure 5.1** and **Figure 5.2**, the mixture of the two erythrocytes contained cells loaded with both Cy5 and TAMRA and cells loaded with TAMRA alone. This indicates TAMRA-C18 is exchanging between membranes. Cy5-C18 did not appear to exchange as readily and may be a function of the increased hydrophobic nature of the fluorophore. However, it has been reported that use of a phospholipid is sufficient to anchor cyanine dyes to erythrocyte membranes, even in the presence of serum or in mice.^[113-116] Therefore, we propose to use phospholipids that contain more hydrophobic tails such as phosphatidylcholine or phosphatidylserine (**Figure 5.3**). These

phospholipids will also have the added benefit that they are more biologically relevant and should reduce risk of eliciting an immune response. Identifying phospholipids that increase the association of the Drug-Cbl derivatives for the membrane could have a two-fold benefit: 1) The increased association will enhance compatibility with biologically relevant system where the presence of serum becomes problematic. 2) Enhanced compatibility could allow for orthogonal control over drug-release. In an ideal system, erythrocytes could be loaded with Drug**A**-Cbl-lipid complex in the presence of Fluorophore**C**-C18. Other erythrocytes could be loaded with Drug**B**-Cbl-Lipid in the presence of Fluorophore**D**-C18 and then illuminating using Fluorophore**C** excitation would only release Drug**A** while illuminating with Fluorophore**D** excitation would furnish release of Drug**B**. In the current system (reported in Chapter 4), exchange between the membranes would dramatically reduce our ability to control drug release orthogonally; thus facilitating the need for a new lipid anchor.

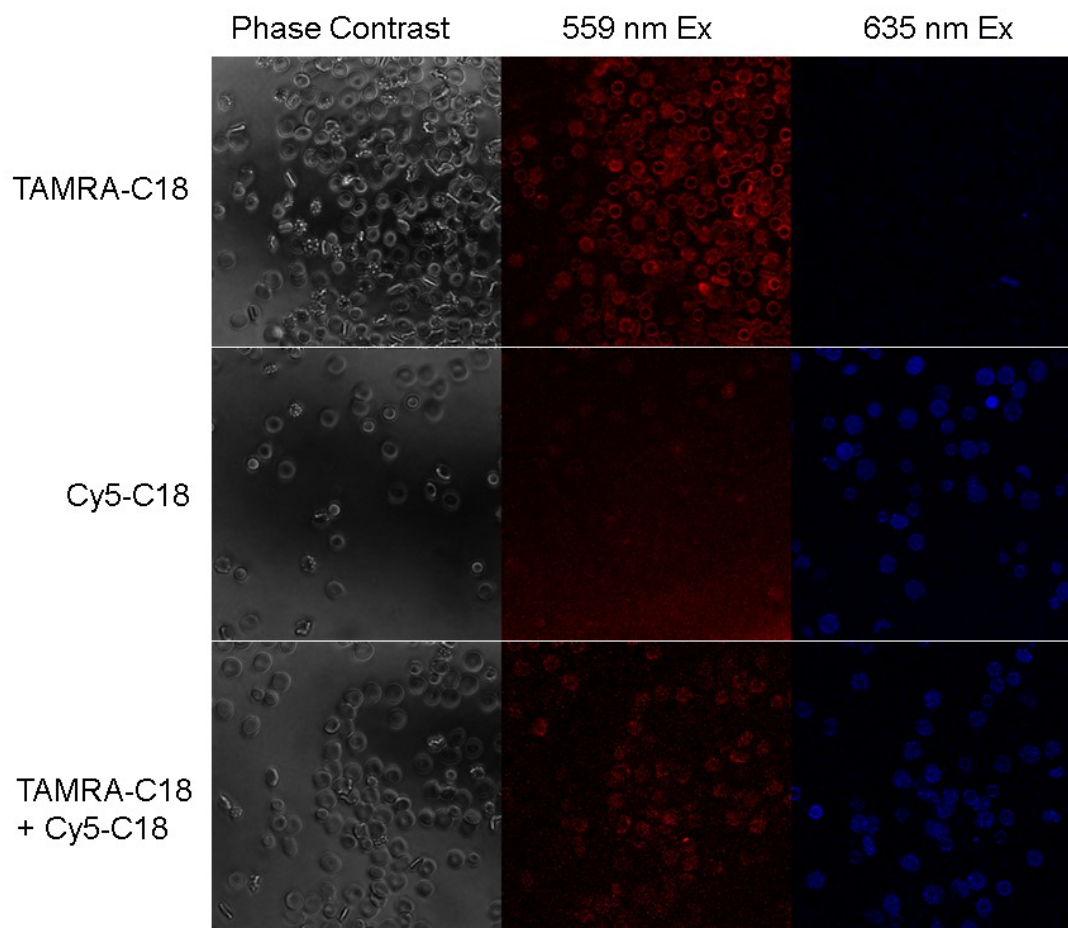


Figure 5.1 Confocal images of erythrocyte loaded with Cy5-C18 and TAMRA-C18. Erythrocytes were loaded with 5 μ M TAMRA-C18 or 5 μ M Cy5-C18 then mixed. The sample was imaged by confocal microscopy.

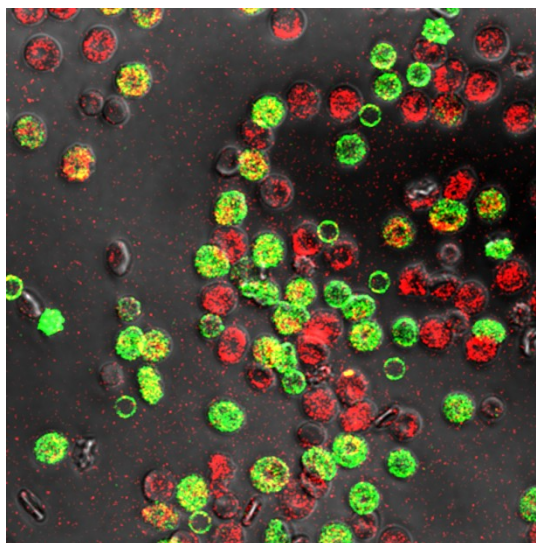


Figure 5.2 Overlay of Cy5-C18 and TAMRA-C18 loaded erythrocytes mixed together.

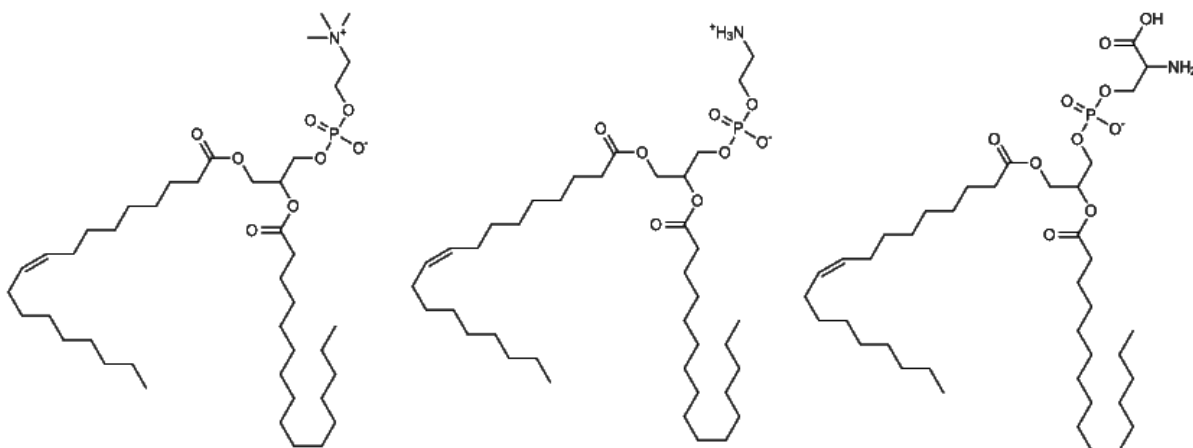


Figure 5.3 Chemical Structure of phosphatidylcholine (left), phosphatidylethanolamine (middle), and phosphatidylserine (right).

Loading therapeutics into erythrocytes. An alternative method to anchoring therapeutic agents to the outside of erythrocytes is to load them into erythrocytes. This method has been demonstrated using dexamethasone to treat ulcerative colitis and L-asparaginase to treat acute lymphoblastic leukemia (ALL).^[117, 118] However, dexamethasone loading uses diffusion as a method of drug release and L-asparaginase is active within the circulating erythrocytes and is unable to escape erythrocytes as such, neither of these methods are able to be spatially controlled. We propose loading erythrocytes with Drug-Cbl derivatives. Using this design cobalamin would localize the drug to the erythrocyte interior. After photolysis the drug should be able to rapidly diffuse through the lipid bilayer. As erythrocyte pore formation, including size after resealing, can be affected by the loading procedure, the loading procedure could be optimized to allow for drugs to rapidly exit the cells (including drugs that are not able to diffuse through the membrane). As a proof of concept, erythrocytes were loaded with a Bodipy-Cbl derivative that releases bodipy (membrane permeable fluorescent membrane marker) at 660 nm light. We were able to

follow bodipy release from erythrocytes using fluorescence spectroscopy and confocal microscopy (**Figure 5.4** and **Figure 5.5**). This method provides several obvious advantages over systemic administration and even over our current membrane anchoring technology. Loading the drug into erythrocytes completely removes the possibility that the drugs could be modified by extracellular proteases or other proteins involved in metabolism. This method eliminates the need to identify fluorophores that can be modified to contain a lipid anchor and as a result all commercially available fluorophores become a potential antenna to control drug release. Lastly, loading the conjugates into the erythrocytes also ensures orthogonal control of drug release. Two batches of erythrocytes, containing different drugs with different fluorophores, can be simultaneously loaded and mixed. The desired drug could be released with the corresponding fluorophore excitation wavelength. Future studies will involve the use of other therapeutic agents in combination with commercially available red fluorophores.

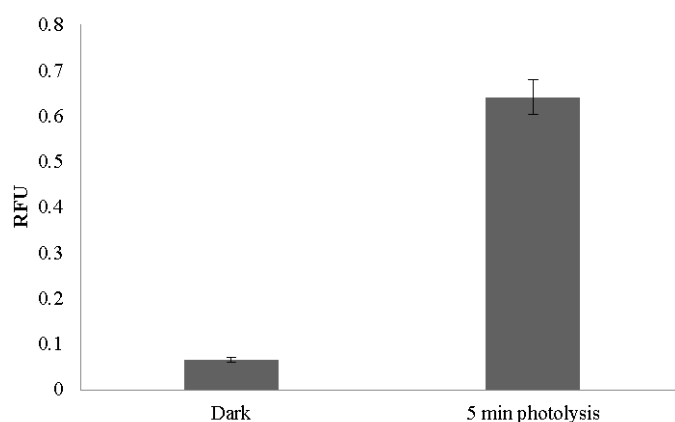


Figure 5.4 Fluorescence increase in supernatant of bodipy loaded erythrocytes in the presence and absence of light (660 nm).

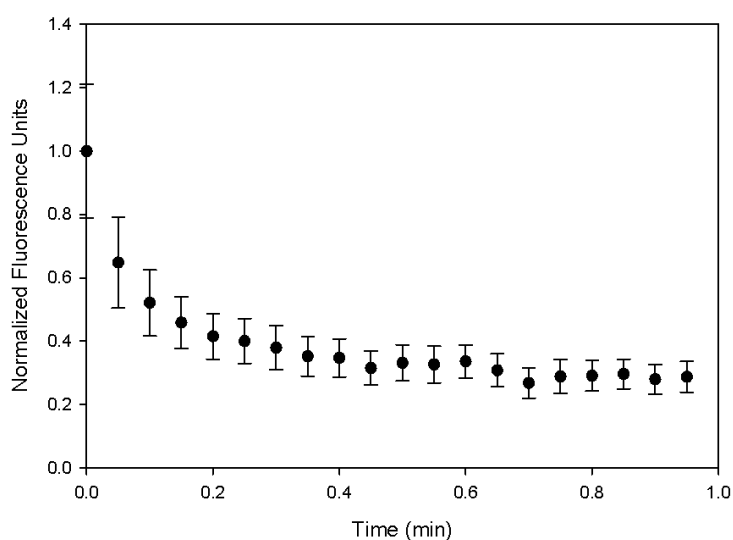
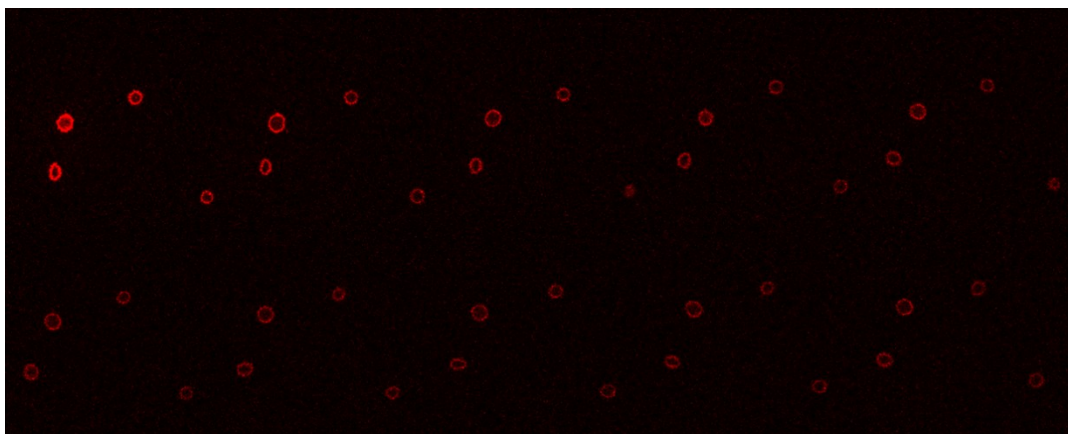


Figure 5.5 Erythrocytes loaded with Bodipy-Cbl and imaged by confocal microscopy. Top; confocal images captured every 6 s of bodipy fluorescence; final frame represents fluorescence after 1 min. Bottom; normalized fluorescence loss of bodipy containing erythrocytes from top figure.

Other carriers (hybrid erythrocytes nano-vesicles, nanoparticles, liposomes/micelles).

Although erythrocytes represent an excellent source of drug delivery vesicles they are not the only ones. Other types include ‘manufactured’ carriers; such as, hybrid erythrocyte nano-vesicles,^[119] nanoparticles,^[120] and liposomes or

micelles.^[121] Each of these manufactured carriers has several advantages and disadvantages as compared to erythrocyte carriers. While immunogenicity can be a problem with each method, one of the primary advantages of these methods is that size can be controlled. This could allow for delivery to tissue outside the reach of erythrocytes which are unable to pass through vessels less than 3 μm in diameter or through the vessel wall and directly to the diseased tissue.

Furthermore, as these delivery vehicles are manufactured in the lab they are easy to append with targeting agents. As an example, nanoparticles can be formulated to contain doxorubicin and targeting by appending antibodies towards a particular cancer target.^[122] Indeed, this method was demonstrated to increase uptake and cytotoxicity in a human carcinoma cell line.^[123] Synthesizing nanoparticles that contain a cancer cell targeting agent and a cobalamin-chemotherapeutic could provide targeted delivery in a temporal manner. This could significantly reduce side effects of chemotherapy treatments and could increase treatment success by increasing the concentration of the therapeutic at the cancerous site.

Using cobalamin to control enzymatic activity.

Lastly, using all of the strategies outlined through this dissertation, we could create an assay to monitor protein kinase activity in real time using light that operates within the optical window of tissue. As depicted in **Figure 5.6**, erythrocytes can be loaded with a peptide-Cbl-lipid moiety, free quencher, and

lipidated quencher. Upon photolysis of the construct, the peptide would be released into the cytosol and in the absence of phosphorylation would remain quenched. In the presence of active enzyme a fluorescence increase would occur due to phosphorylation. This could be used to study erythrocyte kinase activity and more importantly could be used to study how these enzymes respond to external stimuli such as sheer stress, low oxygen, or exposure to nitric oxide.

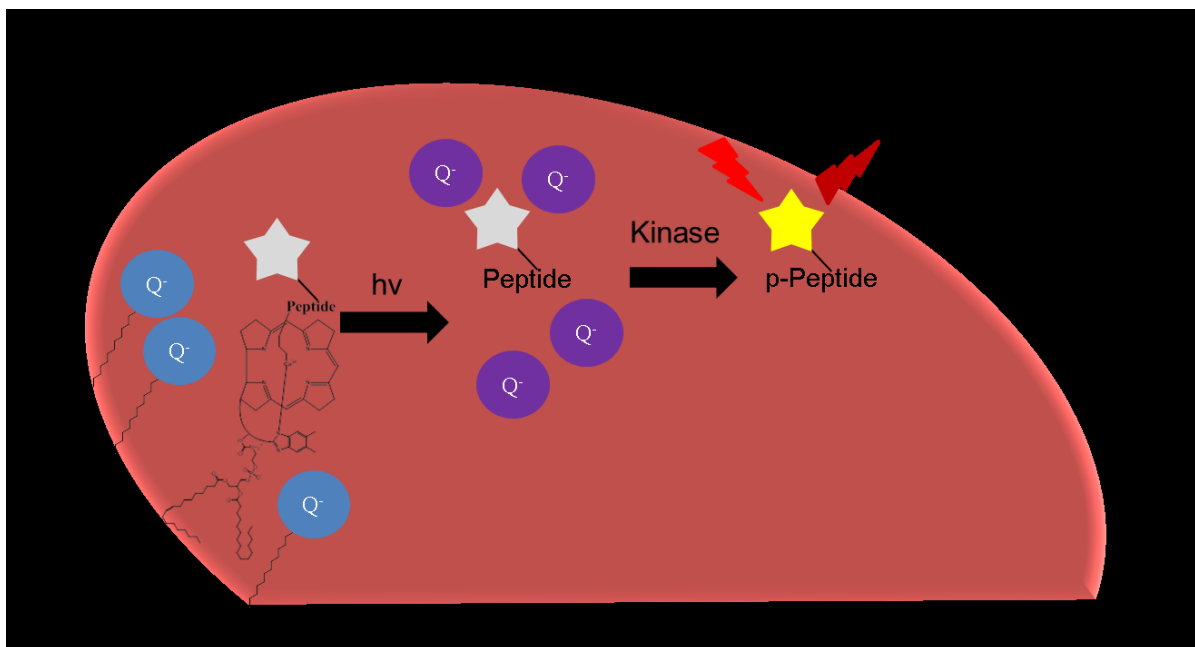


Figure 5.6 Schematic representation for long wavelength control to measure erythrocyte kinase activity in real time

REFERENCES

- [1] K. Leykauf, M. Treeck, P. R. Gilson, T. Nebl, T. Braulke, A. F. Cowman, T. W. Gilberger, B. S. Crabb, *PLoS Pathog*, **6**, e1000941.
- [2] S. Biagiotti, M. F. Paoletti, A. Fraternale, L. Rossi, M. Magnani, *IUBMB Life*, **63**, 621.
- [3] A. Zarrin, M. Foroozesh, M. Hamidi, *Expert Opin Drug Deliv*, **11**, 433.
- [4] A. R. Migliaccio, *Haematologica*, **95**, 1985.
- [5] S. M. Hattangadi, P. Wong, L. Zhang, J. Flygare, H. F. Lodish, *Blood*, **118**, 6258.
- [6] A. D'Alessandro, P. G. Righetti, L. Zolla, *J Proteome Res*, **9**, 144.
- [7] E. M. Pasini, M. Kirkegaard, P. Mortensen, H. U. Lutz, A. W. Thomas, M. Mann, *Blood* **2006**, **108**, 791.
- [8] R. M. Hochmuth, R. E. Waugh, *Annu Rev Physiol* **1987**, **49**, 209.
- [9] R. Rodvien, A. Gillum, L. R. Weintraub, *Blood* **1974**, **43**, 281.
- [10] F. C. Mokken, M. Kedaria, C. P. Henny, M. R. Hardeman, A. W. Gelb, *Ann Hematol* **1992**, **64**, 113.
- [11] M. R. Lieber, T. L. Steck, *J Biol Chem* **1982**, **257**, 11660.
- [12] F. Alexis, E. Pridgen, L. K. Molnar, O. C. Farokhzad, *Mol Pharm* **2008**, **5**, 505.
- [13] M. Magnani, L. Rossi, *Expert Opin Drug Deliv*.
- [14] N. Mohandas, E. Evans, *Annu Rev Biophys Biomol Struct* **1994**, **23**, 787.

- [15] J. A. Chasis, N. Mohandas, *Blood* **1992**, 80, 1869.
- [16] S. E. Lux, K. M. John, R. R. Kopito, H. F. Lodish, *Proc Natl Acad Sci U S A* **1989**, 86, 9089.
- [17] J. C. Murciano, S. Medinilla, D. Eslin, E. Atochina, D. B. Cines, V. R. Muzykantov, *Nat Biotechnol* **2003**, 21, 891.
- [18] V. R. Muzykantov, *Expert Opin Drug Deliv*, 7, 403.
- [19] M. D. Scott, K. L. Murad, F. Koumpouras, M. Talbot, J. W. Eaton, *Proc Natl Acad Sci U S A* **1997**, 94, 7566.
- [20] P. R. Mishra, N. K. Jain, *Int J Pharm* **2002**, 231, 145.
- [21] P. R. Mishra, N. K. Jain, *J Drug Target* **2000**, 8, 217.
- [22] D. V. Godin, S. L. Schrier, *J Membr Biol* **1972**, 7, 285.
- [23] R. C. Gaudreault, B. Bellemare, J. Lacroix, *Anticancer Res* **1989**, 9, 1201.
- [24] V. R. Muzykantov, J. C. Murciano, R. P. Taylor, E. N. Atochina, A. Herraez, *Anal Biochem* **1996**, 241, 109.
- [25] V. R. Muzykantov, M. D. Smirnov, A. L. Klibanov, *J Immunol Methods* **1993**, 158, 183.
- [26] Y. Fu, N. Klonis, C. Suarna, G. J. Maghzal, R. Stocker, L. Tilley, *Cytometry A* **2009**, 75, 390.
- [27] C. G. Millan, M. L. Marinero, A. Z. Castaneda, J. M. Lanao, *J Control Release* **2004**, 95, 27.
- [28] S. K. Doberstein, G. Wiegand, L. M. Machesky, T. D. Pollard, *Cytometry* **1995**, 20, 14.

- [29] R. Mukthavaram, G. Shi, S. Kesari, D. Simberg, *J Control Release*.
- [30] L. Zolla, G. Lupidi, M. Marcheggiani, G. Falcioni, M. Brunori, *Ann Ist Super Sanita* **1991**, 27, 97.
- [31] F. Lang, S. M. Qadri, *Blood Purif*, 33, 125.
- [32] C. Gutierrez Millan, A. Zarzuelo Castaneda, M. L. Sayalero Marinero, J. M. Lanao, *Blood Cells Mol Dis* **2004**, 33, 132.
- [33] G. M. Ihler, R. H. Glew, F. W. Schnure, *Proc Natl Acad Sci U S A* **1973**, 70, 2663.
- [34] A. De Flora, U. Benatti, L. Guida, E. Zocchi, *Proc Natl Acad Sci U S A* **1986**, 83, 7029.
- [35] O. Skorokhod, E. V. Kulikova, N. M. Galkina, P. V. Medvedev, E. E. Zybunova, V. M. Vitvitsky, A. V. Pivnik, F. I. Ataulakhanov, *Haematologica* **2007**, 92, 570.
- [36] X. Xu, H. L. Persson, D. R. Richardson, *Mol Pharmacol* **2005**, 68, 261.
- [37] S. S. Legha, R. S. Benjamin, B. Mackay, M. Ewer, S. Wallace, M. Valdivieso, S. L. Rasmussen, G. R. Blumenschein, E. J. Freireich, *Ann Intern Med* **1982**, 96, 133.
- [38] M. Haritou, D. Yova, D. Koutsouris, S. Loukas, *Clin Hemorheol Microcirc* **1998**, 19, 205.
- [39] M. Magnani, *Erythrocyte engineering for drug delivery and targeting*, Landes Bioscience/Eurekah.com ;Kluwer Academic/Plenum Publishers, Georgetown, Tex.New York, **2003**.
- [40] G. Saulis, *Cell Mol Biol Lett* **2005**, 10, 23.
- [41] G. Flynn, L. McHale, A. P. McHale, *Cancer Lett* **1994**, 82, 225.
- [42] J. L. Sandell, T. C. Zhu, *J Biophotonics*, 4, 773.

- [43] L. M. Matovcik, I. G. Junga, S. L. Schrier, *Blood* **1985**, 65, 1056.
- [44] F. L. Ginn, P. Hochstein, B. F. Trump, *Science* **1969**, 164, 843.
- [45] S. L. Schrier, *Methods Enzymol* **1987**, 149, 260.
- [46] Benbassa.I, K. G. Bensch, S. L. Schrier, *Journal of Clinical Investigation* **1972**, 51, 1833.
- [47] H. Y. Pan, A. R. DeVault, D. Wang-Iverson, E. Ivashkiv, B. N. Swanson, A. A. Sugerman, *J Clin Pharmacol* **1990**, 30, 1128.
- [48] D. Harisa Gel, M. F. Ibrahim, F. K. Alanazi, *Int J Med Sci*, 8, 222.
- [49] M. G. Ihler, *Bibl Haematol* **1985**, 127.
- [50] C. Saadeh, *South Med J* **1998**, 91, 220.
- [51] M. Brahler, R. Georgieva, N. Buske, A. Muller, S. Muller, J. Pinkernelle, U. Teichgraber, A. Voigt, H. Baumler, *Nano Lett* **2006**, 6, 2505.
- [52] A. A. Bogdanov, M. Lewin, R. Weissleder, *Adv Drug Deliv Rev* **1999**, 37, 279.
- [53] H. C. Spencer, W. E. Collins, W. Chin, J. C. Skinner, *Am J Trop Med Hyg* **1979**, 28, 927.
- [54] M. L. Ellsworth, C. G. Ellis, D. Goldman, A. H. Stephenson, H. H. Dietrich, R. S. Sprague, *Physiology (Bethesda)* **2009**, 24, 107.
- [55] G. R. Bergfeld, T. Forrester, *Cardiovasc Res* **1992**, 26, 40.
- [56] H. H. Dietrich, T. Horiuchi, C. Xiang, K. Hongo, J. R. Falck, R. G. Dacey, Jr., *J Vasc Res* **2009**, 46, 253.

- [57] H. Jiang, A. G. Zhu, M. Mamczur, J. R. Falck, K. M. Lerea, J. C. McGiff, *Br J Pharmacol* **2007**, *151*, 1033.
- [58] S. E. Francis, D. J. Sullivan, Jr., D. E. Goldberg, *Annu Rev Microbiol* **1997**, *51*, 97.
- [59] S. M. Huber, A. C. Uhlemann, N. L. Gamper, C. Duranton, P. G. Kremsner, F. Lang, *EMBO J* **2002**, *21*, 22.
- [60] S. L. Jacques, *Phys Med Biol*, *58*, R37.
- [61] K. Konig, *J Microsc* **2000**, *200*, 83.
- [62] V. Ntziachristos, C. Bremer, R. Weissleder, *Eur Radiol* **2003**, *13*, 195.
- [63] N. P. Oien, L. T. Nguyen, F. E. Jernigan, M. A. Priestman, D. S. Lawrence, *Angew Chem Int Ed Engl*, *53*, 3975.
- [64] P. Klan, T. Solomek, C. G. Bochet, A. Blanc, R. Givens, M. Rubina, V. Popik, A. Kostikov, J. Wirz, *Chem Rev*, *113*, 119.
- [65] N. Jamshidi, J. S. Edwards, T. Fahland, G. M. Church, B. O. Palsson, *Bioinformatics* **2001**, *17*, 286.
- [66] F. Lang, K. S. Lang, P. A. Lang, S. M. Huber, T. Wieder, *Antioxid Redox Signal* **2006**, *8*, 1183.
- [67] G. J. Bosman, F. L. Willekens, J. M. Werre, *Cell Physiol Biochem* **2005**, *16*, 1.
- [68] H. M. Lee, M. A. Priestman, D. S. Lawrence, *J Am Chem Soc*, *132*, 1446.
- [69] F. W. Herberg, S. M. Bell, S. S. Taylor, *Protein Eng* **1993**, *6*, 771.
- [70] L. T. Nguyen, N. P. Oien, N. L. Allbritton, D. S. Lawrence, *Angew Chem Int Ed Engl*, *52*, 9936.

- [71] T. G. Cross, D. Scheel-Toellner, N. V. Henriquez, E. Deacon, M. Salmon, J. M. Lord, *Exp Cell Res* **2000**, 256, 34.
- [72] C. Ortutay, J. Valiaho, K. Stenberg, M. Vihinen, *Hum Mutat* **2005**, 25, 435.
- [73] R. Das, V. Esposito, M. Abu-Abed, G. S. Anand, S. S. Taylor, G. Melacini, *Proc Natl Acad Sci U S A* **2007**, 104, 93.
- [74] R. Zennadi, E. J. Whalen, E. J. Soderblom, S. C. Alexander, J. W. Thompson, L. G. Dubois, M. A. Moseley, M. J. Telen, *Blood*, 119, 1217.
- [75] H. K. Jindal, Z. Ai, P. Gascard, C. Horton, C. M. Cohen, *Blood* **1996**, 88, 1479.
- [76] C. Syin, D. Parzy, F. Traincard, I. Boccaccio, M. B. Joshi, D. T. Lin, X. M. Yang, K. Assemet, C. Doerig, G. Langsley, *Eur J Biochem* **2001**, 268, 4842.
- [77] J. Li, L. S. Cox, *Mol Biochem Parasitol* **2000**, 109, 157.
- [78] V. Sharma, R. S. Agnes, D. S. Lawrence, *J Am Chem Soc* **2007**, 129, 2742.
- [79] P. Tsou, B. Zheng, C. H. Hsu, A. T. Sasaki, L. C. Cantley, *Cell Metab*, 13, 476.
- [80] N. Chen, J. Zou, S. Wang, Y. Ye, Y. Huang, G. Gadda, J. J. Yang, *Biochemistry* **2009**, 48, 3519.
- [81] L. Shi, V. De Paoli, N. Rosenzweig, Z. Rosenzweig, *J Am Chem Soc* **2006**, 128, 10378.
- [82] P. Wu, S. B. Nicholls, J. A. Hardy, *Biophys J*, 104, 1605.
- [83] C. H. Tung, U. Mahmood, S. Bredow, R. Weissleder, *Cancer Res* **2000**, 60, 4953.

- [84] X. Huang, S. Lee, X. Chen, *Am J Nucl Med Mol Imaging*, **1**, 3.
- [85] A. Wunder, C. H. Tung, U. Muller-Ladner, R. Weissleder, U. Mahmood, *Arthritis Rheum* **2004**, *50*, 2459.
- [86] A. Specht, F. Bolze, Z. Omran, J. F. Nicoud, M. Goeldner, *HFSP J* **2009**, *3*, 255.
- [87] M. R. Lieber, T. L. Steck, *J Biol Chem* **1982**, *257*, 11651.
- [88] H. Bodemann, H. Passow, *J Membr Biol* **1972**, *8*, 1.
- [89] D. B. Glass, H. C. Cheng, L. Mende-Mueller, J. Reed, D. A. Walsh, *J Biol Chem* **1989**, *264*, 8802.
- [90] H. Flotow, G. Thomas, *J Biol Chem* **1992**, *267*, 3074.
- [91] J. J. Olearczyk, A. H. Stephenson, A. J. Lonigro, R. S. Sprague, *Med Sci Monit* **2001**, *7*, 669.
- [92] I. Koshino, N. Mohandas, Y. Takakuwa, *J Biol Chem*, *287*, 35244.
- [93] M. Rask-Andersen, S. Masuram, H. B. Schioth, *Annu Rev Pharmacol Toxicol*, *54*, 9.
- [94] J. Arrowsmith, *Nat Rev Drug Discov*, *10*, 328.
- [95] G. Bort, T. Gallavardin, D. Ogden, P. I. Dalko, *Angew Chem Int Ed Engl*, *52*, 4526.
- [96] G. Chen, H. Qiu, P. N. Prasad, X. Chen, *Chem Rev*, *114*, 5161.
- [97] L. D. Sun, Y. F. Wang, C. H. Yan, *Acc Chem Res*, *47*, 1001.
- [98] T. A. Shell, J. R. Shell, Z. L. Rodgers, D. S. Lawrence, *Angew Chem Int Ed Engl*, *53*, 875.

- [99] N. T. Ashley, Z. M. Weil, R. J. Nelson, *Annual Review of Ecology, Evolution, and Systematics*, **43**, 385.
- [100] R. Medzhitov, *Nature* **2008**, *454*, 428.
- [101] J. W. K. Park, Y.; Lee, K. J.; Kim, D. J., *Bioconjugate Chemistry* **2012**, *23*, 12.
- [102] W. J. Smith, N. P. Oien, R. M. Hughes, C. M. Marvin, Z. L. Rodgers, J. Lee, D. S. Lawrence, *Angewandte Chemie International Edition*.
- [103] D. Martinez Molina, R. Jafari, M. Ignatushchenko, T. Seki, E. A. Larsson, C. Dan, L. Sreekumar, Y. Cao, P. Nordlund, *Science*, **341**, 84.
- [104] D. Huscher, K. Thiele, E. Gromnica-Ihle, G. Hein, W. Demary, R. Dreher, A. Zink, F. Buttgereit, *Ann Rheum Dis* **2009**, *68*, 1119.
- [105] U. Baschant, N. E. Lane, J. Tuckermann, *Nat Rev Rheumatol*, **8**, 645.
- [106] S. Mitragotri, J. W. Yoo, *Arch Pharm Res*, **34**, 1887.
- [107] C. Fiehn, *Clin Exp Rheumatol*, **28**, S40.
- [108] W. Ulbrich, A. Lamprecht, *J R Soc Interface*, **7 Suppl 1**, S55.
- [109] J. J. McGuire, *Curr Pharm Des* **2003**, *9*, 2593.
- [110] B. D. Markovic, S. M. Vladimirov, O. A. Cudina, J. V. Odovic, K. D. Karljickovic-Rajic, *Molecules*, **17**, 480.
- [111] C. Civiale, F. Bucaria, S. Piazza, O. Peri, F. Miano, V. Enea, *J Ocul Pharmacol Ther* **2004**, *20*, 75.
- [112] F. J. Martin, R. C. MacDonald, *Biochemistry* **1976**, *15*, 321.
- [113] J. L. Unthank, J. M. Lash, J. C. Nixon, R. A. Sidner, H. G. Bohlen, *Microvasc Res* **1993**, *45*, 193.

- [114] S. Akerman, C. C. Reyes-Aldasoro, M. Fisher, K. L. Pettyjohn, M. A. Bjorndahl, H. Evans, G. M. Tozer, *Med Eng Phys*, **33**, 805.
- [115] Q. F. Ahkong, J. P. Desmazes, D. Georgescauld, J. A. Lucy, *J Cell Sci* **1987**, *88 (Pt 3)*, 389.
- [116] Q. F. Ahkong, J. M. Baldwin, R. O'Reilly, J. A. Lucy, *Mol Membr Biol* **1994**, *11*, 171.
- [117] F. Bossa, A. Latiano, L. Rossi, M. Magnani, O. Palmieri, B. Dallapiccola, S. Serafini, G. Damonte, E. De Santo, A. Andriulli, V. Annese, *Am J Gastroenterol* **2008**, *103*, 2509.
- [118] C. Domenech, X. Thomas, S. Chabaud, A. Baruchel, F. Gueyffier, F. Mazingue, A. Auvrignon, S. Corm, H. Dombret, P. Chevallier, C. Galambrun, F. Huguet, F. Legrand, F. Mechinaud, N. Vey, I. Philip, D. Liens, Y. Godfrin, D. Rigal, Y. Bertrand, *Br J Haematol*, *153*, 58.
- [119] B. Bahmani, D. Bacon, B. Anvari, *Sci Rep*, *3*, 2180.
- [120] A. Z. Wilczewska, K. Niemirowicz, K. H. Markiewicz, H. Car, *Pharmacol Rep*, *64*, 1020.
- [121] T. M. Allen, P. R. Cullis, *Adv Drug Deliv Rev*, *65*, 36.
- [122] L. Brannon-Peppas, J. O. Blanchette, *Adv Drug Deliv Rev* **2004**, *56*, 1649.
- [123] H. S. Yoo, T. G. Park, *J Control Release* **2004**, *100*, 247.